Brigham Young University
BYU ScholarsArchive

All Theses and Dissertations

2015-07-01

Lateral Resistance of Pipe Piles Near 20-ft Tall MSE Abutment Wall with Strip Reinforcements

Jason James Besendorfer
Brigham Young University - Provo

Follow this and additional works at: https://scholarsarchive.byu.edu/etd

 Part of the Civil and Environmental Engineering Commons

BYU ScholarsArchive Citation

Besendorfer, Jason James, "Lateral Resistance of Pipe Piles Near 20-ft Tall MSE Abutment Wall with Strip Reinforcements" (2015). *All Theses and Dissertations*. 5922.
https://scholarsarchive.byu.edu/etd/5922

This Thesis is brought to you for free and open access by BYU ScholarsArchive. It has been accepted for inclusion in All Theses and Dissertations by an authorized administrator of BYU ScholarsArchive. For more information, please contact scholarsarchive@byu.edu, ellen_amatangelo@byu.edu.

Lateral Resistance of Pipe Piles Near 20-ft Tall MSE Abutment Wall with Strip Reinforcements

Jason James Besendorfer

A thesis submitted to the faculty of
Brigham Young University
in partial fulfillment of the requirements for the degree of

Master of Science

Kyle M. Rollins, Chair
Kevin W. Franke
Norman L. Jones

Department of Civil and Environmental Engineering

Brigham Young University

July 2015

Copyright © 2015 Jason James Besendorfer

All Rights Reserved

ABSTRACT

Lateral Resistance of Pipe Piles Near 20-ft Tall MSE Abutment Wall with Strip Reinforcements

Jason James Besendorfer
Department of Civil and Environmental Engineering, BYU
Master of Science

Full scale lateral load testing was performed on four 12.75x0.375 pipe piles spaced at 3.9, 2.9, 2.8, and 1.7 pile diameters behind an MSE wall which was constructed for this research to determine appropriate reduction factors for lateral pile resistance based on pile spacing behind the back face of the wall. The load induced on eight soil reinforcements located at various transverse distances from the pile and at different depths was monitored to determine the relationship between lateral load on the pile and load induced in the reinforcement. Each pile was loaded towards the wall in 0.25 in. increments to a total deflection of 3.0 in. Additionally, wall panel displacement was also monitored to determine if it remained in acceptable bounds.

The results of the research indicate that pile resistance tends to decrease as spacing decreases. P-multipliers for the 3.9, 2.9, 2.8, 1.7D tests were found to be 1.0, 1.0, 1.0, and 0.5, respectively using back-analysis with the computer model LPILE. However, these multipliers are higher than expected based on previous testing and research. Piles spaced further than 3.8D can be assumed to have no interaction with the wall. The resistance of piles spaced closer to the wall than 3.8D can be modeled in LPILE using a p-multiplier less than 1.0. The reinforced backfill can be modeled in LPILE using the API Sand (1982) method with a friction angle of 31º and a modulus of approximately 60 pci when a surcharge of 600 psf is applied. If no surcharge is applied, a friction angle of 39º and modulus of 260 pci is more appropriate. Maximum wall panel displacement was highest for the 2.8D test and was 0.35 in. at 3.0 in. of pile head displacement. For all the other tests, the maximum wall displacement at 3.0 in. of pile head displacement was similar and was approximately 0.15 inches. Induced load in the soil reinforcement increases with depth to the 2nd or 3rd layer of reinforcement after which it decreases. Induced load in the reinforcement increases as pile spacing decreases. Induced load in the reinforcement decreases rapidly with increased transverse distance from the pile. Induced load in the reinforcement can be estimated using a regression equation which considers the influence of pile load, pile spacing behind the wall, reinforcement depth or vertical stress, and transverse spacing of the reinforcement.

Keywords: laterally loaded pile, MSE wall, p-y curve, p-multiplier

ACKNOWLEDGEMENTS

Funding for this study was provided by an FHWA pooled fund study TPF-5(272) "Evaluation of Lateral Pile Resistance Near MSE Walls at a Dedicated Wall Site" supported by Departments of Transportation from the states of Florida, Iowa, Kansas, Massachusetts, Minnesota, Montana, New York, Oregon, Texas, and Utah. Utah served as the lead agency with Jason Richards as the project manager. This support is gratefully acknowledged; however, the opinions, conclusions and recommendations in this paper do not necessarily represent those of the sponsoring organizations.

In addition, significant in-kind contributions from a number of entities made it possible for this project to be undertaken with a scope sufficient to accomplish the project objectives. We gratefully acknowledge the assistance of Chris Ragan at Atlas Tube in donating the circular and square steel piles along with Price Bethel at Spartan Steel in donating the H piles used in this study. Eric Hendricksen at Desert Deep Foundations, Inc. provided pile driving services at cost and Carl Clyde at Geneva Rock, Inc. donated site grading services and the use of their land for the MSE abutment test site. Lastly, Reinforced Earth Company and SSL, Inc. donated wall panels and reinforcing elements necessary to construct the abutment wall.

I would like to express my appreciation to each of my committee members, Dr. Kyle M. Rollins, Dr. Kevin W. Franke, and Dr. Norman L. Jones who have all influenced my decision to pursue a master's degree in Geotechnical engineering and have been influential teachers as I have studied at BYU. I would also like to thank my wife for her encouragement and patience throughout my studies.

TABLE OF CONTENTS

LIST OF TABLES ..... **viii**

LIST OF FIGURES ..... **x**

1 Introduction **1**

1.1 Objectives 2

1.2 Scope 3

1.3 Thesis Organization 3

2 Literature Review **5**

2.1 MSE Wall Design 5

2.2 Laterally Loaded Pile Design 12

2.3 Previous Testing and Research 17

2.3.1 Tests with Drilled Shafts and Geogrid Reinforcement (Pierson et al. 2009) 18

2.3.2 Tests with Driven Pipe Piles and Metallic Reinforcements (Rollins et al. 2013) 21

2.3.3 Lateral Load Tests on Pipe Piles Near MSE Wall with Metallic Reinforcement (Hatch 2014, Han 2014) 27

3 Test Layout **33**

3.1 MSE Wall 34

3.1.1 Backfill 36

3.1.2 Surcharge 39

3.2 Piles 40

3.3 Loading Apparatus 41

4 Instrumentation **43**

4.1 Load Cell and Pressure Transducers 43

4.2 String Potentiometers 44

4.3 Strain Gauges 45

4.3.1 Soil Reinforcement Strain Gauges 45
4.3.2 Pile Strain Gauges 47
4.4 Shape Arrays 48
4.5 Digital Image Correlation (DIC) 48
5 Lateral Load Testing 51
5.1 Load Displacement Curves 51
5.2 Soil Reinforcement Performance 54
5.3 Statistical Analysis of Load in the Reinforcement 62
5.3.1 Model with Depth as a Variable 62
5.3.2 Model with Vertical Stress as a Variable 65
5.3.3 Model Parameter Range and Use 68
5.4 Ground Displacement 69
5.5 Wall Panel Displacement 72
5.6 Pile Performance 83
6 Lateral Pile Load Analysis 89
6.1 Material Properties 90
6.2 Results of LPILE Analysis 94
6.2.1 Load-Deflection Curves 94
6.2.2 P-Multipliers versus Pile Spacing Curves 99
6.2.3 Pile Head Load versus Rotation Curves 101
6.2.4 Bending Moment versus Depth Curves 103
7 Conclusion 107
7.1 Conclusions Relative to Lateral Pile Resistance 107
7.2 Conclusions Relative to Force Induced in the Reinforcements 108
7.3 Recommendations for Further Research 109

REFERENCES **111**

Appendix A. Factor of Safety Against Pullout Calcualtions **113**

Appendix B. Geneva Rock Laboratory Test Reports **115**

Phase 1 116

Phase 2 117

Appendix C. Load Displacement Curves **119**

Appendix D. Ground Displacement Curves **123**

Appendix E. Induced Force in the Reinforcement Curves **129**

1.7D Soil Reinforcement Curves 129

2.8D Soil Reinforcement Curves 134

2.9D Soil Reinforcement Curves 138

3.9D Soil Reinforcement Curves 142

Appendix F. Pile Driving Blowcounts **147**

LIST OF TABLES

Table 2-1: Shaft spacing and length.....20

Table 3-1: Soil properties for soil between test piles and MSE wall.....39

Table 3-2: Soil properties for soil behind test piles.....39

Table 3-3: Combined soil properties.....39

Table 4-1: String potentiometer locations.....45

Table 4-2: Reinforcement number and horizontal distance from pile center to reinforcement center for all instrumented soil reinforcements.....47

Table 4-3: Transverse distance of shape array to center of pile.....48

Table 5-1: Multiple regression model results for model with depth as a variable.....63

Table 5-2: Multiple regression model results for model with vertical stress as a variable.....66

Table 5-3: Range of values for each variable applied in the multiple regression models.....69

Table 6-1: Pile properties for LPILE analysis.....91

Table 6-2: Soil properties used in LPILE analysis with simulated surcharge.....93

Table 6-3: Soil properties used in LPILE analysis with surcharge not simulated.....94

Table 6-4: P-Multipliers for each test.....95

Table F-1: Pile driving blowcounts at various depths for each of the test piles.....147

LIST OF FIGURES

Figure 2-1: Typical cross section of an MSE wall (Berg et al, 2009). 7

Figure 2-2: Potential external failure mechanisms for an MSE wall (Berg et al, 2009).....8

Figure 2-3: Variation of the coefficient of lateral stress ratio (K_r/K_a) with depth in an MSE wall (Berg et al, 2009). 9

Figure 2-4: Assumed failure surface for inextensible reinforcement (Berg et al, 2009). 10

Figure 2-5: Assumed failure surface for extensible reinforcement (Berg et al, 2009). 10

Figure 2-6: Conceptual model of the p-y method (After Reese et al. 2004). 13

Figure 2-7: Soil modulus reaction based on soil friction angle or relative density (API, 1982). 14

Figure 2-8: Illustration of wedge failure for laterally loaded piles at shallow depths (Reese et al. 2004).....15

Figure 2-9: Coefficients C_1, C_2, and C_3 as a function of soil friction angle. 16

Figure 2-10: Soil modulus reduction using the p-multiplier approach. 17

Figure 2-11: Peak load versus displacement curves for tested shafts (After Pierson et al. 2009).....20

Figure 2-12: Load-deflection curves for the test piles (Price, 2012). 23

Figure 2-13: P-multipliers for piles based on pile distance from the wall and L/H ratio (Price, 2012).....24

Figure 2-14: Tentative failure envelope for soil reinforcement (Price, 2012).....25

Figure 2-15. Load-displacement curves for piles tested. (Nelson, 2013) 26

Figure 2-16: Pile head load versus deflection for peak load of grid reinforcement (Hatch, 2014). 29

Figure 2-17: Pile head load versus deflection for peak load of ribbed steel strip reinforcement (Han, 2014).....29

Figure 2-18: Normalized induced force in grid versus normalized distance from pile (Hatch, 2014). 31

Figure 2-19: P-multipliers from previous testing and research (Rollins et al. 2013, Hatch 2014, Han 2014). 32

Figure 3-1: Location of the research site. 33

Figure 3-2: Elevation and plan view of the site. 35

Figure 3-3: Soil gradation of the backfill for both phases of construction and testing. 36

Figure 3-4: Measured relative compaction of backfill. 38

Figure 3-5: Measured moisture content of backfill. 38

Figure 3-6: An example of surcharge and reaction beam. 41

Figure 3-7: Loading apparatus setup. 42

Figure 4-1: Several instrumented soil reinforcement strips. 46

Figure 4-2: Typical DIC setup. 49

Figure 4-3: Facets used in DIC analysis. 50

Figure 5-1: Peak pile load versus displacement. 52

Figure 5-2: Final pile head load versus displacement. 52

Figure 5-3: Induced loads in the second layer of soil reinforcement at various pile head loads and distances from the wall. (2.9D test, 38 in. reinforcement transverse spacing). 56

Figure 5-4: Induced loads in the third layer of soil reinforcement at various pile head loads and distances from the wall. (2.9D test, 37 in. reinforcement transverse spacing). 56

Figure 5-5: Max tensile force in close soil reinforcement at each pile head load for 1.7D test. 57

Figure 5-6: Max tensile force in far soil reinforcement at each pile head load for 1.7D test. 57

Figure 5-7: Max tensile force in close soil reinforcement at each pile head load for 2.8D test. 58

Figure 5-8: Max tensile force in far soil reinforcement at each pile head load for 2.8D test. 58

Figure 5-9: Max tensile force in close soil reinforcement at each pile head load for 2.9D test. 59

Figure 5-10: Max tensile force in far soil reinforcement at each pile head load for 2.9D test. 59

Figure 5-11: Max tensile force in close soil reinforcement at each pile head load for 3.9D test. 60

Figure 5-12: Max tensile force in far soil reinforcement at each pile head load for 3.9D test. 60

Figure 5-13: Interaction of soil and MSE wall reinforcement when pile is laterally loaded. 61

Figure 5-14: Predicted versus measured tensile force for model with depth as a variable. 64

Figure 5-15: Residuals for the variables used in the multiple regression model with depth as a variable. 64

Figure 5-16: Predicted versus measured tensile force for model with vertical stress as a variable. 67

Figure 5-17: Residuals for the variables used in the multiple regression model with vertical stress as a variable. 67

Figure 5-18: Vertical ground displacement for all test piles. 70

Figure 5-19: Horizontal ground displacement for 2.9D test at several pile head load levels. 71

Figure 5-20: Normalized ground displacement. 72

Figure 5-21: Wall panel displacement at 0.5 in. pile head displacement for all piles tested. 73

Figure 5-22: Wall panel displacement at 3.0 in. pile head deflection. Note different scale on 2.8D. 74

Figure 5-23: Panel displacement at the reinforcement connection location for the 1.7D test. 78

Figure 5-24: Panel displacement at the reinforcement connection location for the 2.8D test. 78

Figure 5-25: Panel displacement at the reinforcement connection location for the 2.9D test. 79

Figure 5-26: Panel displacement at the reinforcement connection location for the 3.9D test. 79

Figure 5-27: Comparison of wall displacement measured by the shape arrays to DIC and string potentiometer data for the 1.7D test at 3.0 in. pile head deflection. 81

Figure 5-28: Comparison of wall displacement measured by the shape arrays to DIC and string potentiometer data for the 2.8D test at 1.75 in. pile head deflection. 81

Figure 5-29: Comparison of wall displacement measured by the shape arrays to DIC and string potentiometer data for the 2.9D test at 3.0 in. pile head deflection. 82

Figure 5-30: Comparison of wall displacement measured by the shape arrays to DIC and string potentiometer data for the 3.9D test at 3.0 in. pile head deflection. 82

Figure 5-31: Measurement of y to correct strain measurement for pile rotation. 84

Figure 5-32: Moment versus depth for various loads on the 1.7D test. 85

Figure 5-33: Moment versus depth for various loads on the 2.8D test. 86

Figure 5-34: Moment versus depth for various loads on the 2.9D test. 86

Figure 5-35: Moment versus depth for various loads on the 3.9D test. 87

Figure 5-36: Pile head load versus rotation of the tip of the four test piles and the reaction pile. 88

Figure 6-1: Soil modulus reaction based on soil friction angle or relative density (API, 1982). 93

Figure 6-2: Comparison of load versus deflection curves computed by LPILE to measured load-deflection curves. 96

Figure 6-3: Comparison of load versus displacement curves for the 3.9D pile to other piles at similar spacings tested during this study. 98

Figure 6-4: Comparison of load versus displacement curves for the 2.8D pile to other piles at similar spacings tested during this study. 98

Figure 6-5: Comparison of load versus displacement curves for the 1.7D pile to other piles at similar spacings tested during this study. 99

Figure 6-6: P-multiplier curve versus normalized distance from the wall from this study in comparison with previous test results. 100

Figure 6-7: Comparison of pile head load versus rotation curves computed by LPILE to measured pile head load versus rotation curves for the 1.7D test. 102

Figure 6-8: Comparison of pile head load versus rotation curves computed by LPILE to measured pile head load versus rotation curves for the 2.9D test. 102

Figure 6-9: Measured and computed pile bending moment at multiple pile head load levels for the 1.7D test. 103

Figure 6-10: Measured and computed pile bending moment at multiple pile head load levels for the 2.8D test. 104

Figure 6-11: Measured and computed pile bending moment at multiple pile head load levels for the 2.9D test. 104

Figure 6-12: Measured and computed pile bending moment at multiple pile head load levels for the 3.9D test. 105

Figure C-1: Load-deflection curves for 1.7D test. 119

Figure C-2: Load-deflection curves for 2.8D test. 120

Figure C-3: Load-deflection curves for 2.9D test. 120

Figure C-4: Load-deflection curves for 3.9D test. 121

Figure D-1: Horizontal ground displacement at several load levels for 1.7D test. 123

Figure D-2: Horizontal ground displacement at several load levels for 2.8D test. 124

Figure D-3: Horizontal ground displacement at several load levels for 2.9D test. 124

Figure D-4: Horizontal ground displacement at several load levels for 3.9D test. 125

Figure D-5: Vertical ground displacement at peak pile load for 1.7D test. 125

Figure D-6: Vertical ground displacement at peak pile load for 2.8D test. 126

Figure D-7: Vertical ground displacement at peak pile load for 2.9D test. 126

Figure D-8: Vertical ground displacement at peak pile load for 3.9D test. 127

Figure E-1: Induced force in soil reinforcement at varying pile head loads and distances from the back face of the MSE wall for the 1.7D test; 15 in. depth and 9.5 in. transverse spacing from center of pile. 129

Figure E-2: Induced force in soil reinforcement at varying pile head loads and distances from the back face of the MSE wall for the 1.7D test; 15 in. depth and 35 in. transverse spacing from center of pile. 130

Figure E-3: Induced force in soil reinforcement at varying pile head loads and distances from the back face of the MSE wall for the 1.7D test; 45 in. depth and 11 in. transverse spacing from center of pile. 130

Figure E-4: Induced force in soil reinforcement at varying pile head loads and distances from the back face of the MSE wall for the 1.7D test; 45 in. depth and 37.5 in. transverse spacing from center of pile. 131

Figure E-5: Induced force in soil reinforcement at varying pile head loads and distances from the back face of the MSE wall for the 1.7D test; 75 in. depth and 9 in. transverse spacing from center of pile. 131

Figure E-6: Induced force in soil reinforcement at varying pile head loads and distances from the back face of the MSE wall for the 1.7D test; 75 in. depth and 36 in. transverse spacing from center of pile. 132

Figure E-7: Induced force in soil reinforcement at varying pile head loads and distances from the back face of the MSE wall for the 1.7D test; 105 in. depth and 9 in. transverse spacing from center of pile. 132

Figure E-8: Induced force in soil reinforcement at varying pile head loads and distances from the back face of the MSE wall for the 1.7D test; 105 in. depth and 35 in. transverse spacing from center of pile. 133

Figure E-9: Induced force in soil reinforcement at varying pile head loads and distances from the back face of the MSE wall for the 2.8D test; 15 in. depth and 24.5 in. transverse spacing from center of pile. 134

Figure E-10: Induced force in soil reinforcement at varying pile head loads and distances from the back face of the MSE wall for the 2.8D test; 15 in. depth and 50 in. transverse spacing from center of pile. 134

Figure E-11: Induced force in soil reinforcement at varying pile head loads and distances from the back face of the MSE wall for the 2.8D test; 45 in. depth and 20.5 in. transverse spacing from center of pile. 135

Figure E-12: Induced force in soil reinforcement at varying pile head loads and distances from the back face of the MSE wall for the 2.8D test; 45 in. depth and 47 in. transverse spacing from center of pile. 135

Figure E-13: Induced force in soil reinforcement at varying pile head loads and distances from the back face of the MSE wall for the 2.8D test; 75 in. depth and 22.5 in. transverse spacing from center of pile. 136

Figure E-14: Induced force in soil reinforcement at varying pile head loads and distances from the back face of the MSE wall for the 2.8D test; 75 in. depth and 49.5 in. transverse spacing from center of pile. 136

Figure E-15: Induced force in soil reinforcement at varying pile head loads and distances from the back face of the MSE wall for the 2.8D test; 105 in. depth and 23.5 in. transverse spacing from center of pile. 137

Figure E-16: Induced force in soil reinforcement at varying pile head loads and distances from the back face of the MSE wall for the 2.8D test; 105 in. depth and 50 in. transverse spacing from center of pile. 137

Figure E-17: Induced force in soil reinforcement at varying pile head loads and distances from the back face of the MSE wall for the 2.9D test; 15 in. depth and 10 in. transverse spacing from center of pile. 138

Figure E-18: Induced force in soil reinforcement at varying pile head loads and distances from the back face of the MSE wall for the 2.9D test; 15 in. depth and 35.5 in. transverse spacing from center of pile. 138

Figure E-19: Induced force in soil reinforcement at varying pile head loads and distances from the back face of the MSE wall for the 2.9D test; 45 in. depth and 12 in. transverse spacing from center of pile. 139

Figure E-20: Induced force in soil reinforcement at varying pile head loads and distances from the back face of the MSE wall for the 2.9D test; 45 in. depth and 38 in. transverse spacing from center of pile. 139

Figure E-21: Induced force in soil reinforcement at varying pile head loads and distances from the back face of the MSE wall for the 2.9D test; 75 in. depth and 11.5 in. transverse spacing from center of pile. 140

Figure E-22: Induced force in soil reinforcement at varying pile head loads and distances from the back face of the MSE wall for the 2.9D test; 75 in. depth and 37 in. transverse spacing from center of pile. 140

Figure E-23: Induced force in soil reinforcement at varying pile head loads and distances from the back face of the MSE wall for the 2.9D test; 105 in. depth and 10.5 in. transverse spacing from center of pile. 141

Figure E-24: Induced force in soil reinforcement at varying pile head loads and distances from the back face of the MSE wall for the 2.9D test; 105 in. depth and 38 in. transverse spacing from center of pile. 141

Figure E-25: Induced force in soil reinforcement at varying pile head loads and distances from the back face of the MSE wall for the 3.9D test; 15 in. depth and 26 in. transverse spacing from center of pile. 142

Figure E-26: Induced force in soil reinforcement at varying pile head loads and distances from the back face of the MSE wall for the 3.9D test; 15 in. depth and 51 in. transverse spacing from center of pile. 142

Figure E-27: Induced force in soil reinforcement at varying pile head loads and distances from the back face of the MSE wall for the 3.9D test; 45 in. depth and 22.5 in. transverse spacing from center of pile. 143

Figure E-28: Induced force in soil reinforcement at varying pile head loads and distances from the back face of the MSE wall for the 3.9D test; 45 in. depth and 49 in. transverse spacing from center of pile. 143

Figure E-29: Induced force in soil reinforcement at varying pile head loads and distances from the back face of the MSE wall for the 3.9D test; 75 in. depth and 24.5 in. transverse spacing from center of pile. 144

Figure E-30: Induced force in soil reinforcement at varying pile head loads and distances from the back face of the MSE wall for the 3.9D test; 75 in. depth and 50 in. transverse spacing from center of pile. 144

Figure E-31: Induced force in soil reinforcement at varying pile head loads and distances from the back face of the MSE wall for the 3.9D test; 105 in. depth and 24.5 in. transverse spacing from center of pile. 145

Figure E-32: Induced force in soil reinforcement at varying pile head loads and distances from the back face of the MSE wall for the 3.9D test; 105 in. depth and 51.5 in. transverse spacing from center of pile. 145

1 INTRODUCTION

Piles within the reinforcement zone of Mechanically Stabilized Earth (MSE) walls are commonly used to support Integral Abutment Bridges (IAB). These piles must support the axial load from the bridge as well as lateral loads from thermal expansion and contraction and earthquake loads. There are commonly used methods for designing laterally loaded piles; however, little guidance on the design of these piles within the zone of reinforcement of a MSE wall is available. Also, little is known about the effects of laterally loaded piles on the reinforcement used for the MSE wall, thus it is not known how to account for the induced stresses on the soil reinforcement caused by the laterally loaded piles. Right-of-way constraints often require traditional sloped fills to be removed and replaced with MSE walls. Several approaches have been used for design of laterally loaded piles within the reinforced mass of an MSE wall. One design approach is to place piles back far enough from the wall face so that no interaction between the wall and pile is assumed to take place. However, this may require an offset of six to eight pile diameters which increases the bridge span length. Another method is to assume that the pile near the wall has no resistance. Although conservative, this approach leads to larger piles or more piles at a bridge abutment which increases the foundation cost. Reduction factors to account for the decreased resistance of pile near the wall could be used, but there is insufficient data to define what they should be at present.

To investigate this problem further, full-scale lateral load testing of cast-in-place shafts was first performed by Pierson et al. (2009). The results clearly indicated that as spacing behind the wall of the laterally loaded shafts decreased, lateral resistance decreased. However, these tests involved geosynthetic reinforcements and short drilled shafts which are not typical of routine design practice. Price (2012) and Nelson (2013) also conducted full-scale pile lateral load tests and further investigated the effects of the MSE wall-pile interaction for long driven piles and metallic reinforcements. They were able to propose a preliminary reduction factor design curve for lateral resistance of piles near MSE walls, but their tests all involved relatively high reinforcement length (L) to wall height (H) ratios near 1.0 which are typical of seismic loadings. Their results suggested that the reduction factor curves might be a function of reinforcement L/H ratios, but no data were available for L/H values of about 0.70 which are more typical of static loading conditions. They also investigated the loads induced on the soil reinforcement caused by the lateral pile loading and proposed a failure envelope for the soil reinforcement near the laterally loaded piles. This research will focus on an L/H ratio which is shorter than previously tested to investigate the effects of the L/H ratio further. Furthermore, circular piles and ribbed steel strip reinforcements are used which is typical of routine design practice.

1.1 Objectives

The objectives of this research study are to determine appropriate reduction factors for lateral pile resistance of pipe piles based on spacing behind the back face of the wall for walls with a shorter L/H ratio than has previously been studied, determine if wall panel displacement remains within acceptable limits during lateral pile loading for walls with a shorter L/H ratio, and to determine how to predict loads induced by lateral pile loading on the soil reinforcement in the vicinity of the piles being loaded.

1.2 Scope

To further improve our understanding of the MSE wall-pile interaction, a full-scale MSE wall was constructed and piles within the zone of reinforcement were laterally loaded towards the wall. Three different pile types spaced at varying distances behind the wall and two reinforcement types including welded wire grids and ribbed steel strips were tested. Wall face displacement, pile strain, soil reinforcement strain, and pile load were all monitored during testing. Data from previous studies and the additional data gathered through this research should allow design curves to be made to predict lateral load resistance of piles at varying distances behind the MSE wall face. Additionally, the possibility of developing a method to account for induced stress on soil reinforcement due to lateral pile loading will be explored using the data gathered. Previous testing at the site with L/H ratios near 1.0 have confirmed the preliminary design curves for this reinforcement ratio (Hatch, 2014 & Han, 2014). This thesis focuses on the lateral load tests conducted on circular pipe piles with ribbed strip reinforcements having L/H ratios near 0.70. These test represent the first of their kind with reinforcement ratios typical of static conditions and metallic strip reinforcements.

1.3 Thesis Organization

The remainder of this thesis will have the following organization. First, a review of the literature will be completed followed by an overview of the test layout of the wall, piles, and loading device. The instrumentation employed during testing will then be discussed. After that, the lateral load testing results for both the piles and the soil reinforcement will be given. Finally, the lateral pile load analysis will be reviewed followed by conclusions drawn from the research.

2 LITERATURE REVIEW

As the amount of research conducted to determine the effects of laterally loaded piles on MSE walls and their reinforcement has increased, it has become clear that the strength of laterally loaded piles decreases as they are placed closer to the face of the MSE wall. However, a finalized design approach has not been determined. As the research results from each series of tests is combined, a design approach to account for the decreased resistance of these piles may be possible. The literature review contained herein reviews MSE wall design, laterally loaded pile design, and the previous research and testing which has been performed on laterally loaded piles that has brought us to our current state of knowledge.

2.1 MSE Wall Design

In general, an MSE wall consists of multiple layers of soil reinforcement attached to a wall facing which prevents raveling of the soil between the reinforcement layers. There are various types of soil reinforcement that are used, generally classified as metallic or non-metallic with varying degrees of extensibility. Extensible soil reinforcement may deform as much or more as the soil at failure. Inextensible reinforcement is much more rigid and deforms very little at failure. The types of facing used are also variable including precast concrete panels, dry cast modular blocks, gabions, welded wire mesh, shotcrete, timber lagging and panels, polymeric cellular confinement systems, and wrapped sheets of geosynthetics (Berg et al, 2009).

The design of MSE walls has been done based on both Allowable Stress Design (ASD) and the Load and Resistance Factor Design (LRFD) method. Both methods are based on the evaluation of the external and internal stability of the stabilized mass; the primary difference between the two design approaches is the way uncertainty is treated in the design. LRFD design is based on the equation

$$\gamma L = \phi R \tag{2-1}$$

where

γ is the load factor which is greater than 1,

L is the load,

ϕ is the resistance factor which is less than 1, and

R is the resistance.

Using LRFD, the following strength and service limits must be evaluated in the design of an MSE wall. External stability strength limit states for MSE walls include limiting eccentricity, sliding, and bearing resistance failures. Internal stability parameters which must be evaluated include tensile and pullout resistance of reinforcement as well as structural resistance of face elements and face element connections. The service state limits which must be evaluated for the external stability are vertical and lateral wall movements. Global stability must also be considered including the overall stability and the compound stability.

Figure 2-1 shows a typical cross section of an MSE wall. When evaluating the external stability of an MSE wall, important engineering parameters such as the unit weight, friction angle, cohesion, and coefficient of consolidation of the foundation soil need to be determined as well as the unit weight, friction angle, and cohesion of the retained backfill. Additionally, the unit weight

and friction angle of the reinforced wall fill are also necessary. Loads considered in the design of the external stability of the wall include horizontal and vertical earth pressure, live load surcharge, earth surcharge, as well as water and seismic loads if applicable. The reinforced mass is treated as a rigid body which acts vertically on the foundation soil and which has earth pressures acting horizontally behind it caused by the retained backfill. Hence, the external stability is largely based on the length of reinforcement used. The minimum length of reinforcement is generally 8 ft. or 0.7H, whichever is larger, with H being the design height of the wall plus the surcharge. Forces resisting sliding, overturning, and bearing failure of the mass are compared to driving forces, applying the appropriate load and resistance factors for each case. The worst case of the load combinations is considered based on limiting eccentricity (overturning), sliding, and bearing resistance failure. Figure 2-2 shows the three cases evaluated for external stability.

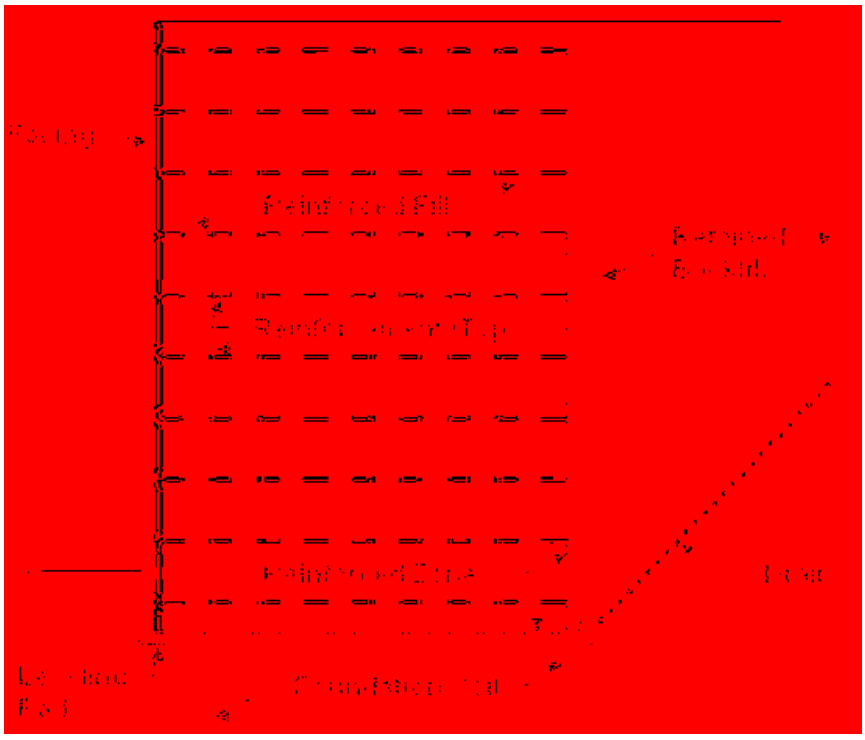

Figure 2-1: Typical cross section of an MSE wall (Berg et al, 2009).

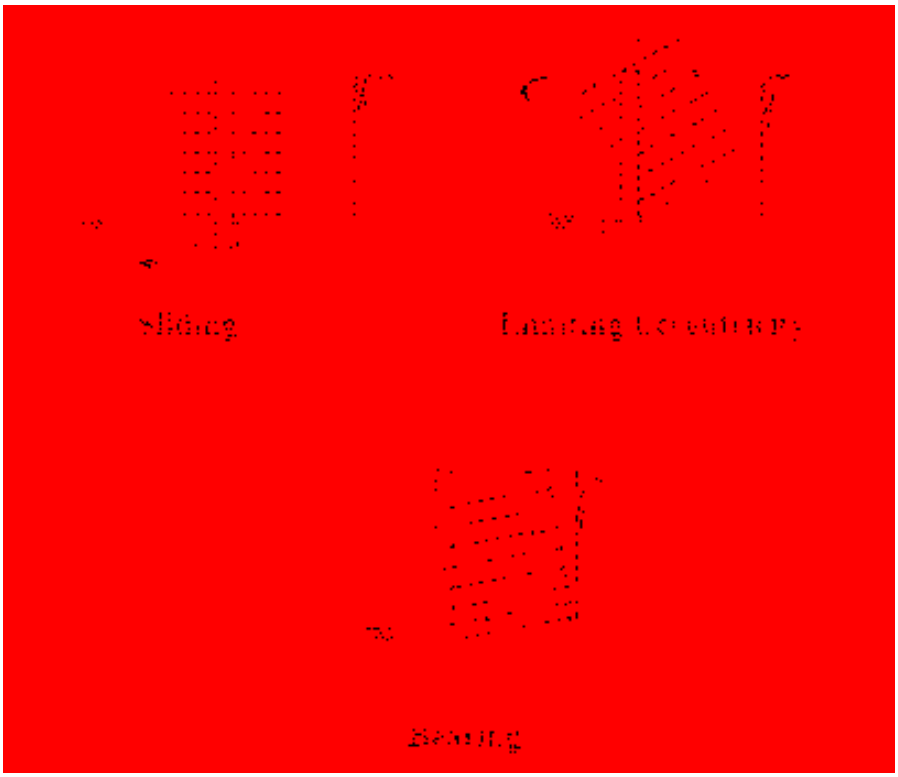

Figure 2-2: Potential external failure mechanisms for an MSE wall (Berg et al, 2009).

Evaluation of the internal stability of an MSE wall requires the consideration of two main reinforcement failure modes: pullout and elongation or breakage. Pullout failure occurs when the tensile force in the reinforcement is greater than the pullout resistance and elongation failure occurs when the tensile force in the reinforcement is large enough to cause excessive elongation or breakage. Loads in the reinforcement are primarily caused by earth pressure of the reinforced fill and surcharge but may also include water, seismic, and other loads. Horizontal earth pressures acting on the wall vary depending on what type of reinforcement is used. Figure 2-4 and Figure 2-5 show the assumed failure surface for inextensible and extensible reinforcement respectively. Vertical and horizontal spacing of the reinforcement must be considered. The horizontal stress within the reinforced zone is given by the equation

$$\sigma_H = K_r \sigma_V + \Delta\sigma_H \qquad (2\text{-}2)$$

where

K_r is the coefficient of lateral earth pressure in the reinforced zone which is a fraction of K_a, the coefficient of active earth pressure (As given in Figure 2-3),

σ_V is the factored vertical pressure at the depth of the reinforcement with 1.35 being the load factor, and

$\Delta\sigma_H$ is the factored horizontal stress due to external surcharge with 1.35 being the load factor because the surcharge is represented as an equivalent uniform soil height.

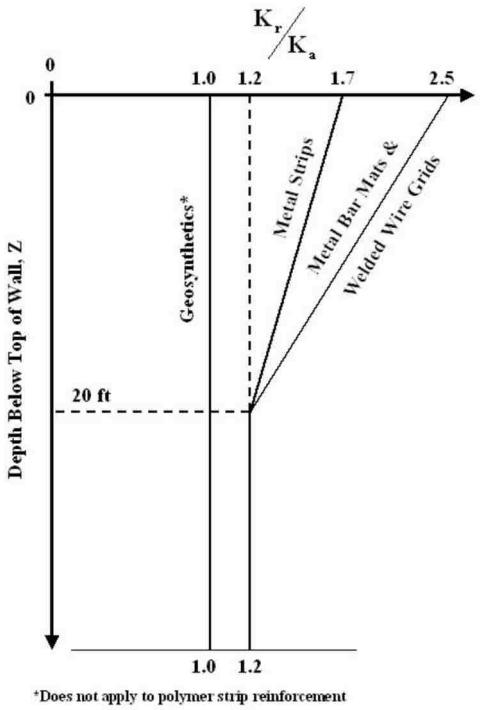

Figure 2-3: Variation of the coefficient of lateral stress ratio (K_r/K_a) with depth in an MSE wall (Berg et al, 2009).

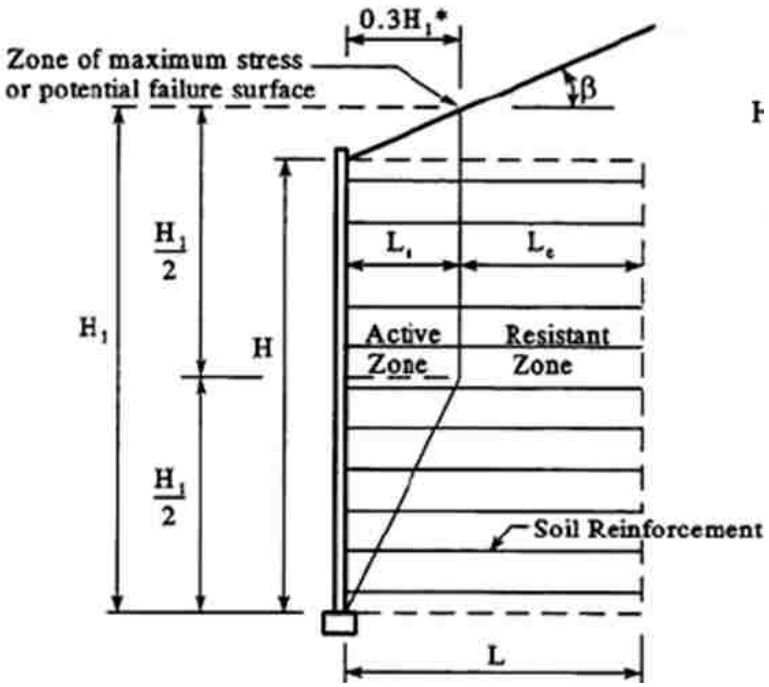

Figure 2-4: Assumed failure surface for inextensible reinforcement (Berg et al, 2009).

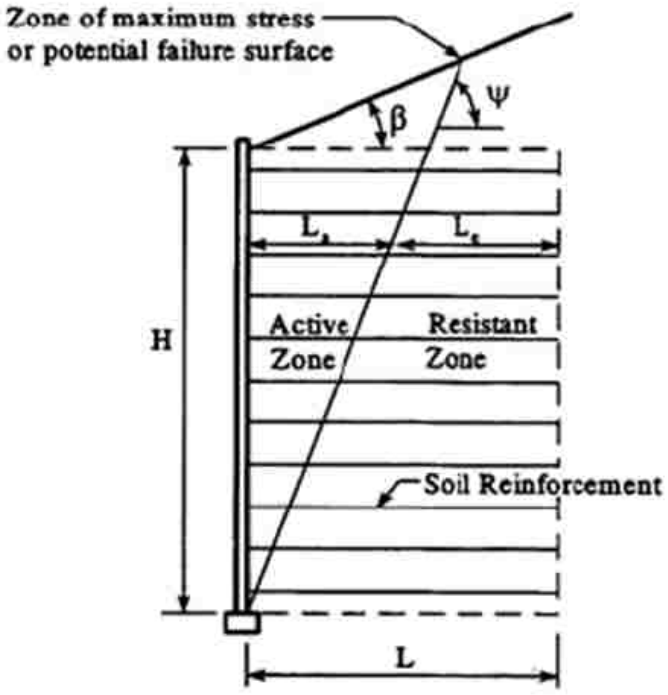

Figure 2-5: Assumed failure surface for extensible reinforcement (Berg et al, 2009).

After calculating the horizontal earth pressure, the maximum tension in the reinforcement per unit width of the wall, T_{MAX} can be determined using Equation (2-3):

$$T_{MAX} = \sigma_H S_V \tag{2-3}$$

where

S_V is the vertical spacing of the reinforcement which is 2.5 ft., and

σ_H is the horizontal earth pressure at the center of the contributory height.

If the reinforcement is not horizontally continuous or if panels of known size are used as the facing, additional variables can be added to this equation to determine the maximum tension in the reinforcement. The maximum tension in the reinforcement must be less than the resistance of the reinforcement to breaking or pullout. The length of reinforcement that must extend beyond the active zone, L_e, to resist pullout is determined with Equation (2-4) below.

$$\phi L_e \geq \frac{T_{MAX}}{F^* \alpha \sigma_V C R_C} \tag{2-4}$$

where

ϕ is the resistance factor for soil reinforcement which is 0.75 for statically loaded metal strips,

F^* is the pullout resistance factor which varies with depth,

α is the scale correction factor equal to 1.0 for inextensible strips unless otherwise indicated by pullout tests,

C = 2 for strip, grid, and sheet reinforcement, and

R_C is the coverage ratio which is the ratio of strip width to horizontal spacing equal to 0.067 for this test.

The total length of the reinforcement is the sum of the active and effective length as shown in Figure 2-5. The active length of inextensible reinforcement for the bottom half of the wall is calculated using Equation (2-5), and the active length of inextensible reinforcement for the top half of the wall is calculated using Equation (2-6).

$$L_{\alpha} = 0.6(H - Z) \tag{2-5}$$

$$L_{\alpha} = 0.3H \tag{2-6}$$

where

H is the design height of the wall, and

Z is the depth of the reinforcement.

Connection strength of the reinforcement to the panels is dependent on many factors and must be determined on a case by case basis through testing and is generally provided by the manufacturer.

2.2 Laterally Loaded Pile Design

A common approach to analyzing laterally loaded piles is the p-y method. With this method, the soil surrounding the piles is modeled as a series of springs at various depths along the pile. The spring stiffness varies nonlinearly with displacement. The displacement of a pile at any depth at a given lateral load can be determined through an iterative approach using this method. Figure 2-6 shows a conceptual model of the p-y method. The load depends on soil type and state, pile geometry, and loading method. Hence, various p-y curves are necessary for different types of soil.

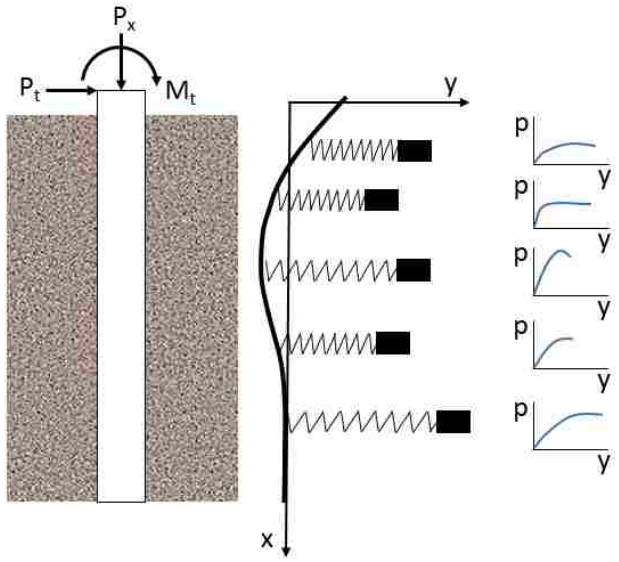

Figure 2-6: Conceptual model of the p-y method (After Reese et al. 2004).

A computer program called LPILE is available for laterally loaded pile design. LPILE is the commercial version of the computer program COM624 which was originally developed by Reese and Matlock at the University of Texas in the 1970s and is one of the most widely used programs for lateral pile load analysis. LPILE is a finite difference program that uses the p-y method described previously. The program computes deflection, bending moment, shear force, and soil response over the length of the pile. Various options are available within the program for determining p-y curves based on different soil types. Some of the options available to model different soil types in LPILE include stiff clay with or without free water (Reese), sand (Reese), American Petroleum Institute (API) sand (O'Neill), liquefied sand (Rollins), and weak rock (Reese). The accuracy of the analysis depends on how accurately the reaction of the soil is modeled by the p-y curve selected for the analysis. The API sand (O'Neill) method is used for laterally loaded pile analysis in this report. The soil unit weight, friction angle, and modulus of subgrade reaction (soil stiffness) are required inputs for this method.

The API p-y curve is defined by the equation

$$p = AP_u \tanh\left[\frac{(kZ)}{(AP_u)}y\right] \qquad (2\text{-}7)$$

where

A is a factor to account for cyclic or static loading and is equal to 3.0-0.8(Z/D) ≥0.9 for static loading and 0.9 for cyclic loading,

Z is the depth below the ground surface,

D is pile diameter,

P_u is the ultimate lateral resistance which is the lower value calculated using Equation (2-8) and (2-9),

k is the initial modulus of subgrade reaction determined from Figure 2-7 based on the soil friction angle, and

y is the lateral deflection at depth Z.

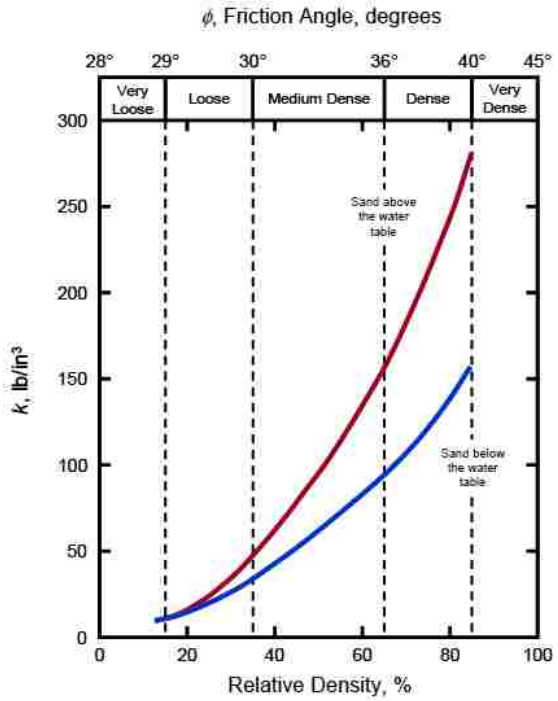

Figure 2-7: Soil modulus reaction based on soil friction angle or relative density (API, 1982).

The ultimate lateral resistance for sand, P_u, has been found to vary from wedge type failure at shallow depths determined by Equation (2-8) to a flow-around type failure at greater depths defined by Equation (2-9). The equation giving the smallest value of P_u should be used as the ultimate resistance in Equation (2-7). The typical wedge type failure shape is illustrated in Figure 2-8. The angle β is typically assumed to be 45° + ϕ/2 while the fan angle, α, is thought to be between ϕ/2 and ϕ for dense sand and approximately ϕ/2 for loose sand.

$$P_{us} = (C_1 x + C_2 b)\gamma' x \tag{2-8}$$

$$P_{ud} = C_3 b \gamma' x \tag{2-9}$$

where

γ' is the effective soil unit weight,

x is the depth below the ground surface, and

C_1, C_2, and C_3 are coefficients determined from Figure 2-9.

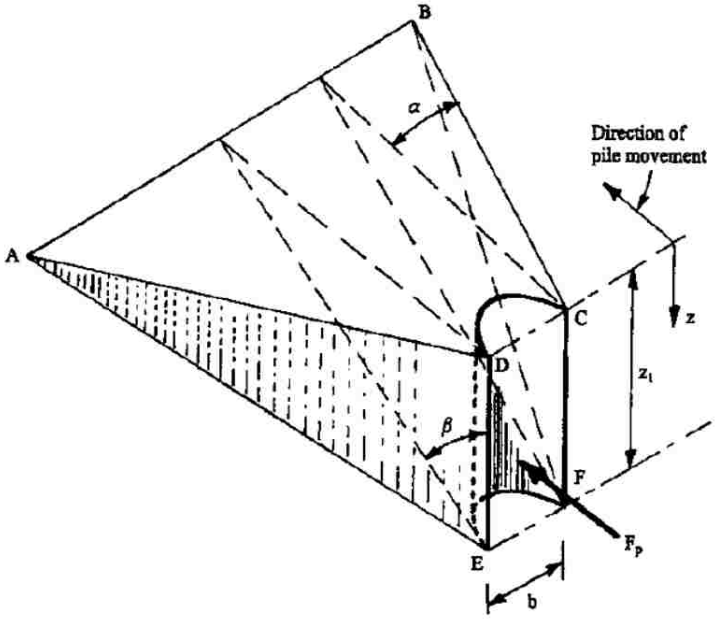

Figure 2-8: Illustration of wedge failure for laterally loaded piles at shallow depths (Reese et al. 2004).

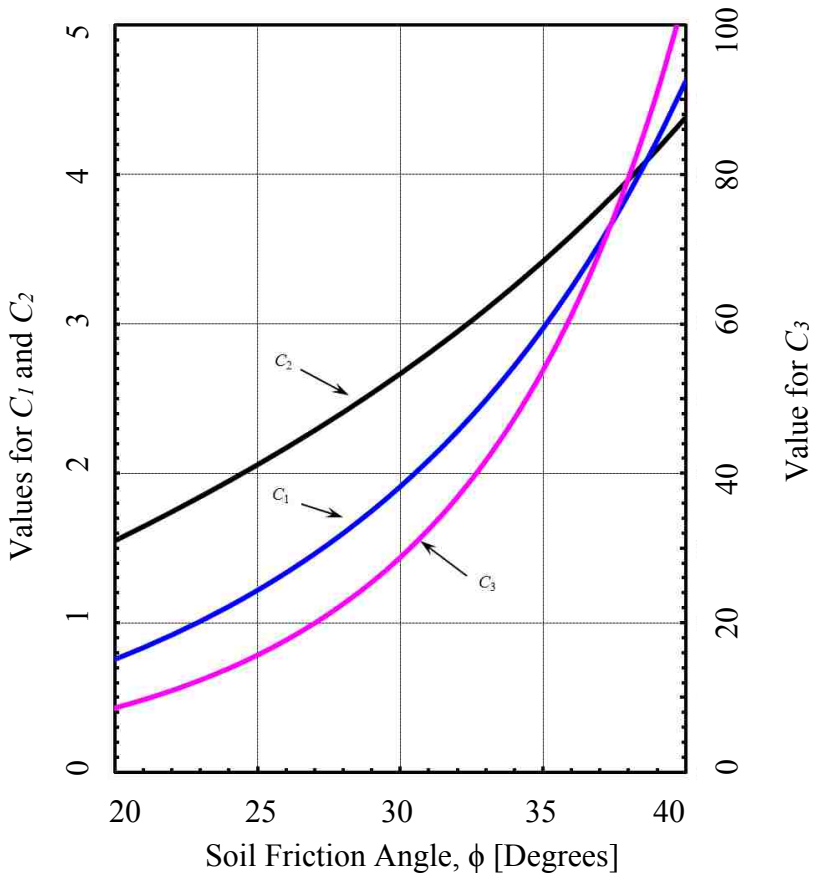

Figure 2-9: Coefficients C_1, C_2, and C_3 as a function of soil friction angle.

Previous testing and research has shown that laterally loaded piles within the reinforcement zone of an MSE wall have reduced resistance. A common approach is to use a p-multiplier (usually less than 1) to reduce the p-y curve to account for the reduced resistance of the pile near the wall. Prior to this research, very few tests have been done to determine the correct multiplier to use for a given situation. Figure 2-10 illustrates how the p-multiplier is used to reduce the p-y curve.

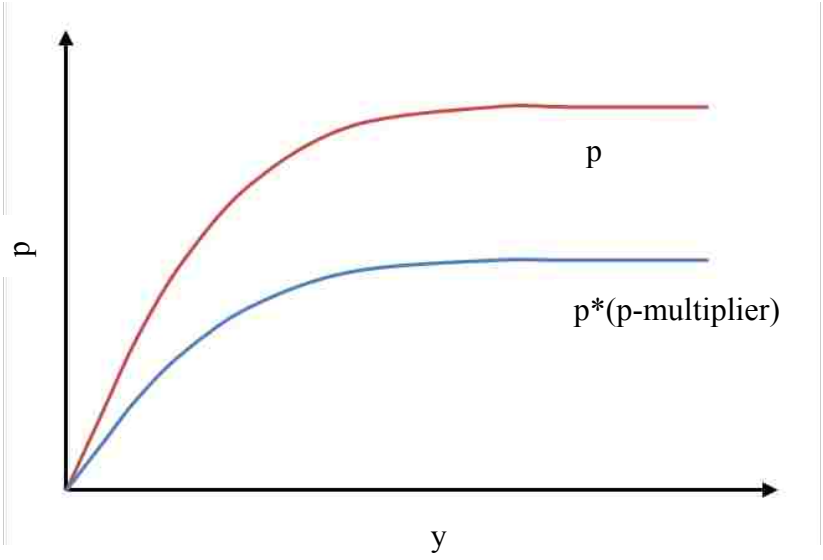

Figure 2-10: Soil modulus reduction using the p-multiplier approach.

2.3 Previous Testing and Research

It has been recognized for quite some time that research needs to be conducted to investigate the effects of laterally loaded piles within the reinforcement zone of MSE walls. To date, three full scale tests have been conducted. The first study conducted by the University of Kansas with funding from the Kansas Department of Transportation investigated the lateral resistance of short drilled shafts behind a block masonry wall reinforced with geogrid sheets (Pierson et al. 2009). The wall and shafts were specifically constructed for the testing purposes. The second study conducted by BYU with funding from the Utah Department of Transportation investigated lateral resistance of driven pipe piles at three bridge sites that were under construction (Rollins et al. 2013). Test involved welded wire (Price, 2012) and ribbed strip reinforcements (Nelson, 2013). The third test series, of which this study is a part, investigates the lateral resistance of driven pipe, square, and H-piles with both welded wire and ribbed strip reinforcements at a site specifically dedicated to testing. This BYU investigation, supported by an FHWA pooled fund,

has already produced reports regarding pipe piles with ribbed strip reinforcement (Han, 2014) and welded wire reinforcement (Hatch, 2014). These earlier reports deal with reinforcement length to wall height ratios of about 0.90, which are typical of seismic design, whereas the current study involves a reinforcement ratio of about 0.70 which is more typical of static design.

2.3.1 Tests with Drilled Shafts and Geogrid Reinforcement (Pierson et al. 2009)

When laterally loaded drilled shafts are used within the reinforcement limits of an MSE wall, common practice is to anchor the end of the drilled shaft into the underlying foundation material. While this method works, it was recognized that considerable cost savings may be realized if it were possible to support the shaft with the MSE mass alone. To determine the resistance of drilled shafts supported by the MSE mass alone, a 20 ft. high segmental block MSE wall was designed and constructed according to the Federal Highway Administration (FHWA) design procedure for MSE walls without shafts. Tensar International Inc. provided the design of the wall as well as the materials, including Mesa standard unit concrete blocks and UX1400 and UX1500 extensible geogrid reinforcement. The stiffness and tensile strength of the two types of extensible geogrid soil reinforcement varied. Both geogrid types consisted of punched-drawn uniaxial high density polyethylene (HDPE). The geogrids were spaced 2 ft. vertically and the ratio of geogrid reinforcement length to wall height was 0.7. Corrugated metal pipe (CMP), 36 inches in diameter, was used as a form for eight drilled shafts located within the MSE mass so drilling would not be necessary after the wall was constructed. Before construction began, the site was excavated down to limestone. The geogrid reinforcement was cut to fit around the CMP as the wall was constructed. Select backfill was used and compacted behind the wall. The backfill consisted of crushed limestone gravel, specified as Kansas Department of Transportation (KDOT) clean aggregate backfill (CA-5) with a measured friction angle of 51 degrees. It was compacted using a

steel wheel/pneumatic tire roller behind the shafts and a walk behind tamper between the shafts and the wall. The dry density of the backfill was 110 pcf. Steel reinforcement cages were placed in the vertical CMP and high slump concrete was poured to create the shafts.

This research explored the effects of shaft length, shaft spacing behind the wall, geogrid stiffness, and group interaction. All of the shafts lengths were equal to the height of the wall (20 ft.) except for one that was 75% of the wall height. The four shafts that were equal to the wall height were spaced at 1, 2, 3, and 4 diameters behind the wall. Three additional shafts were spaced at 2 diameters and were used to explore the group interaction of shafts near the wall. The shorter shaft was also spaced at 2 diameters. The shafts were monitored using Linear Variable Differential Transformers (LVDTs), a hydraulic pressure gauge, a load cell, and an inclinometer. Earth pressure cells and strain gages were used to monitor the MSE wall along with photogrammetry and telltales to determine wall deflection. The data collected from these shafts was used to provide a comparison of the performance of the wall, reinforcement, and shafts based on the different shaft lengths. The area of influence on the wall of the loading, the displacement of the wall versus the displacement of the drilled shaft, and the load versus displacement of the shafts were all compared. It was found that as the spacing between the wall and the shaft decreased, the lateral load resistance substantially decreased and that the shorter shaft had substantially less lateral load capacity than the shaft that extended the full depth of the wall. However, the shorter drilled shaft was still able to carry substantial loads. The load-displacement curves for the shafts spaced at 1, 2, 3, and 4 diameters and the short shaft is shown below in Figure 2-11. The spacing of the shafts is given in Table 2-1.

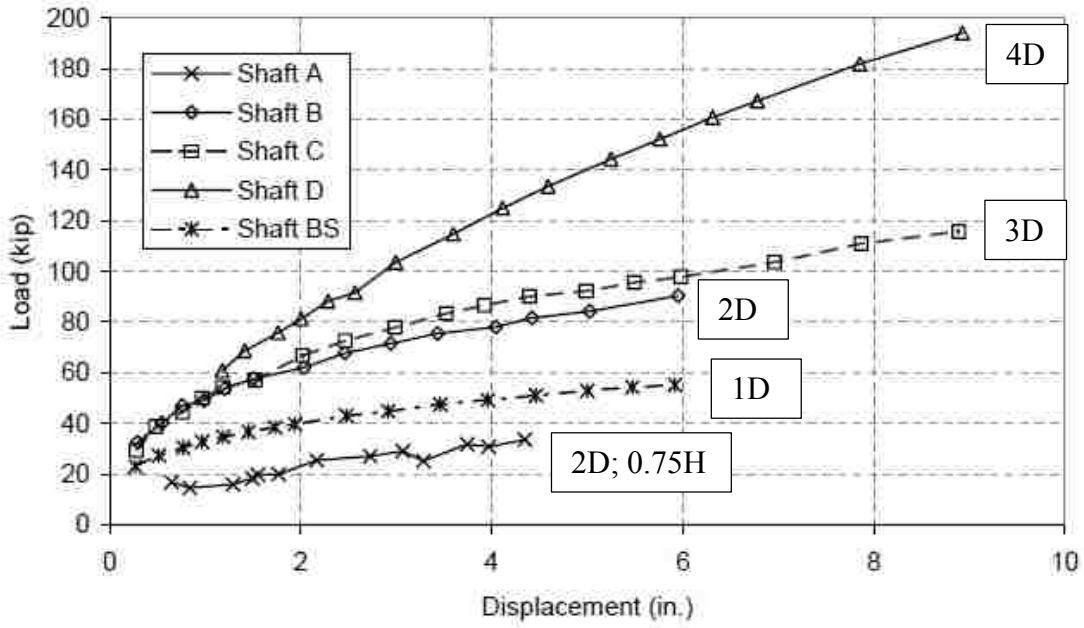

Figure 2-11: Peak load versus displacement curves for tested shafts (After Pierson et al. 2009).

Table 2-1: Shaft spacing and length

Shaft	Distance from Facing to Center of Shaft [in]	Normalized Spacing	Shaft Length [ft]
A	36	1D	20
B	72	2D	20
C	108	3D	20
D	144	4D	20
BS	72	2D	15

To gain a better understanding of the MSE system, data from this study was used to calibrate a finite difference model of the MSE wall and shafts (Huang et al. 2011). The blocks were modeled individually to be as accurate as possible. The stiffness of the geogrid was considered in the strong (perpendicular to the wall), weak (parallel to the wall), and shearing direction. The stiffness of the geogrid was calculated based on its elastic modulus and Poison's ratio and applied to the model. The stiffness was then varied to gain a better understanding of its

influence on the lateral shaft load and wall face displacement. The results indicate that the stiffness of the geogrid has the largest effects on the shaft and wall face displacement for a given pile load. Stiffer geogrids reduce the wall face displacement for a given pile load.

This test clearly demonstrates that strength decreases as spacing between the pile and wall decreases. However, the results of the study have limited application. Large drilled shafts were used so additional information on the interaction of smaller driven piles and MSE walls is not explored. Also, the wall was constructed of extensible geogrid reinforcement and blocks so additional testing is necessary to make conclusions about the pile-wall interaction of walls with inextensible reinforcement and other wall types. The friction angle of the backfill was found to be 51 degrees which is only typical of gravels and too high for many other backfill types. Additionally, p-multipliers were not back calculated in order to make the design applicable to other situations.

2.3.2 Tests with Driven Pipe Piles and Metallic Reinforcements (Rollins et al. 2013)

To investigate the relationship between the lateral resistance of driven steel pile piles near MSE walls reinforced with metallic reinforcement, multiple tests were performed on piles where MSE walls were being constructed during expansion of Interstate-15 in central Utah. Two common types of soil reinforcement were tested including welded wire grid reinforcement and ribbed steel strip reinforcement. Routine design practice typically calls for driven steel piles and metallic reinforcement.

2.3.2.1 Welded Wire Reinforcement

Price (2012) reports on full scale lateral load tests performed on five test piles that were spaced at varying distances behind MSE walls at two bridge sites. Welded wire grids were used as

the MSE wall reinforcement in both cases. Three of the piles were production piles designed to support a bridge and two of the piles were test piles located on the wing walls of the MSE wall next to a bridge abutment. All of the piles tested were closed ended steel pipe piles with 0.375 in. wall thickness. Two of the piles tested were 12.75 in. diameter and three piles were 16 in. diameter. The test piles were typically driven approximately 50 and 60 ft. below the base of the wall respectively into a dense sand bearing layer. All the piles were hollow at the time of testing but later filled with concrete. Prior to placing backfill and constructing the wall, the 16 in. test piles were wrapped with two layers of 10 mil low-density polyethylene (LDPE). This is a common practice to reduce down drag on the pile as the soil is compacted around the piles. The reinforcement was spaced vertically every 2.5 ft. and the typical horizontal spacing was 6 ft. for the production piles and 5 ft. for the test piles. The walls were constructed of 6 in. thick panels that were typically 6 ft. high by 12 ft. wide for the site where the production piles were located and 5 ft. high by 10 ft. wide at the site with the test piles. Sandy gravel fill American Association of State Highway and Transportation Officials (AASHTO) A-1-a classification was compacted behind the wall to approximately 97% of standard proctor density with 5% moisture content. A load cell and hydraulic pressure gauge were used to monitor the load on the piles as they were tested. The bending moment of the piles and the load in the soil reinforcement were monitored by strain gauges. One to three layers of soil reinforcement were instrumented depending on the test. String potentiometers were used to monitor the displacement and rotation of the pile as well as the displacement of the ground in front of the pile. Shape arrays and LVDTs were used to monitor the wall displacement. The piles were loaded based on displacement control criteria. The load-displacement curves for the three test piles are shown in Figure 2-12.

After testing, the finite difference computer program LPILE was used to perform back analyses to predict the lateral resistance of the piles which were assumed to be placed far enough back that there was no interaction with the wall. The friction angle of the soil and p-y modulus values (k) were varied until the computed and measured load displacement curves matched well. Using the piles which showed no wall interaction as a baseline, a p-multiplier was applied to reduce the soil resistance until the model predicted correct load-displacement curves for piles located closer to the wall. The results are shown in Figure 2-13. From these tests, it appears that the pile resistance may be dependent on the L/H ratio as well as on the spacing of the pile behind the wall although the data is limited.

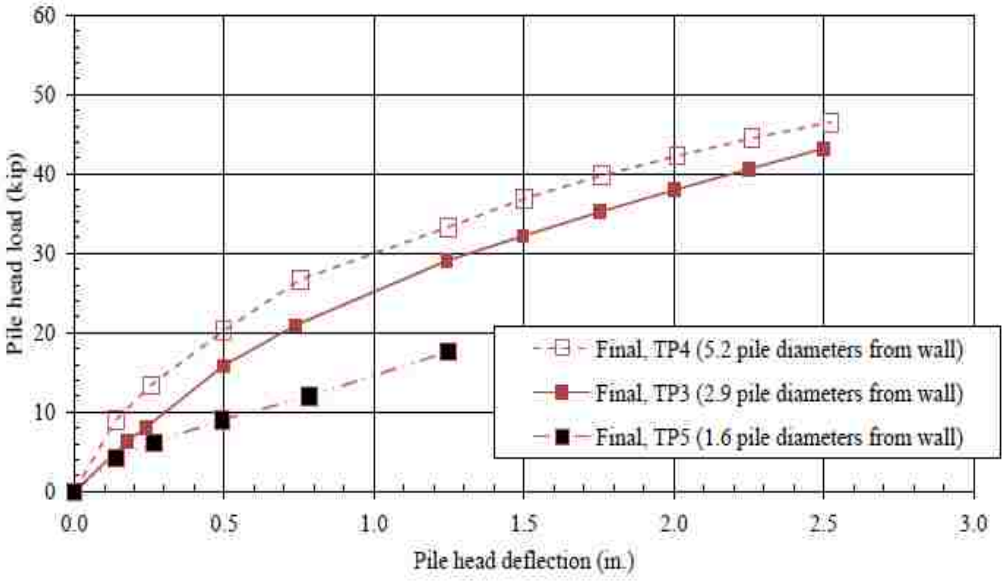

Figure 2-12: Load-deflection curves for the test piles (Price, 2012).

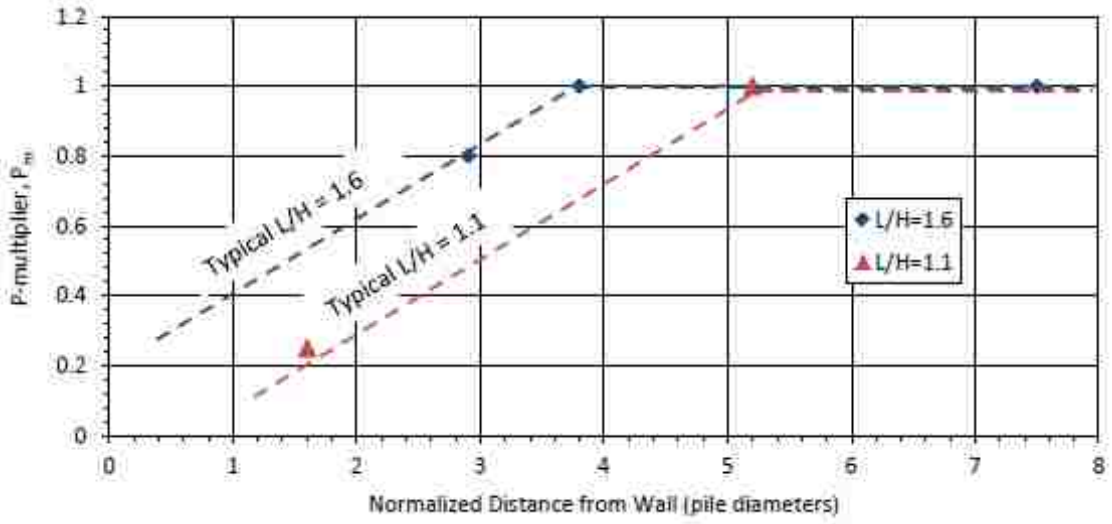

Figure 2-13: P-multipliers for piles based on pile distance from the wall and L/H ratio (Price, 2012).

Additionally, the data gathered from the soil reinforcement was used to create a proposed failure envelope for the soil reinforcement. The envelope is based on the distance from the center of the pile normalized by the spacing of the pile behind the wall and the maximum force induced in the reinforcement normalized by the load on the pile. The results are shown in Figure 2-14.

The results of these tests build upon the work done by Pierson and additionally explore inextensible steel grid reinforcement, driven steel piles, and a move towards design parameters. However, the tests also indicate that additional research is needed. The 16 in. test piles have a lower observed resistance than the 12.75 in. piles. This may be due to the LDPE wrapping but could be based on other factors. Too few piles were tested to provide a broad correlation between pile spacing and resistance to adequately develop a p-multiplier curve which can be used for design. Also, ribbed steel strip reinforcement was not investigated.

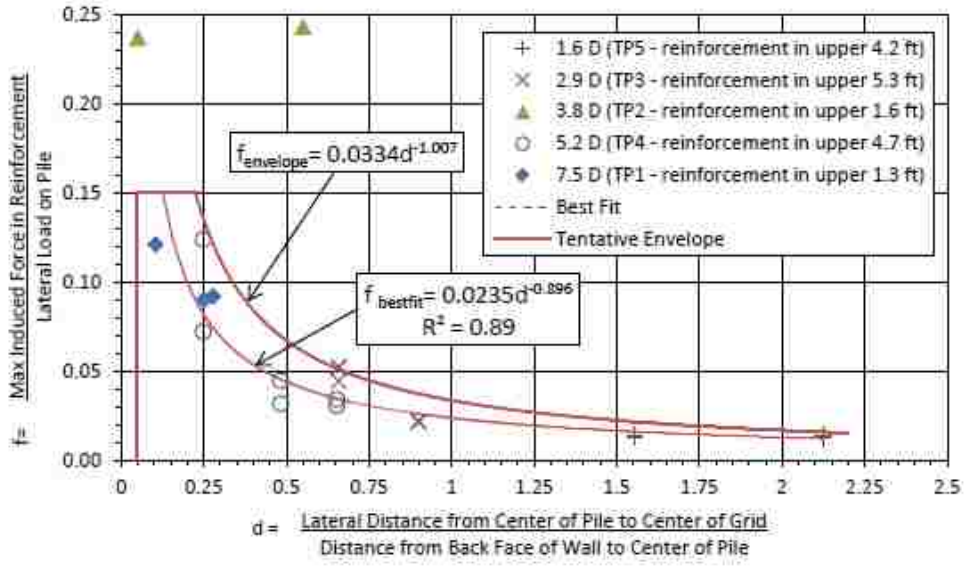

Figure 2-14: Tentative failure envelope for soil reinforcement (Price, 2012).

2.3.2.2 Ribbed Strip Reinforcement

Nelson (2013) reports on four lateral pile load tests that were performed similar to those performed by Price (2012) but with ribbed strip reinforcement. Two of the piles were production piles designed to support a bridge and two of the piles were test piles located behind a two stage MSE wall being constructed for a bridge abutment. All of the piles tested were closed ended steel pipe piles with 0.375 in. wall thickness. The production piles were driven approximately 120 ft. below the base of the wall into a sand bearing layer while the test piles extended approximately 20 ft. below the base of the wall. The spacing of the piles behind the wall varied from 1.3 to 7.7 pile diameters. All the piles were hollow at the time of testing. Galvanized ribbed steel strips were used as the MSE wall reinforcement. The reinforcement was spaced vertically every 2 ft. The length of reinforcement varied throughout the wall but was approximately 28 ft. near the test piles. The wall panels were non rigid welded wire panels covered with geo fabric and were approximately 5 ft.

high by 10 ft. wide. The wall height at the time of testing was approximately 22 ft. and the L/H ratio varied from approximately 1.0 to 1.2. Sandy gravel fill with AASHTO A-1-a classification and a standard Proctor maximum density of 132.2 pcf and optimum moisture content of 7% was compacted behind the wall to approximately 97% of standard Proctor density with 5% moisture content. A free draining backfill with reduced compaction requirements was used adjacent to the wall.

A load cell and hydraulic pressure gauge were used to monitor the load on the piles as they were tested. The bending moment of the piles and the load in the soil reinforcement were monitored by strain gauges. Two layers of soil reinforcement were instrumented. String potentiometers were used to monitor the displacement and rotation of the pile as well as the displacement of the ground in front of the pile. LVDTs were used to monitor the wall displacement. The piles were loaded based on displacement control criteria to various total displacements. The load-displacement curves for the piles are shown in Figure 2-15.

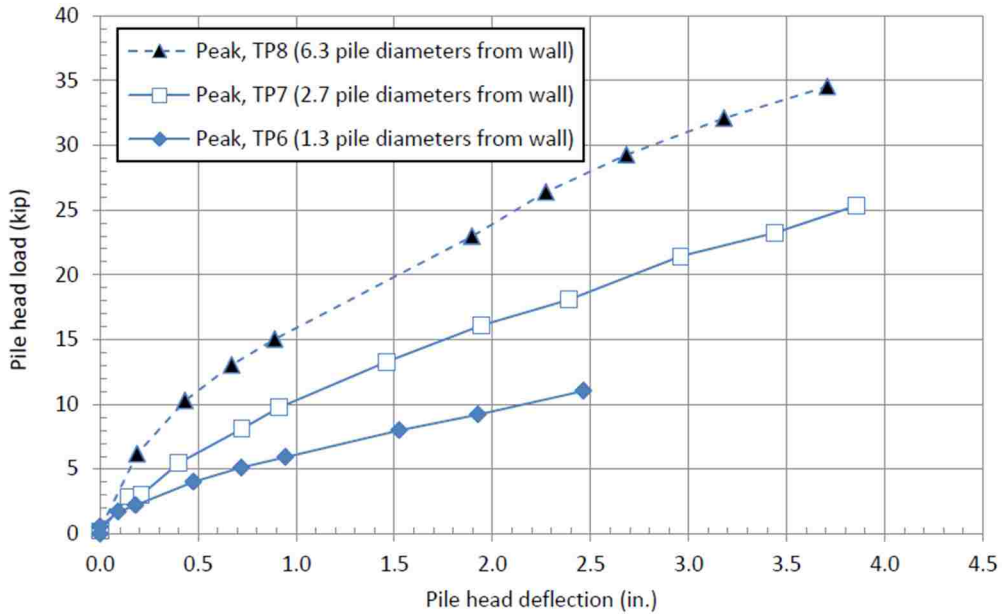

Figure 2-15: Load-displacement curves for piles tested (Nelson, 2013).

After testing, the finite difference computer program LPILE was used to perform back analyses to predict the lateral resistance of the piles which were assumed to be placed far enough back that there was no interaction with the wall. The friction angle of the soil and p-y modulus values (k) were varied until the computed and measured load displacement curves matched well. Using the piles which showed no wall interaction as a baseline, a p-multiplier was applied to reduce the soil resistance until the model predicted correct load-displacement curve for piles located closer to the wall. Additionally, the data gathered from the soil reinforcement was used to create a proposed failure envelope for ribbed steel strip soil reinforcement. As with the envelope proposed by Price, the envelope is based on the distance from the center of the pile normalized by the spacing of the pile behind the wall and the maximum force induced in the reinforcement normalized by the load on the pile.

2.3.3 Lateral Load Tests on Pipe Piles Near MSE Wall with Metallic Reinforcement (Hatch 2014, Han 2014)

As part of the current investigation, Hatch (2014) and Han (2014) report on full scale lateral load testing performed on pipe piles to further investigate the effects of pile spacing behind the wall. A full scale single stage MSE wall was constructed for the testing. Testing and analysis occurred in two different phases corresponding to different total wall elevations. Both phases of construction and testing have been completed, however the analysis of Phase 2 data is currently underway at the time of this report, and this thesis is part of the second phase of the analysis.

For the first phase of construction and testing, the MSE wall was constructed to an elevation of 15 ft. with a 2 ft. embedment depth. The wall consisted of two wall types separated by a slip joint. The west side of the wall with ribbed steel strip reinforcement was designed by Reinforced Earth Company (RECO) and the east side of the wall with welded wire grid soil reinforcement

was designed by SSL according to AASHTO 2012 LRFD. Both types of reinforcement were 18 ft. in length. Concrete panels approximately 5x10 ft. were used as the wall facing for both reinforcement types and were provided by the respective companies along with the soil reinforcement. The total wall length was approximately 180 ft., the main full height section being approximately 100 ft. with two 40 ft. wing walls at a 2:1 slope to bring the wall down to the elevation of the native material.

12.75x0.375 (A252-Grade 3) pipe piles, 12x12x313 square piles, and HP12x74 piles were driven prior to wall construction at design spacings of 2, 3, 4, and 5 diameters behind the future location of the back face of the MSE wall. Actual spacing after driving and construction varied somewhat from these target values. All piles were instrumented with strain gauges in order to determine bending moment in the pile. Two of the soil reinforcements on the top two layers were instrumented with strain gauges to further investigate the relationship between the loads induced on the reinforcement from the lateral pile load. Several reaction piles were driven behind the reinforced mass and spanned with a 3 ft. deep reaction beam in order to create a reaction for the load applied to the test piles. The soil backfill was AASHTO A-1-a classification with a standard proctor maximum density of 128 pcf and an optimum moisture content of 7.8%. The fill was compacted to approximately 95% of the standard proctor density. A 600 psf surcharge was applied above the zone of reinforcement adjacent to each test pile using concrete blocks to simulate a bridge abutment pile cap.

The piles were loaded based on displacement control criteria in 0.25 in. increments out to a total displacement of 3 in., measured at the load point. Pile load and displacement, pile strain, wall displacement, horizontal and vertical ground movement between the pile and the wall, and strain on the soil reinforcement were all monitored during testing using string potentiometers,

shape arrays, strain gauges, and digital imaging correlation. The results of the testing confirm that there is a relationship between the spacing of the pile behind the MSE wall and the lateral resistance of the pile. Figure 2-16 shows the load-displacement curves for the pipe piles on the side of the wall with grid reinforcement. Figure 2-17 shows the load-displacement curve for the pipe piles and the ribbed strip soil reinforcement.

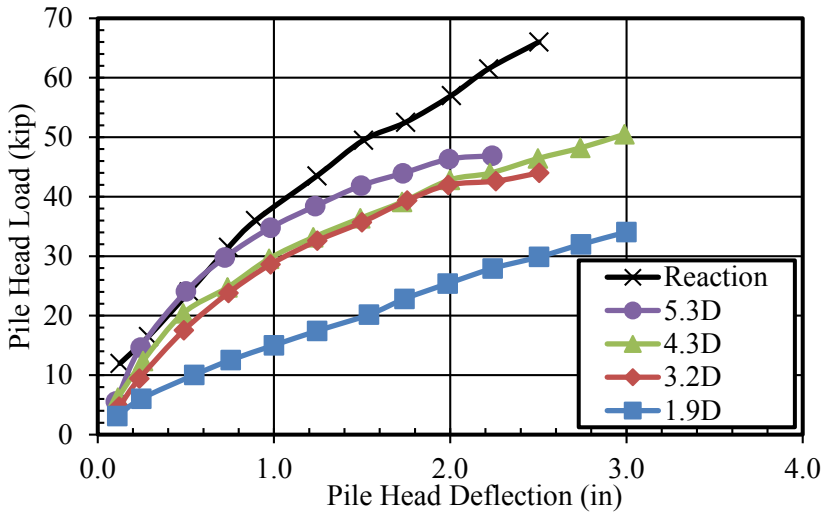

Figure 2-16: Pile head load versus deflection for peak load of grid reinforcement (Hatch, 2014).

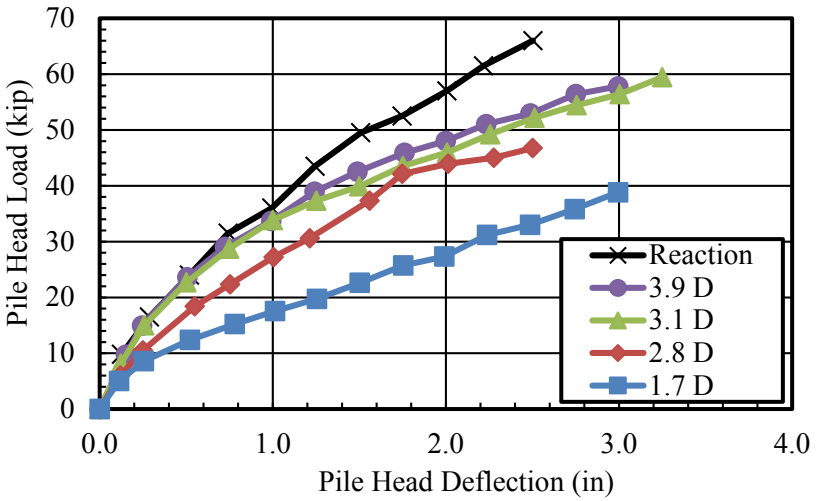

Figure 2-17: Pile head load versus deflection for peak load of ribbed steel strip reinforcement (Han, 2014).

Based on these results, an LPILE model of the piles was created. Using the pile with the maximum spacing behind the wall as a baseline, p-multipliers were determined to apply to the piles spaced closer to the wall. The results are shown in Figure 2-19. These results show the same trend established by previous testing and research performed by Price and Nelson. However, the preliminary design curve proposed by Price and Nelson had two different curves for different L/H ratios ranging from 1.1 to 1.6 as shown in Figure 2-13. The height of the surcharge was not applied to the height of the wall as it was in subsequent L/H ratio calculations so the L/H ratio of 1.6 calculated without the surcharge is closer to 1.2 when an equivalent soil surcharge is used. Therefore, a single curve with L/H ratios ranging from approximately 0.9 to 1.2 as shown in Figure 2-19 was used rather than separate curves for different L/H ratios. A new linear regression using the data from Rollins et al. (2013) without creating separate curves for different L/H ratios was calculated. Equation (2-10) gives the new linear regression equation. Additionally, the linear regression equation that includes data from Hatch, 2014 and Han, 2014 as well as data from Rollin et al. (2013) was calculated. Recalculation of the equation shows that no change to the equation occurs when data from Hatch and Han is included. Figure 2-19 shows the linear regression equation based on all previously calculated p-multipliers.

$$p_{mult} = 0.34\frac{S}{D} - 0.29 \qquad (2\text{-}10)$$

where

p_{mult} is the p-multiplier,

S is the distance from the center of the pile to the back face of the MSE wall, and

D is the pile diameter.

As was done by Price and Nelson, loads on the soil reinforcement induced by the lateral loading of the pile were also investigated using the data collected from the strain gauges on the soil reinforcement. Data from this study was added to the data gathered by Price and Nelson for the respective soil reinforcement types. A plot of the results for the grid reinforcement is shown below in Figure 2-18. As can be seen, the envelope does not fit the data well perhaps due to the applied surcharge. Similar results were found by Han (2014). It is clear that the envelope needs revision or that another approach needs to be explored to predict accurately the induced loads on the soil reinforcement.

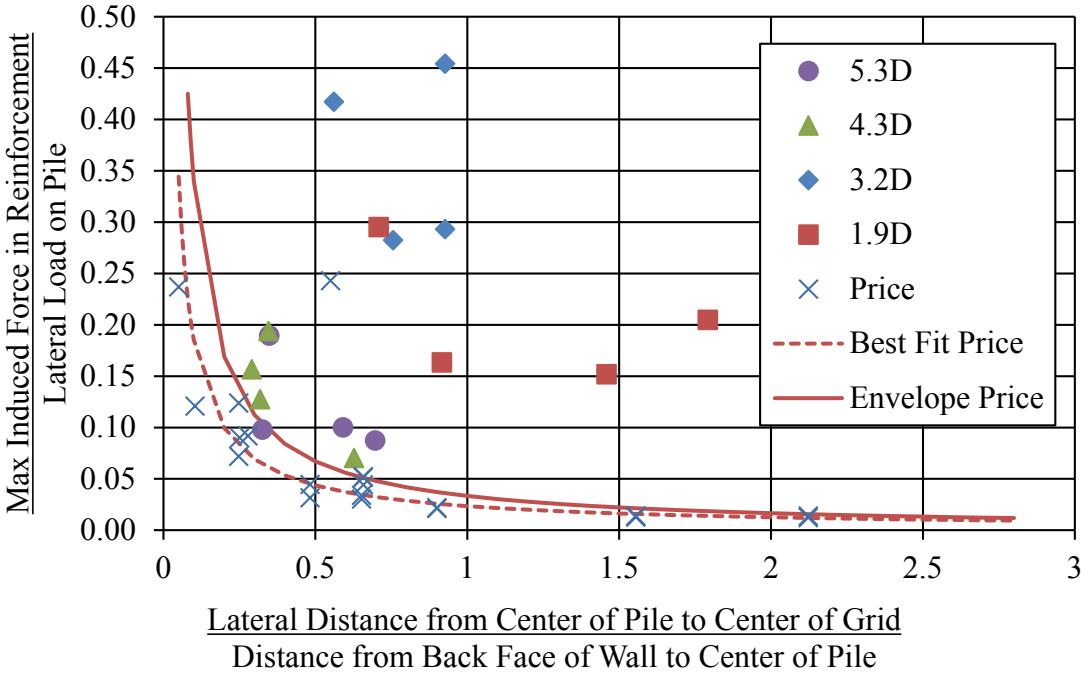

Figure 2-18: Normalized induced force in grid versus normalized distance from pile (Hatch, 2014).

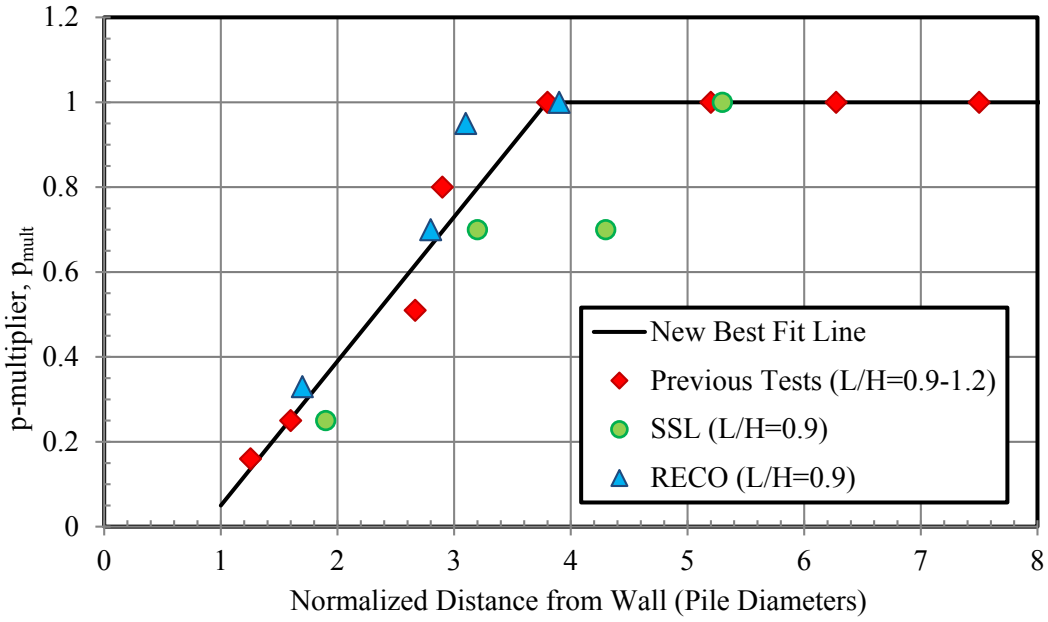

Figure 2-19: P-multipliers from previous testing and research (Rollins et al. 2013, Hatch 2014, Han 2014).

In each of these full scale tests on metallic reinforcement, only the top two layers of soil reinforcement have been instrumented with strain gauges so current data does not make it possible to determine loads induced on lower layers of reinforcement or the depth where maximum induced load on the soil reinforcement is expected to occur. Furthermore, the data gathered by Hatch, 2014 and Han, 2014 is outside of the design envelope proposed by Price and Nelson so a different approach of predicting maximum loads induced in the soil reinforcement is necessary. There seems to be additional factors that affect the induced load on the soil reinforcement other than the load on the pile and the transverse distance from the pile to the reinforcement which are the two parameters the current soil reinforcement design curve is based on. Additionally, the effect of an L/H ratio less than 0.9 on the lateral resistance of the pile has never been tested for driven piles with metallic reinforcement so the validity of the proposed p-multiplier curve needs to be checked for shorter L/H ratios.

3 TEST LAYOUT

Full scale lateral load testing was performed on piles within the reinforcement zone of an MSE wall built for this research. The wall is located near Lehi, Utah on Geneva Rock property that was formerly a gravel pit. A map showing the location of the site is shown in Figure 3-1.

Figure 3-1: Location of the research site.

3.1 MSE Wall

The MSE wall consisted of two different soil reinforcement types: ribbed steel strips and welded wire grids. The welded wire grids were supplied by SSL LLC and the ribbed metal strip reinforcements were provided by Reinforced Earth Company (RECO). The wall panels were also provided by these respective companies. To minimize interaction between the two reinforcement systems and to accommodate small differences in wall panel dimensions between the two companies, a slip joint was installed between the two wall types.

The two sides of the wall were designed by SSL and RECO respectively using AASHTO 2012 LRFD code provisions. An overview of the site is provided in Figure 3-2. Piles were driven open ended prior to wall construction and the wall was built up around the piles. Testing occurred in two different phases. For the first phase, the wall was built to the 15 ft. elevation and all piles were tested. During the second phase, the elevation of the wall was built to 20 ft. and all of the testing was repeated. The two phases allowed different L/H ratios to be investigated. During testing a surcharge load of 600 psf or about 5 ft. of soil was applied behind the piles. Accounting for the surcharge effect, the L/H ratio at the 15 ft. level was about 0.9 which is more typical in seismic design while at the 20 ft. level L/H is 0.72 which is more typical of static design.

The reinforcement length of both the ribbed strips and the wire grids was 18 ft. throughout the entire height of the wall. For each of the pipe piles tested at the 20 ft. level, the top four layers of reinforcement were instrumented. Two reinforcements on each layer at various transverse distances from the wall were instrumented with strain gauges as explained in the Instrumentation section. Hence, a total of eight reinforcements were instrumented and monitored for each test.

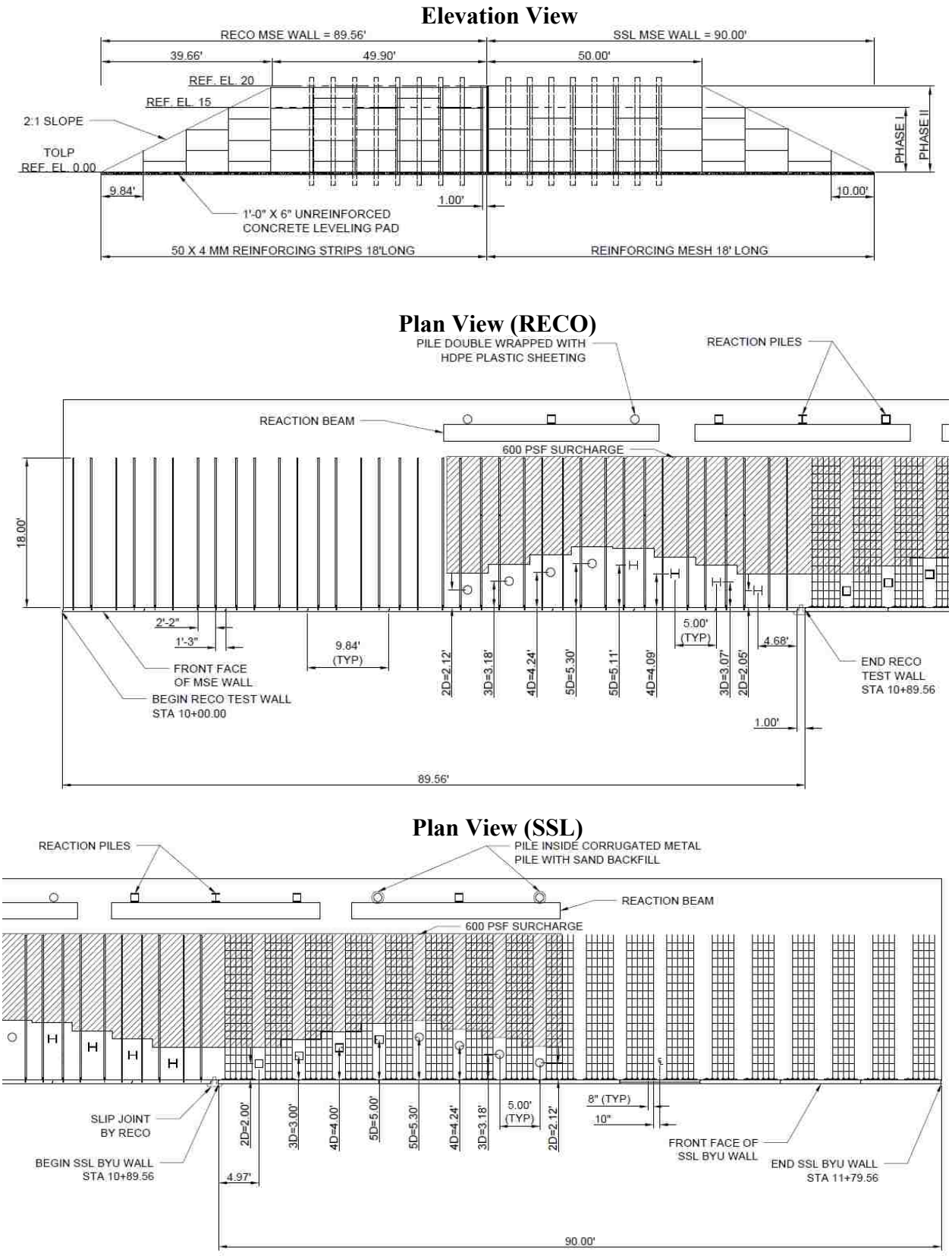

Figure 3-2: Elevation and plan view of the site.

3.1.1 Backfill

A proctor analysis of the soil used as backfill for the MSE wall was obtained at the beginning of both phases of construction. The soil gradation differed slightly between the phases. The backfill used for Phase 1 of construction (0 to 15 ft. wall elevation) classifies as AASHTO A-1-a material and silty sand with gravel (SM) using the Unified Soil Classification System (USCS). This backfill had a maximum standard proctor density of 128.0 pcf and an optimum moisture content of 7.8%. The backfill used for Phase 2 (15 to 20 ft. wall elevation) also classifies as AASHTO A-1-a material but the USCS classification is poorly graded sand with silt and gravel (SP-SM). The standard proctor maximum dry density is 126.7 pcf. The backfill was provided by Geneva Rock in both cases. The assumed backfill friction angle and moist unit weight of the soil used for design of the wall were 34 degrees and 131 pcf respectively. A plot showing the typical grain size distribution of the backfill for both phases is shown below in Figure 3-3.

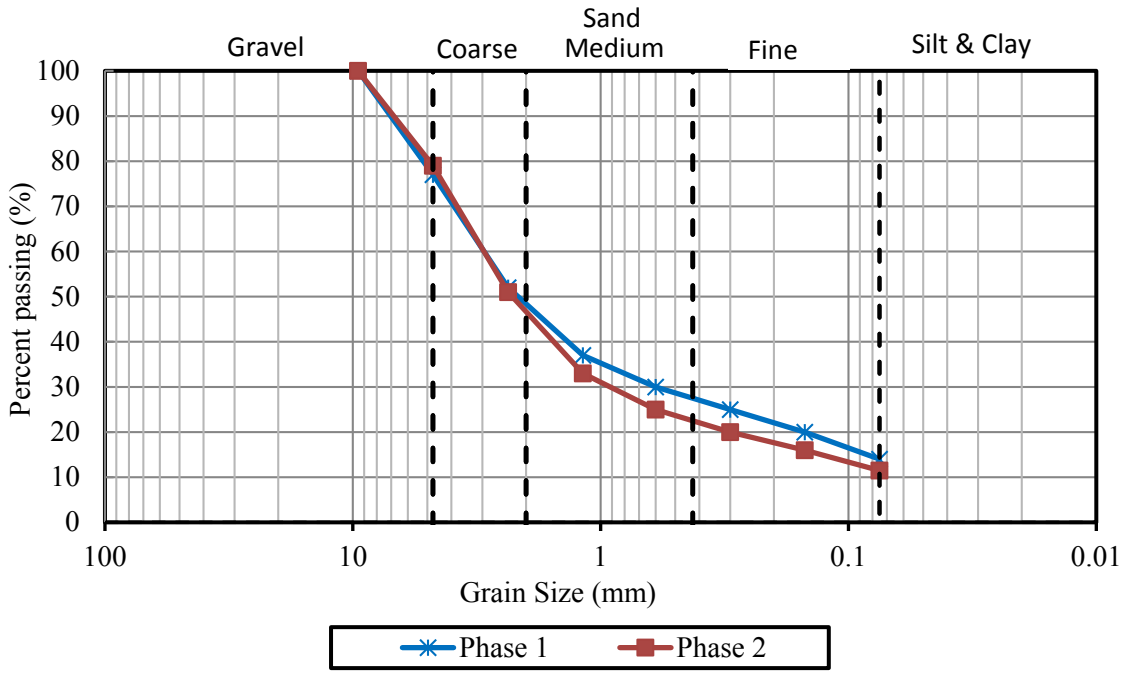

Figure 3-3: Soil gradation of the backfill for both phases of construction and testing.

The soil between the reaction piles and the test piles was compacted using a vibratory roller compactor in two lifts between each layer of reinforcement. Between the test piles and the wall, a vibratory plate compactor was used and the soil was compacted in four six inch lifts between each layer of reinforcement to account for the reduced compaction energy of the plate compactor. The target density of the backfill was 95% of the standard proctor dry density and was measured by BYU students using a nuclear density gauge as the wall was constructed by Hadco, Inc. Measured relative densities and moisture contents are shown in Figure 3-4 and Figure 3-5. Additionally, based on the measurements made from the nuclear density tests, the average, standard deviation, and coefficient of variation of the measured soil properties are shown for the soil between the test piles and the MSE wall, the soil behind the test piles, and the combined measurements in Table 3-1, Table 3-2, and Table 3-3, respectively. Although the backfill compacted by the roller compactor behind the test piles was typically 95% or above, the backfill between the test piles and wall where the vibratory plate compactor was used was generally less than 95%. In addition, there was more scatter in the relative compaction results for the soil between the test piles and the wall. Compaction is not normally specified in this area and similar conditions are likely to be encountered in a typical MSE wall construction project. This experience is confirmed by representatives from the MSE wall suppliers (J. Sankey, personal communication, 2015).

Based on the average unit weight of the backfill for the wall, the soil was compacted to approximately 90% of the Modified Proctor dry density. Correlations between relative compaction and relative density indicated that this equates to a backfill relative density of approximately 50%. (Lee & Singh, 1971).

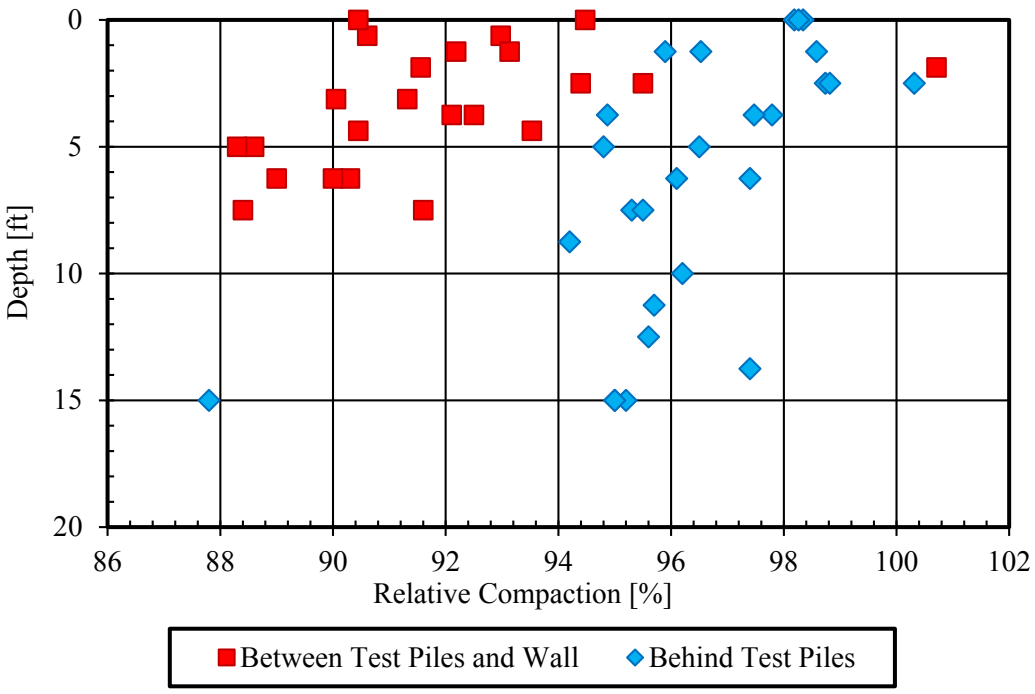

Figure 3-4: Measured relative compaction of backfill.

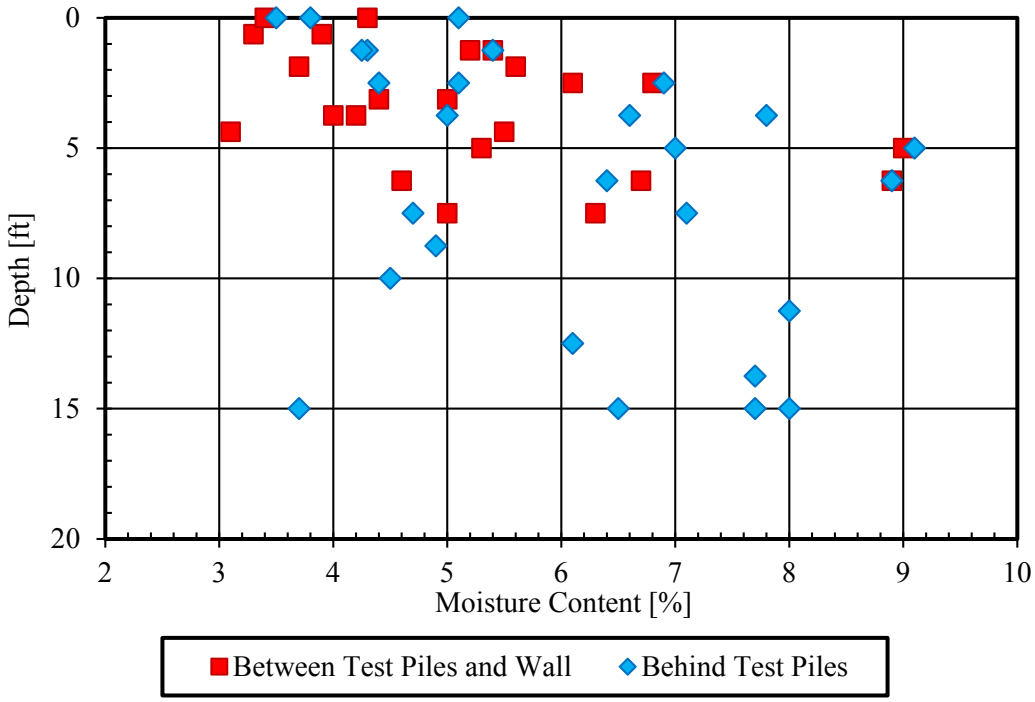

Figure 3-5: Measured moisture content of backfill.

Table 3-1: Soil properties for soil between test piles and MSE wall

	Moisture Content [%]	Dry Unit Weight [pcf]	Moist Unit Weight [pcf]	Relative Compaction [%]
Average	5.2	116.7	122.8	91.8
Standard Deviation	1.58	3.22	3.76	2.78
Coefficient of Variation	0.303	0.028	0.031	0.030

Table 3-2: Soil properties for soil behind test piles

	Moisture Content [%]	Dry Unit Weight [pcf]	Moist Unit Weight [pcf]	Relative Compaction [%]
Average	6.0	122.8	130.1	96.4
Standard Deviation	1.66	2.64	3.14	2.32
Coefficient of Variation	0.276	0.021	0.024	0.024

Table 3-3: Combined soil properties

	Moisture Content [%]	Dry Unit Weight [pcf]	Moist Unit Weight [pcf]	Relative Compaction [%]
Average	5.6	120.0	126.8	94.3
Standard Deviation	1.66	4.20	5.03	3.39
Coefficient of Variation	0.294	0.035	0.040	0.036

3.1.2 Surcharge

Using pre-cast concrete blocks, a 600 psf surcharge (≈ 5 ft. of soil fill) was applied to the zone over the reinforcement within 6 ft. of the pile being tested and extending the length of the soil reinforcement to simulate a bridge abutment pile cap. An example of the applied surcharge is shown in Figure 3-6. The surcharge blocks were moved using a fork lift between each test.

3.2 Piles

The four piles tested were 12.75x0.375 hollow steel pipe piles 40 ft. in length. The piles were donated by Atlas Tube. All piles conform to American Society for Testing and Materials (ASTM) A252-10 GR 3 specification and have a yield strength of approximately 57,000 psi. The piles were driven open ended to a depth of approximately 18 ft. prior to construction of the wall at various distances behind the future location of the back face of the MSE wall. The piles plugged with soil while driving with the plug depth ranging from 25.9 to 27.6 ft. below the elevation of the top of the MSE wall after Phase 2 of construction which corresponds to a distance of 10.4 to 12.1 ft. above the toe of the pile. Therefore, the piles can be considered as hollow at the time of testing. Pile driving was performed by Desert Deep Foundations using an ICE I-30V2 diesel hammer. Driving resistance was minimal and a record of blowcounts per ft. is found in Table F-1 in the appendix. Spacing of the piles behind the wall was normalized by the pile diameter. Design spacing was 2, 3, 4, and 5 pile diameters (D), with the distance being measured from the center of the pile to the back face of the MSE wall. Actual spacing of the piles after the wall was built to the 20 ft. level was 1.7, 2.8, 2.9, and 3.9D equivalent to a distance of 1.82, 2.95, 3.11, and 4.16 ft. Additional piles were driven behind the reinforced mass and were used to react against while load testing. Figure 3-6 shows the reaction beam and reaction piles.

Figure 3-6: An example of surcharge and reaction beam.

3.3 Loading Apparatus

Multiple piles were driven behind the reinforced soil zone and spanned with a W36x150 beam to create the reaction for the lateral load of the piles being tested. The load was applied using a 300 kip hydraulic jack. A hemispherical self-correcting load plate was used between the hydraulic jack and reaction beam to minimize eccentric loading. Steel struts were used as spacers between the jack and the reaction beam as spacing distance changed. A load cell was placed between the hydraulic jack and the pile. A steel C-channel was welded to each of the test piles to provide a flat surface for attachment of the clevis pin on the end of the load cell connection and to protect the strain gauges on the piles. Figure 3-7 shows a typical loading apparatus setup. The surcharge blocks were placed on either side of the jack as explained in section 3.1.2.

Figure 3-7: Loading apparatus setup.

4 INSTRUMENTATION

Various types of instrumentation were employed to gather data for load, displacement, bending moment, and rotation of each pile being tested. Also, the load induced on the soil reinforcement, the heave and horizontal movement of the soil in front of the pile being tested, and the displacement of the wall during lateral load testing of the piles were monitored. Details of the various instrumentation used can be found in the subsequent sections.

4.1 Load Cell and Pressure Transducers

A pressure transducer connected to the line between the hydraulic ram and the pump was the primary method used to monitor the pile load. Additionally, a load cell placed between the hydraulic ram and pile was used as a redundant measurement. Laboratory verification showed that the load from the pressure transducer was the most accurate, so only data from the pressure transducer was used for the analysis. Inaccuracies of the load cell measurements are likely due to eccentrically applied loads. The same pressure transducer and load cell were used throughout testing of all the piles. The data acquisition rate was two reading per second for both the pressure transducer and the load cell.

4.2 String Potentiometers

String potentiometers were used to monitor the horizontal pile deflection during loading at and 3 ft. above the load point. They were also used to monitor horizontal ground movement between the pile and the back face of the MSE wall and horizontal movement of the top of the MSE wall. All string potentiometers were attached to an independent reference frame so movement of the pile, soil, and wall were measured relative to the same datum. The reference frame consisted a of 4x4 in. lumber beam resting on two 2x2x6 ft. concrete surcharge blocks placed approximately 8 ft. away on either side of the pile being tested. The number of string potentiometers used for each test ranged from 4 to 6.

The string potentiometers were attached to the reference frame and positioned as needed using 2x4 in. lumber, clamps, and screws. Eyebolts magnetically attached to the pile were used for the connection of the string potentiometer lines to the pile. An eyebolt was drilled and epoxied into the top of the MSE wall and metal stakes were driven into the ground between the pile and the back face of the MSE wall at approximately 1ft. intervals as spacing allowed and attached to the string potentiometer lines. The data acquisition rate was two readings per second for all string potentiometers. String potentiometer displacements were verified using a measuring tape before each test began and were graphically monitored during testing.

The attachment of the potentiometer lines to the stakes between the pile and the back of the MSE wall was made as close to the ground as possible; however, rotation of some of the stakes between the pile and wall was observed during testing leading to some uncertainty in the accuracy of these measurements. The location of string potentiometers used for each test is shown below in Table 4-1.

Table 4-1: String potentiometer locations

Test	Load Point	3ft Above Load Point	Top of Wall	1ft	2ft	3ft	Other
1.7D	SP37	SP36	SP33				SP32-10in
2.8D	SP37	SP36	SP33	SP31			SP32-20in
2.9D	SP37	SP36	SP33	SP31	SP32		
3.9D	SP36	SP37	SP34		SP32	SP33	SP31-13in

4.3 Strain Gauges

Waterproof electrical resistance strain gauges were used to measure strain on the soil reinforcement induced from the pile loading and also strain induced in the pile from bending. The measured strains were later used to determine the force induced on the reinforcement and the pile bending moment.

4.3.1 Soil Reinforcement Strain Gauges

Two reinforcement strips in each of the top four layers of soil reinforcement were instrumented. Gauges were attached 0.5, 2, 3, 5, 8, 11, and 14 ft. from the wall connection point of the reinforcement except in the case when a gauge would land on a rib of the reinforcement. In this case, the gauge was placed as close as possible to the specified location. None of the gauges were placed more than 1 in. from the above specified distances. Gauges were attached to both the top and bottom of the reinforcement for redundancy and to cancel out bending moment effects. Strain gauge lead wires were bundled and wrapped with electrical tape for additional protection during transport and construction. The lead wires were run along the sides of the reinforcement into a Poly Vinyl Chloride (PVC) conduit placed against the back face of the wall up to the top the MSE wall. The data acquisition rate was two reading per second for all soil reinforcement strain gauges. The instrumented soil reinforcement strips are shown below in Figure 4-1.

Several of the strain gauge wire leads were damaged or cut during transport and installation. Repair of the damaged wires was attempted when possible; however, some of the strain gauges which were repaired did not function properly. Also, due to the testing sequence and location of the strips, some of them were subject to loading and unloading up to four times which seemed to cause additional failures of some of the strain gauges.

Figure 4-1: Several instrumented soil reinforcement strips.

Table 4-2: Reinforcement number and horizontal distance from pile center to reinforcement center for all instrumented soil reinforcements

	Layer Depth							
Test	**15 in**		**45 in**		**75 in**		**105 in**	
1.7D	21 - 9.5in	22-35.0in	20-11.0in	19-37.5in	1 - 9.0in	2-36.0in	10 - 9.0in	9 - 35.0in
2.8D	22-24.5in	21-50.0in	19-20.5in	20-47.0in	2-22.5in	1-49.5in	9 - 23.5in	10-50.0in
2.9D	23-10.0in	24-35.5in	18-12.0in	17-38.0in	5-11.5in	6-37.0in	13-10.5in	12-38.0in
3.9D	24-26.0in	23-51.0in	17-22.5in	18-49.0in	6-24.5in	5-50.0in	12-24.5in	13-51.5in

4.3.2 Pile Strain Gauges

Gauges were attached to each pile at a distance corresponding to 2, 4, 6, 9, 12, 15, and 18 ft. below the ground surface after compaction to the 20 ft. elevation. Gauges were attached on opposite sides of the pile for redundancy. For additional protection against damage during driving and construction, L1 1/2x1 1/2x1/8 in. angle iron was placed over the gauges and lead wires and tack welded to the pile. Care was taken to ensure that none of the welds were closer than 1 ft. to any of the gauges to avoid damage. After the angle iron was attached, it was filled with expansive foam for additional protection against water. The data acquisition rate was two reading per second for all pile strain gauges.

As with the soil reinforcement, several of the strain gauge wire leads were damaged or cut during driving and construction. Repair of the damaged wires was attempted when possible; however, some of the strain gauges which were repaired did not function properly. If multiple lead wires on the same pile were cut and it was not possible to determine the proper location through inspection of the wires, the resistance of the wires and the strain measured during testing was used to estimate the proper location. During driving, some of the piles rotated slightly so the strain gauges were not aligned with the bending axis of the pile. In this case, the rotation of the pile was measured and used to correct the strain measured by the strain gauges.

4.4 Shape Arrays

Measurand ShapeAccelArrays (Shape Arrays) were used to measure the change in deflection of the wall induced by lateral pile loading. Shape arrays consist of an array of rigid segments separated by joints with MEMS gravity sensors which measure tilt along three axes. Much like an inclinometer, the sensors allow the displacement at any point along the array to be calculated relative to the end of the array. Four shape arrays were placed in electrical conduit running vertically up the back face of the MSE wall for each test. The conduit was secured against the back face of the MSE wall with duct tape during construction. One shape array was installed approximately in front of each pile being loaded and the others were installed at various distances to one side of the pile. Table 4-3 shows the distances from the pile center to each of the arrays for all of the tests.

Table 4-3: Transverse distance of shape array to center of pile

	Array Number			
Test	**45104**	**45134**	**45115**	**45112**
1.7D	0	38	96	69
2.8D	0	38	96	69
2.9D	57.5	95.5	0	33
3.9D	0	33	59.5	92.5

4.5 Digital Image Correlation (DIC)

Digital Imaging Correlation (DIC) is an optical measurement method that uses two cameras at a specified distance apart to take images of an object simultaneously during testing. A computer algorithm can then track the location of hundreds to thousands of points on the object to calculate contours of displacement, deformation, and strain in three coordinate axes of the total value. DIC

was used to monitor the deflection of the MSE wall face. A typical setup of the cameras can be seen in Figure 4-2. Images were captured immediately after each loading of the pile and again after a five-minute relaxation period. A high contrast grid was applied to the wall aiding in the location of identical points on each image. During analysis of the images, the images were divided into small local facets as shown in Figure 4-3. The position of the cameras in relationship to one another is calculated when the system is calibrated and pixels within each facet are tracked. This information allows a correlation algorithm to be used to calculate the three dimensional position of each point from which contours of displacement, deformation, and strain of the wall can be determined.

Figure 4-2: Typical DIC setup.

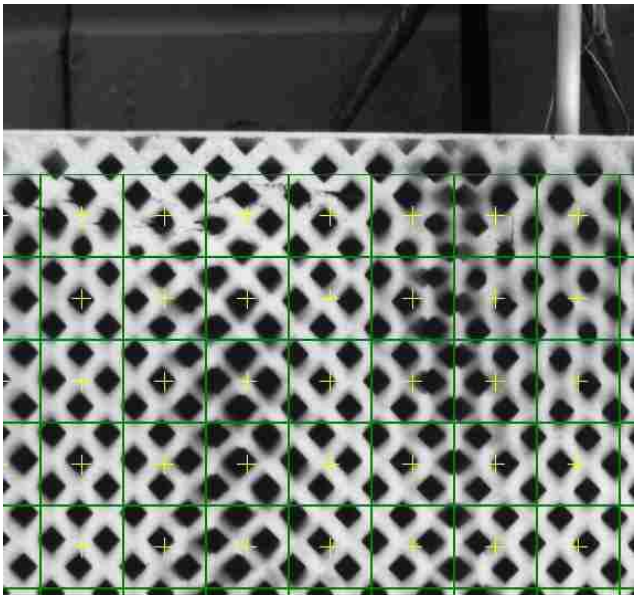

Figure 4-3: Facets used in DIC analysis.

5 LATERAL LOAD TESTING

Lateral load testing of the four piles began on August 4th, 2014 and was complete by August 6th, 2014. For an additional reference, a reaction pile located outside of the reinforced mass but still in the compacted backfill was tested on August 20th, 2014. Displacement control criteria governed the loading procedure. Lateral load was applied to the pile until the target displacement was reached. Target displacement ranged from 0.25 to 3.0 inches, with each loading increment being 0.25 inches. Each target displacement was maintained for a five-minute period between loading increments. The same test approach was used for all of the piles.

5.1 Load Displacement Curves

Pile head load versus deflection plots for the four tests and the reaction pile are shown in Figure 5-1 and Figure 5-2. The load curves are based on the hydraulic pressure gauge monitoring the pressure in the hydraulic jack line. Figure 5-1 shows the peak load applied to the pile versus pile deflection. The pressure in the pump spiked briefly after reaching the target displacement for each load cycle. The peak load at each loading increment is the average of several seconds of data after the highest load was applied. The peak load is likely to only be encountered in situations such as an earthquake but is probably not representative of static loading conditions. Figure 5-2 shows the pile head load versus deflection after a five-minute relaxation period and is more likely representative of static loading conditions caused by thermal expansion and contraction.

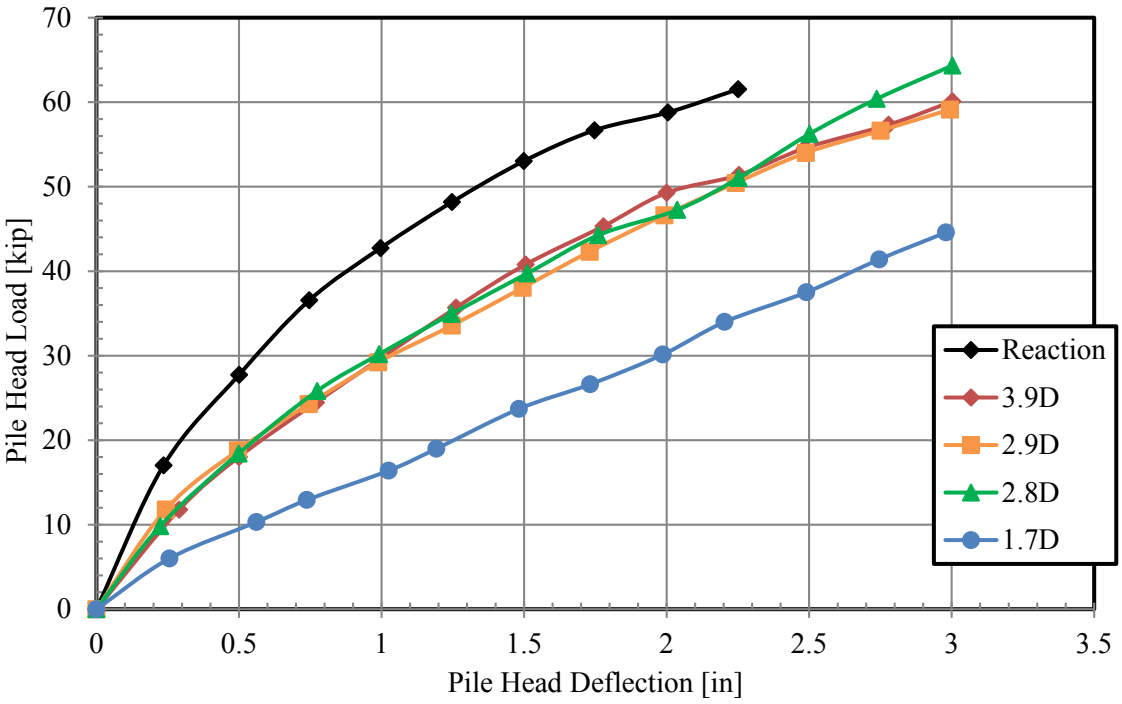

Figure 5-1: Peak pile load versus displacement.

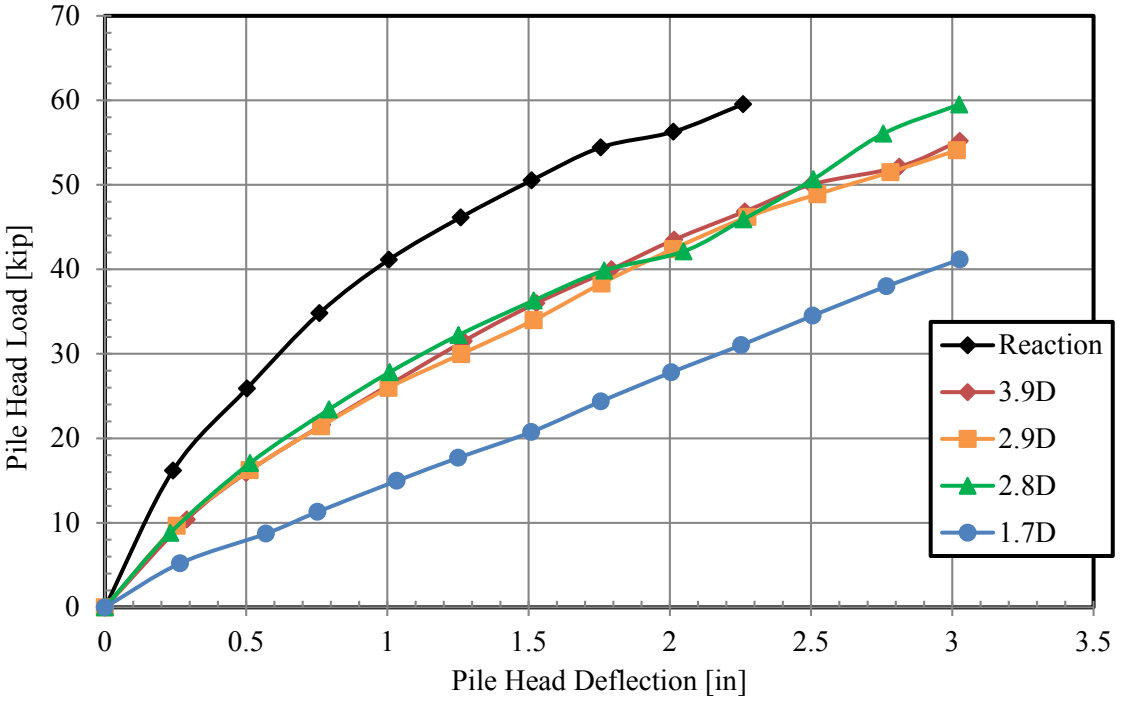

Figure 5-2: Final pile head load versus displacement.

A general comparison of the curves shows that the lateral resistance of the 3.9, 2.9 and 2.8D piles is approximately equal and the resistance of the 1.7D pile is about 70% less than these piles. The spacing of the 2.9D and 2.8D piles is approximately the same so similar load-deflection curves are not unexpected. However, the resistance of the 3.9D pile being similar to that of the 2.9 and 2.8D piles is unexpected based on previous testing and research performed by Hatch (2014), Han (2014), Price (2012), and Nelson (2013). Figure 2-19 indicates that lateral resistance of piles spaced greater than 3.8D should be approximately the same. Based on the testing, either the resistance of the 3.9D pile was lower than expected or the resistance of 2.9 and 2.8D piles was higher than expected. There are several possible explanations for this discrepancy. The night before the 2.8 and 2.9D piles were tested, a significant rainstorm occurred at the site. The USCS material classification of SP-SM indicates that there are some fines in the soil (See section 3.1.1) so perhaps the resistance of the 2.8 and 2.9D tests was increased due to cohesion that added to the strength of the soil. Both of the tests were performed on the day following the rainstorm. Furthermore, the water that infiltrated the soil would increase the unit weight of the soil and may have caused some natural compaction. Another possibility is that the panel configuration varies from test to test. As shown in Figure 3-2, there is a joint directly in front of the 1.7D and 2.9D piles while the 2.8D and 3.9D piles are located in the center of a panel. Also, the size of the panels varies at the top of the wall from tests to test. Perhaps the panel configuration of the 3.9D pile does not provide as much strength as the panel configuration in the vicinity of the 2.9 and 2.8D piles. Another possibility is that the compaction around the piles differed. Compaction between the piles and the wall was done using a vibratory plate compactor. The path of compaction generally was around the pile, next to the wall, and then in-between piles. Assuming the same number of passes of the plate compactor occurred between each pile and the wall, the soil between the wall and piles

on the 2.8 and 2.9D piles would have received more compaction effort than the soil around the 3.9D pile. Although nuclear density testing was performed throughout construction as outlined in section 3.1.1 of this report, the exact location of all tests is not known and cannot be used to verify this. We do know; however, that the compaction tests indicated substantial variation in relative compaction within the zone between the piles and wall panels in comparison with the soil behind the piles as shown in Table 3-1 and Table 3-2. This variation could account for the observed inconsistencies.

5.2 Soil Reinforcement Performance

The load in the soil reinforcement was calculated using the strain data. Strain gauges were applied to both sides of the reinforcement and the average of the values was used. In the case where one of the gauges was damaged, the strain from the working gauge was used and in cases where both were damaged, the data point was omitted. The induced load in the reinforcement was calculated using the following equation:

$$T_i = EA(\mu\varepsilon_i - \mu\varepsilon_o)(10^{-6}) \qquad (5\text{-}1)$$

where

T_i is the equivalent induced force in kips for the wire strip at the i^{th} data point,

E is the modulus of elasticity of the steel strip (29,000 ksi),

A is the cross sectional area of the steel strip (0.31 in^2),

$\mu\varepsilon_i$ is the micro strain for the i^{th} data point, and

$\mu\varepsilon_o$ is the micro strain for the initial data point just before loading the pile.

The measured tensile force represents only the force induced by the lateral load on the pile and does not account for the force induced by earth pressure during construction of the wall itself.

For depths of 45 and 75 inches, the measured load in the soil reinforcement at various distances behind the back face of the MSE wall is shown in Figure 5-3 and Figure 5-4, respectively. The load on the reinforcement is shown at several load levels. Both plots are for the 2.9D test and the transverse distance from the center of the pile to the center of the reinforcement is approximately 38 in. in both cases. As an additional reference, the nominal tensile resistance based on FHWA equations (2009) described in section 3.4.2 has been added to the plots. The tensile force in the reinforcement tends to peak approximately near the center of the pile. The tensile force increases between the wall and pile and tends to decrease between the pile and the back end of the reinforcement. Similar plots for the other reinforcements monitored during each test can be found in Appendix E.

The maximum measured induced load in the reinforcement at each pile head load for the piles at 1.7, 2.8, 2.9, and 3.9D from the wall is shown in Figure 5-5 through Figure 5-12. In these figures, Layer 1 designates the shallowest level of reinforcement while Layer 4 indicates the deepest. Separate figures are provided for strip reinforcements located at close and far distances measured transverse to the direction of loading relative to the center of the test pile. Transverse distance for each of the reinforcements relative to the pile is summarized in Table 4-2. All of the reinforcements underwent testing multiple times and occasionally a residual load was observed in the reinforcement after unlading the pile. Hence, the non-zero load at zero pile head load is due to the residual load from previous tests. In general, the following trends in the soil reinforcement have been observed. The induced tensile force on the reinforcement increases as the load on the pile increases. The load on the reinforcement increases with depth to the second or third layer, after which it again decreases. The induced load on the reinforcement decreases as the transverse distance between the pile and the reinforcement increases. At a given pile load, the induced tensile

force in the reinforcement increases as pile spacing decreases. These trends seem to be somewhat dependent on whether there is a vertical joint between the panels directly in front of the pile and also on the size of the panels at the top of the wall in front of the pile being tested.

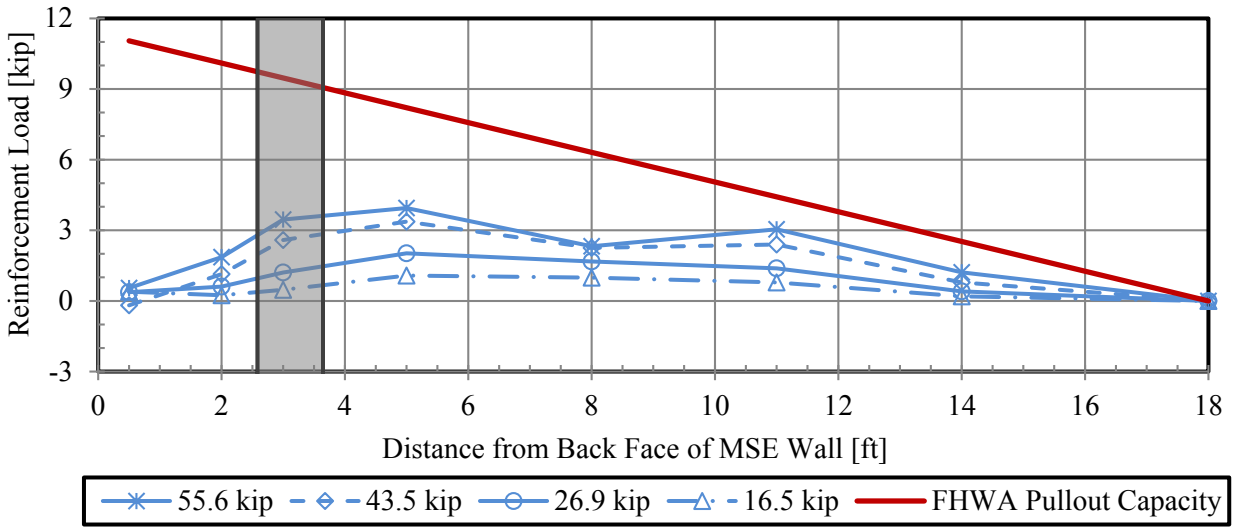

Figure 5-3: Induced loads in the second layer of soil reinforcement at various pile head loads and distances from the wall. (2.9D test, 38 in. reinforcement transverse spacing).

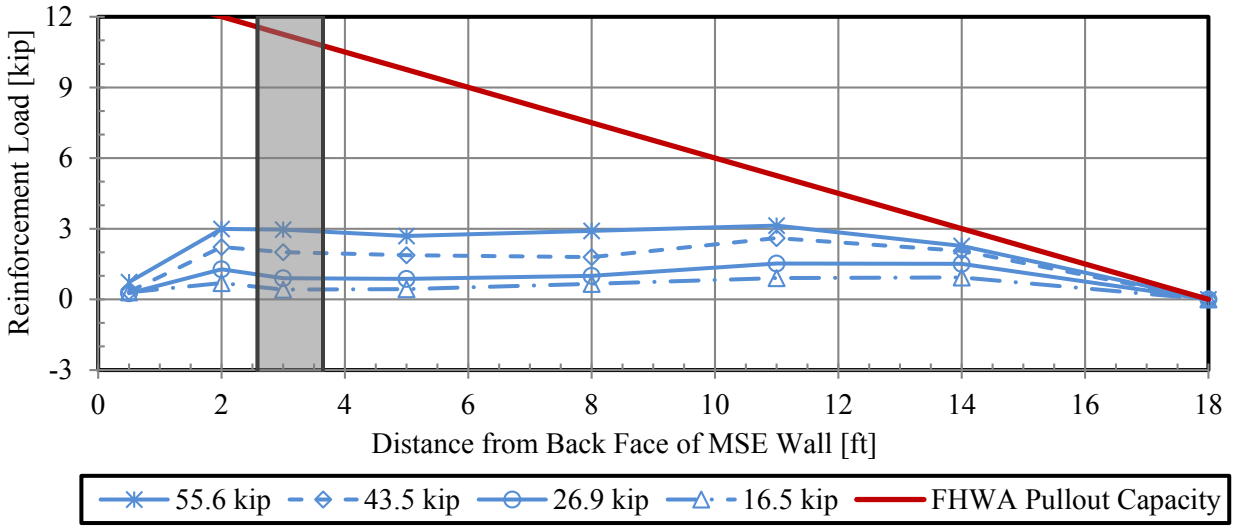

Figure 5-4: Induced loads in the third layer of soil reinforcement at various pile head loads and distances from the wall. (2.9D test, 37 in. reinforcement transverse spacing).

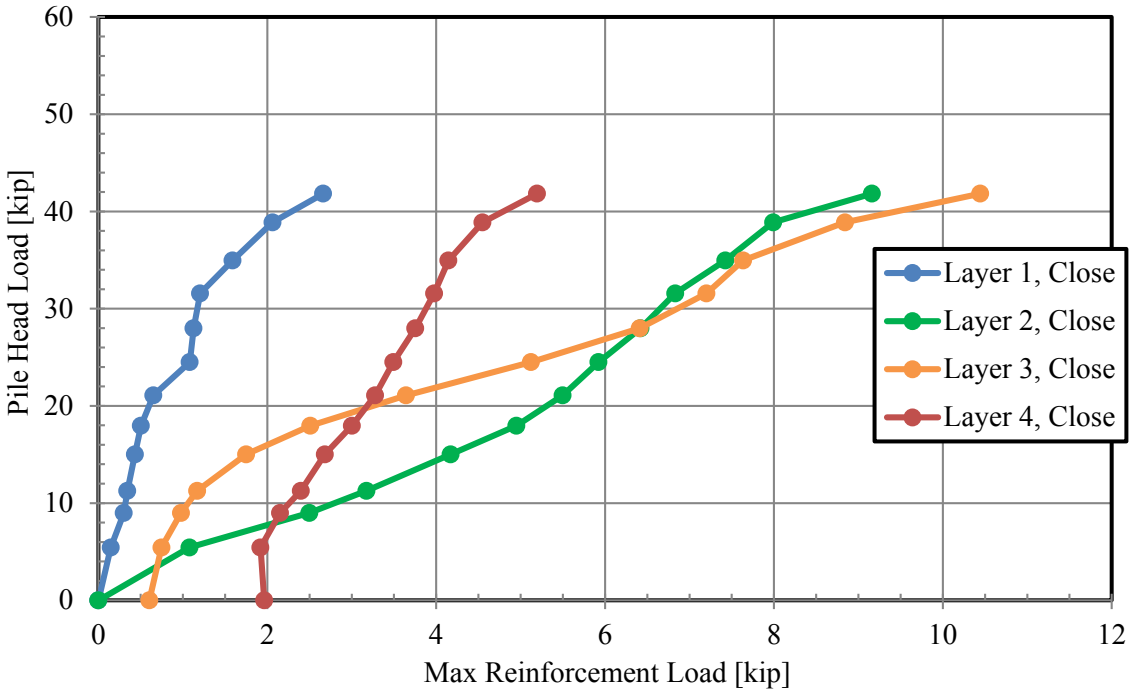

Figure 5-5: Max tensile force in close soil reinforcement at each pile head load for 1.7D test.

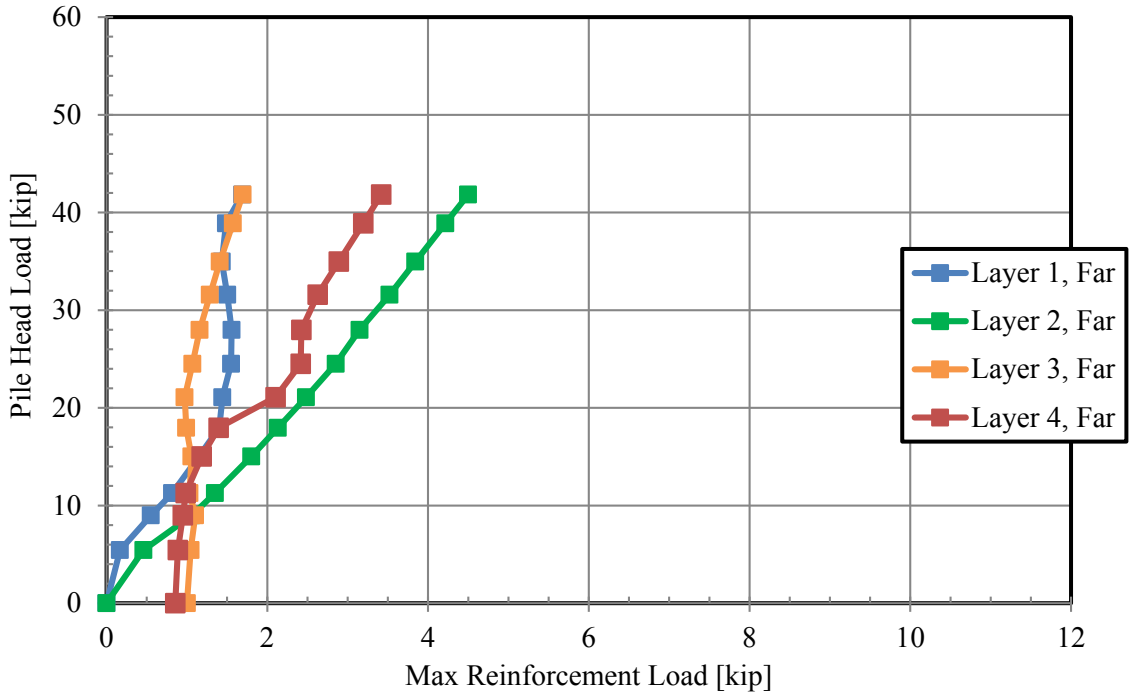

Figure 5-6: Max tensile force in far soil reinforcement at each pile head load for 1.7D test.

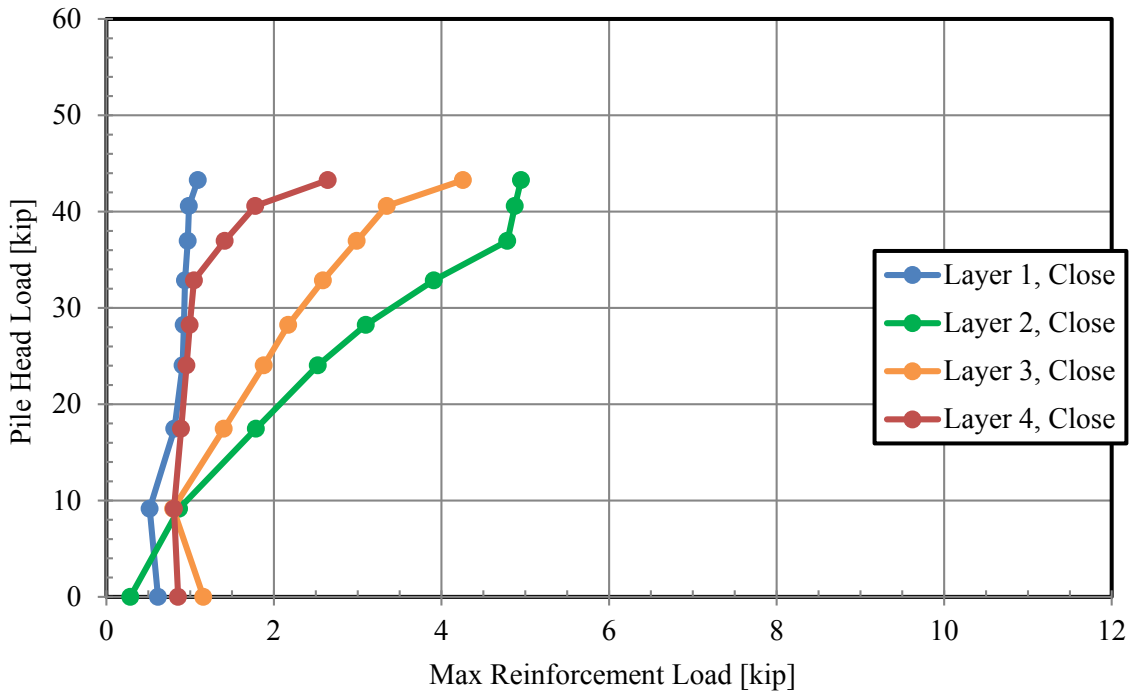

Figure 5-7: Max tensile force in close soil reinforcement at each pile head load for 2.8D test.

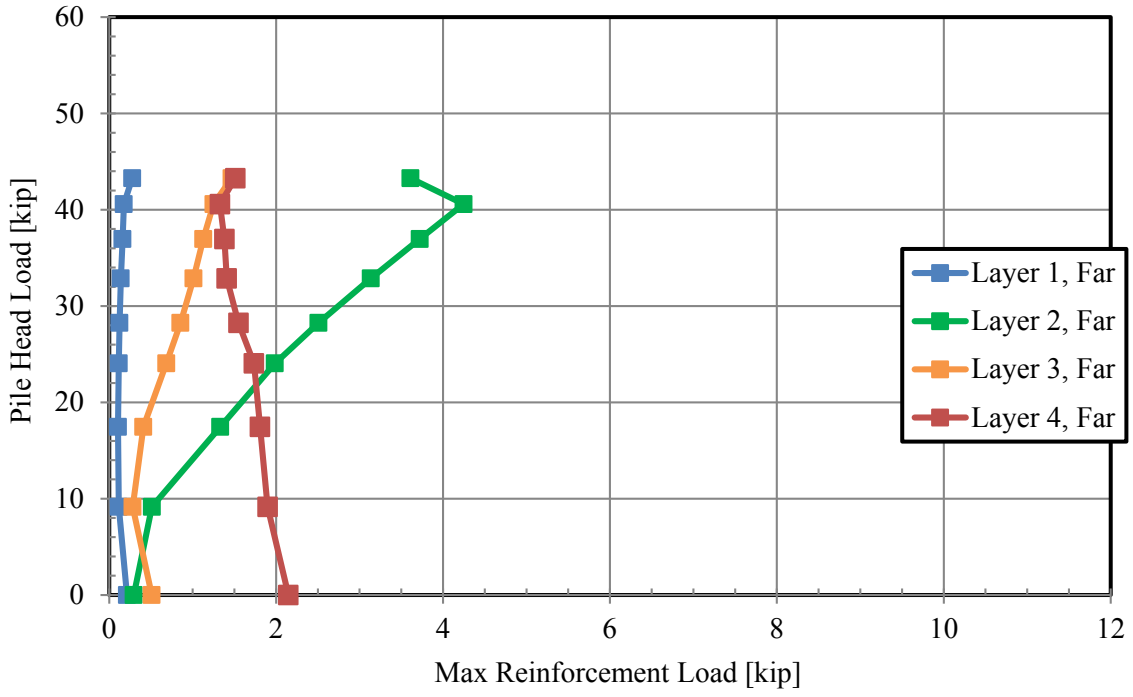

Figure 5-8: Max tensile force in far soil reinforcement at each pile head load for 2.8D test.

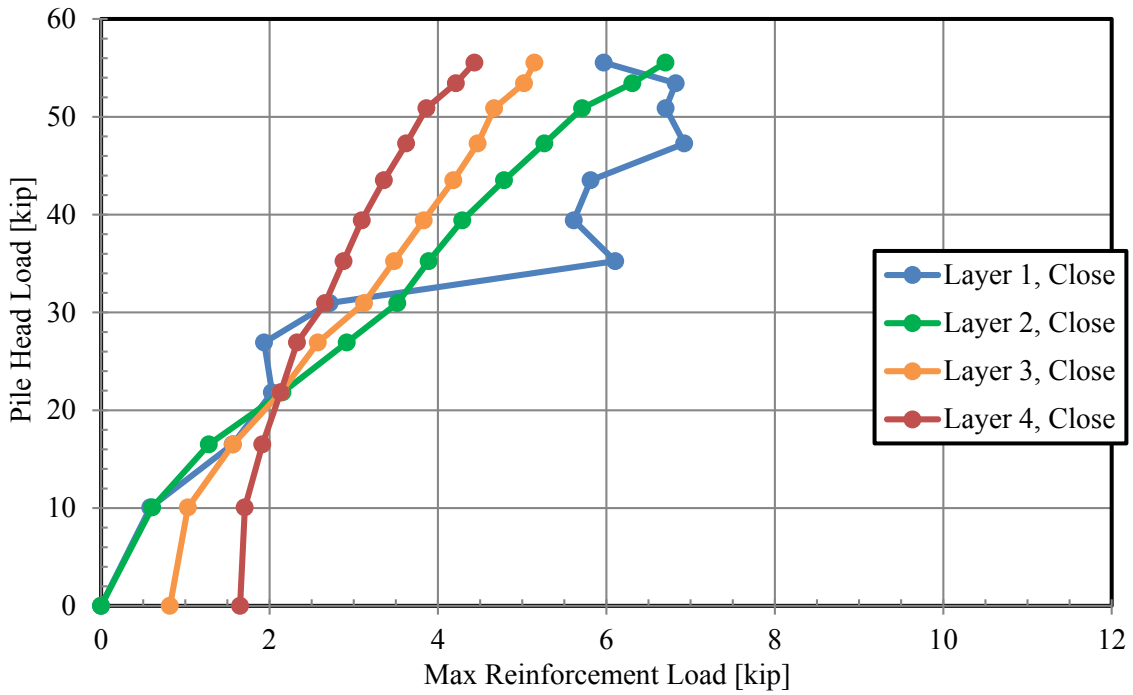

Figure 5-9: Max tensile force in close soil reinforcement at each pile head load for 2.9D test.

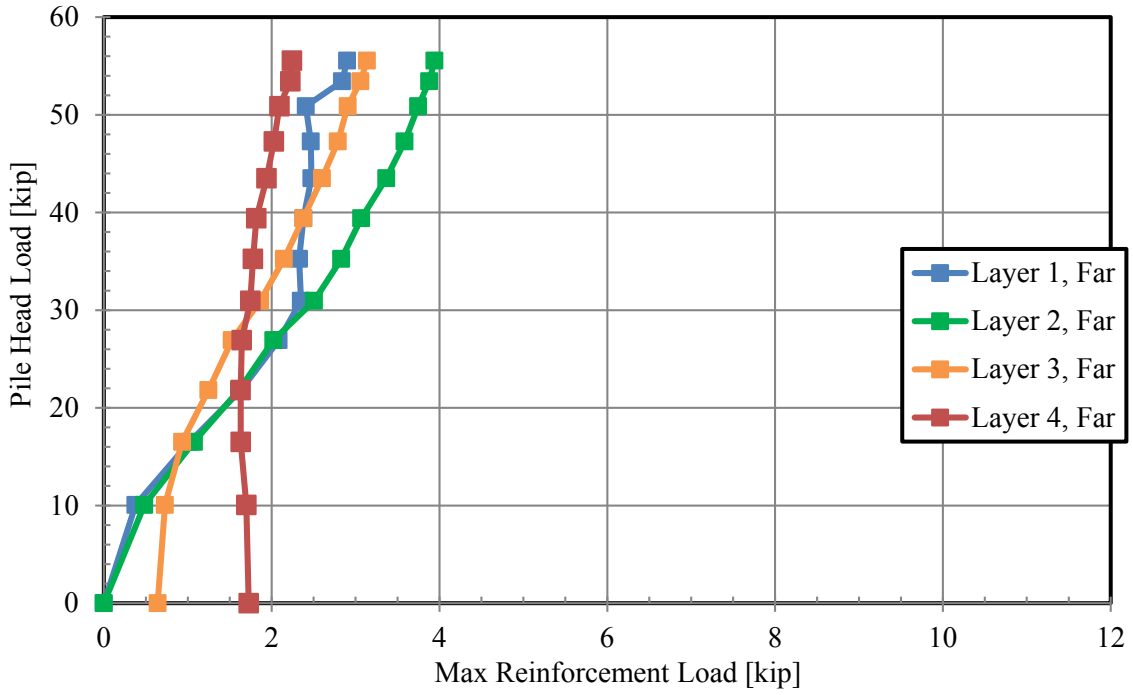

Figure 5-10: Max tensile force in far soil reinforcement at each pile head load for 2.9D test.

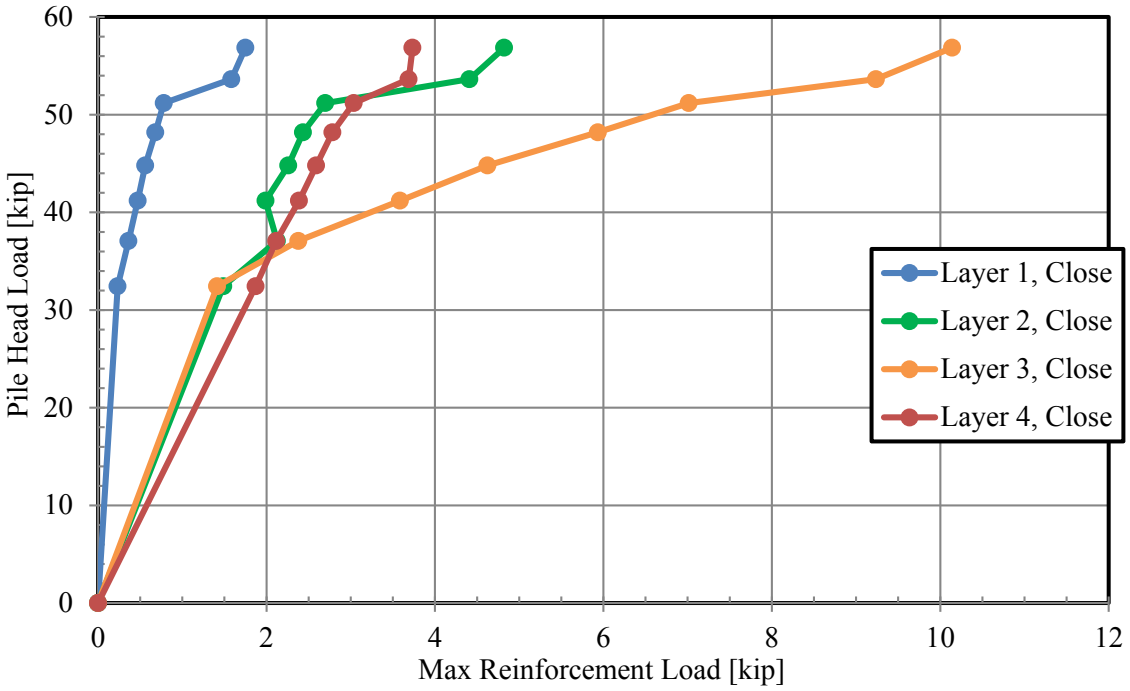

Figure 5-11: Max tensile force in close soil reinforcement at each pile head load for 3.9D test.

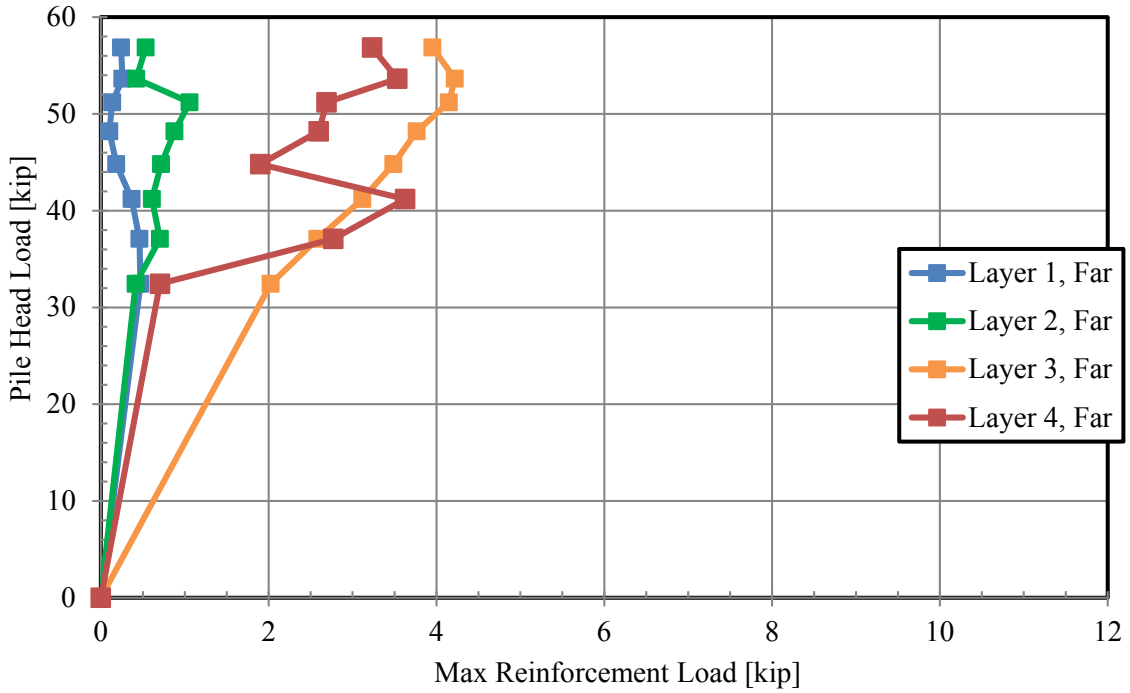

Figure 5-12: Max tensile force in far soil reinforcement at each pile head load for 3.9D test.

Figure 5-13 shows an idealized model of what is likely occurring in the reinforcement. The measured force distribution in the reinforcement suggests that soil in front of the pile is being pushed forward as the pile is loaded and the soil behind the pile is acting as an anchor for the reinforcement. Behind the pile, the strip is moving toward the wall relative to the soil. This leads to decrease tension in the strip behind the pile as load is transferred to the surrounding soil by skin friction. In front of the pile, forward movement of the soil relative to reinforcement increases the force in the reinforcement. Positive tensile force in the reinforcement at the wall face is likely a result of the increased earth pressure on the wall from the pile loading. Occasionally negative values were observed indicating that the reinforcement is in compression rather than tension. This is likely the result of bending in the reinforcement caused by uneven movement of the soil.

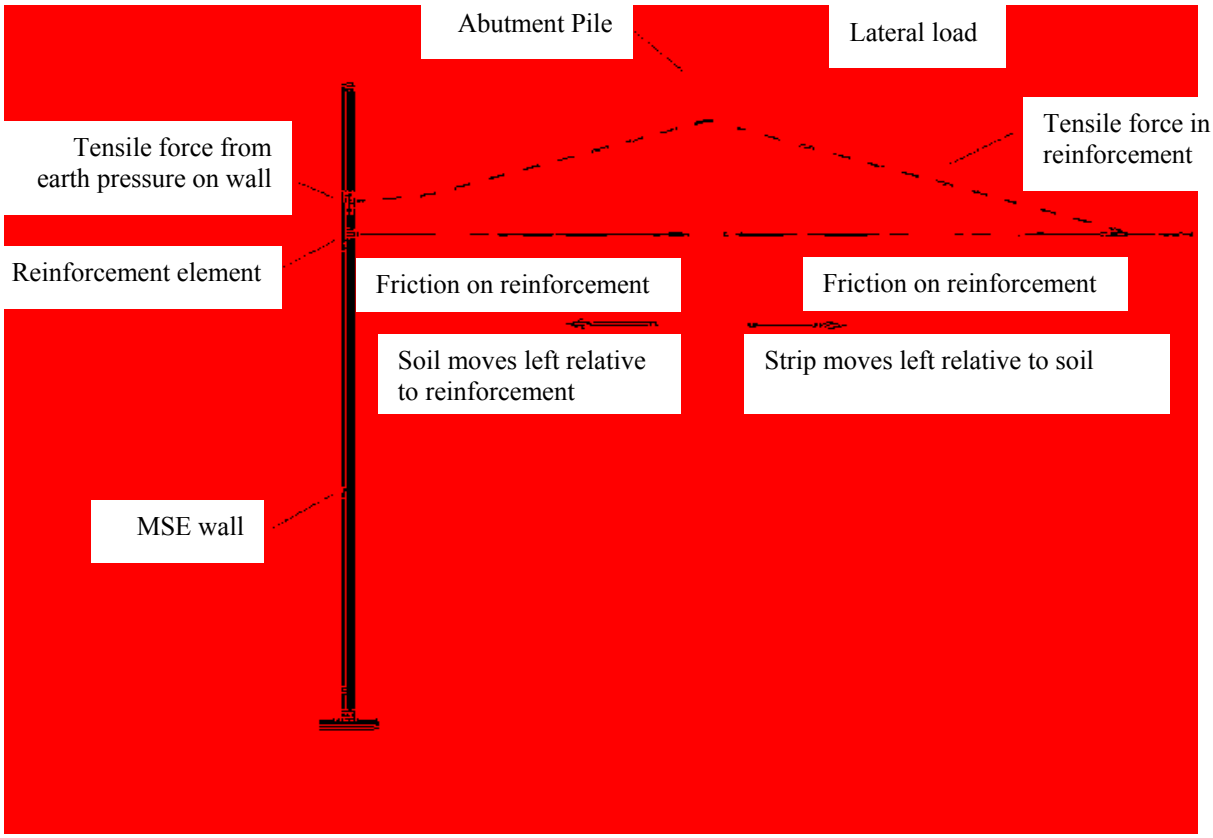

Figure 5-13: Interaction of soil and MSE wall reinforcement when pile is laterally loaded.

5.3 Statistical Analysis of Load in the Reinforcement

Due to the difficulty of predicting loads induced on the soil reinforcement by lateral pile loading through simple observations and calculations, a statistical analysis of the data was performed under the direction of Dr. Dennis Eggett of the Statistics Department at BYU. Data from this study, including data from Phase 1 of testing, and also data from Nelson (2013) were used to create two different multiple regression models to predict the induced force in the soil reinforcement. One model uses depth below ground surface (excluding equivalent depth of surcharge) as a variable while the other uses vertical stress (calculated by adding the surcharge to the vertical stress from the soil).

5.3.1 Model with Depth as a Variable

Using an F-test, the following variables and their two-way interactions were tested to determine if they were statistically significant: the displacement of the wall at the location where the reinforcement attaches to the wall, the transverse distance of the reinforcement to the center of the pile, the depth of the reinforcement below the ground surface, whether the reinforcement was attached near the center or edge of a panel, the pile head load, the pile head displacement, whether the pile being loaded was near a joint or the center of a panel, the normalized pile spacing (distance of the pile behind the wall), the size of the panel the reinforcement is connected to, the type of panel the reinforcement is connected to, the applied surcharge, and the L/H ratio of the wall at the time of testing. Of these parameters, the transverse distance of the reinforcement to the center of the pile being loaded, the pile head load, the normalized pile spacing, and the depth of reinforcement or the interactions of these variables were all statistically significant.

Because the tensile force data was not normally distributed, a base 10 log transformation of the data was applied before running the model. The results of the multiple regression analysis

are summarized in Table 5-1. It is important to note that these values are based on the log transformation of the data.

Table 5-1: Multiple regression model results for model with depth as a variable

Parameter	Coefficient Estimate	Standard Error	t Value	Pr>|t|
Intercept	0.100110702	0.046731	2.14	0.0325
Transverse spacing, T	-0.004212281	0.000810	-5.20	<.0001
Depth, Z	0.007480573	0.000971	7.70	<.0001
Pile load, P	0.025486498	0.001532	16.64	<.0001
Normalized spacing, S/D	-0.051315548	0.023390	-2.19	0.0286
T*Z	0.000047877	0.000013	3.79	0.0002
T*P	-0.000148592	0.000023	-6.57	<.0001
Z^2	-0.000053610	0.000006	-8.51	<.0001
Z*(S/D)	-0.000709904	0.000203	-3.50	0.0005
P^2	-0.000171253	0.000023	-7.49	<.0001
$(S/D)^2$	0.006191141	0.002480	2.50	0.0128

A plot of the predicted tensile force versus measured tensile force in the reinforcement is provided in Figure 5-14. The black dashed lines in Figure 5-14 show an error of 2 (i.e. the measured value is double the predicted value and the measured value is half of the predicted value). The R^2 value of the model is 0.71, indicating that about 71% of the variation in the reinforcement tensile force is accounted for by the equation. The standard error is 0.137 (1.103 with log transformation removed) and the model has 10 degrees of freedom. A plot of the residuals for each of the four main variables used in the equation is provided in Figure 5-15. The residuals for each of the variables seem to be scattered evenly around 0 and do not indicate any serious violation of the model assumptions.

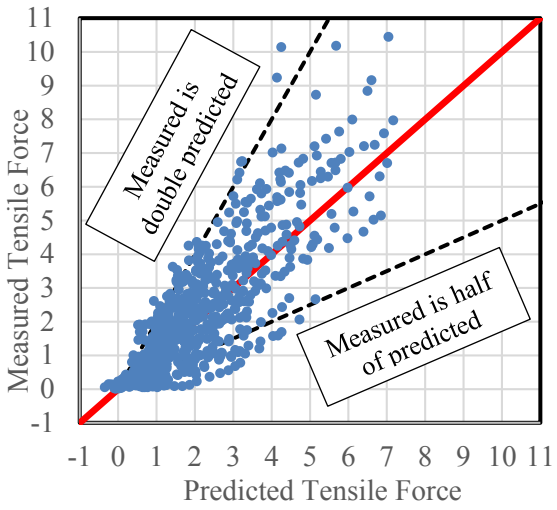

Figure 5-14: Predicted versus measured tensile force for model with depth as a variable.

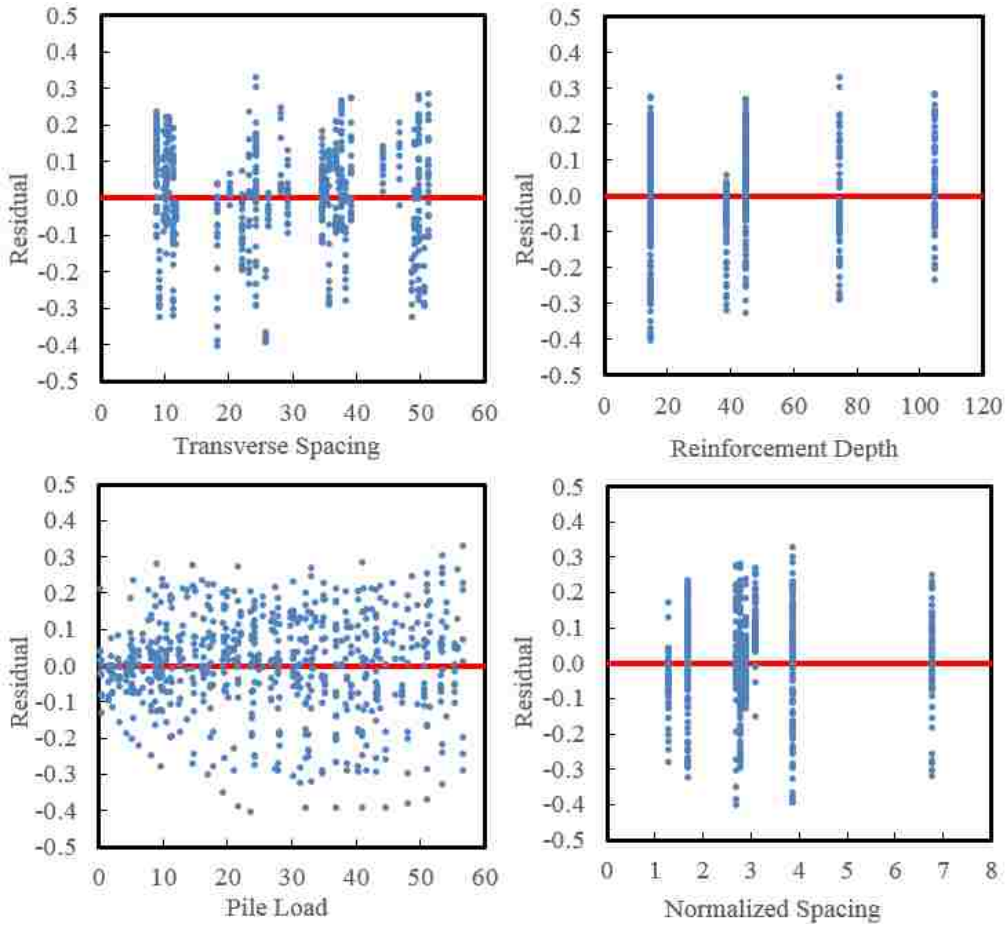

Figure 5-15: Residuals for the variables used in the multiple regression model with depth as a variable.

Applying the coefficients found in Table 5-1, the tensile force in the reinforcement can be predicted using the equation

$$F=10\text{^}(0.1001-0.004212T+0.007481Z+0.02549P-0.05132\frac{S}{D}$$
$$+4.787x10^{-5}TZ-1.486x10^{-4}TP-5.361x10^{-5}Z^2-7.099x10^{-4}Z\frac{S}{D} \quad (5\text{-}2)$$
$$-1.713x10^{-4}P^2+0.006191\left(\frac{S}{D}\right)^2)-1$$

where

F is the tensile force in the reinforcement in kips,

T is the transverse spacing of the reinforcement from the center of the pile in inches,

Z is the depth of the reinforcement below the ground surface in inches,

P is the pile head load in kips, and

S/D is the normalized pile spacing with S being the distance from the center of the pile to the back face of the MSE wall and D being the pile diameter.

5.3.2 Model with Vertical Stress as a Variable

An alternative model that uses the vertical stress on the reinforcement rather than the pile depth was also explored. To calculate the vertical stress, the depth of the reinforcement and the surcharge were combined. The vertical stress includes the full surcharge applied above the reinforcement plus the vertical stress due to the soil above the reinforcement. As with the previous model, the significance of each of the variables and their two way interactions was explored. The transverse distance of the reinforcement to the center of the pile being loaded, the pile head load, the normalized pile spacing, and the vertical stress on the reinforcement were all statistically significant when the interactions were considered.

As with the other model, a base 10 log transformation of the data was applied before running the model. The results of the multiple regression analysis that uses vertical stress rather than depth are summarized in Table 5-2. These values are based on the log transformation of the data. A plot of the predicted tensile force versus measured tensile force in the reinforcement is provided in Figure 5-16. The black dashed lines in Figure 5-16 show an error of 2 (i.e. the measured value is double the predicted value and the measured value is half of the predicted value). The R^2 value of the model is 0.69, indicating that about 69% of the variation in the reinforcement tensile force is accounted for by the equation. The standard error is 0.142 (1.163 with log transformation removed) and the model has 12 degrees of freedom. A plot of the residuals for each of the four main variables used in the equation is provided in Figure 5-17. The residuals for each of the variables seem to be scattered evenly around 0 and do not indicate any serious violation of the model assumptions.

Table 5-2: Multiple regression model results for model with vertical stress as a variable

Parameter	Coefficient Estimate	Standard Error	t Value	Pr>|t|
Intercept	0.024991781	0.070966	0.35	0.7248
Transverse spacing, T	-0.006041202	0.001903	-3.18	0.0016
Vertical stress, σ_v	0.000455909	0.000093	4.90	<.0001
Pile load, P	0.022340729	0.001857	12.03	<.0001
Normalized spacing, S/D	-0.006345214	0.024277	-0.26	0.7939
σ_v^2	-0.000000194	0.000000	-5.19	<.0001
T^2	-0.000060257	0.000031	-1.93	0.0542
P^2	-0.000184272	0.000024	-7.62	<.0001
$T*\sigma_v$	0.000003934	0.000001	3.48	0.0005
T*P	-0.000155229	0.000024	-6.55	<.0001
T*(S/D)	0.001073979	0.000329	3.27	0.0011
σ_v*P	0.000003167	0.000001	2.52	0.0118
σ_v*(S/D)	-0.000056329	0.000021	-2.71	0.0069

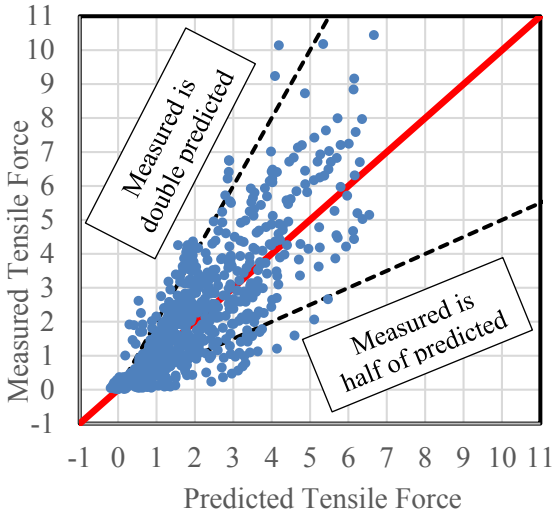

Figure 5-16: Predicted versus measured tensile force for model with vertical stress as a variable.

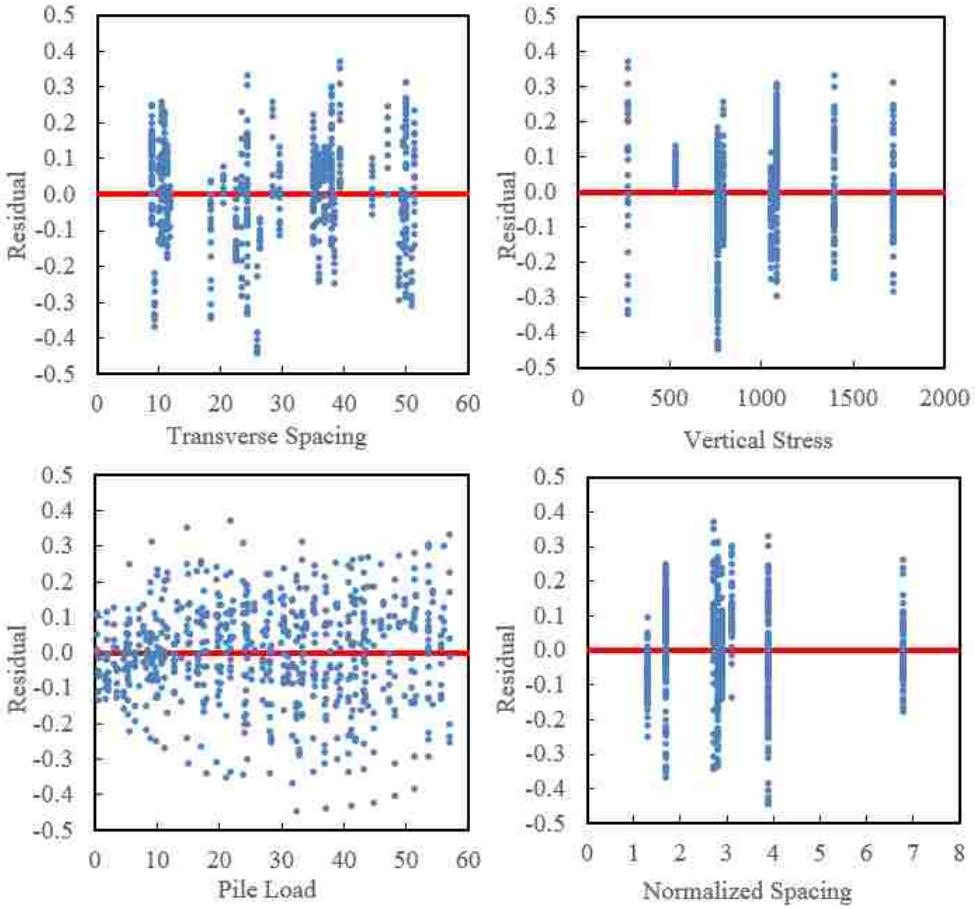

Figure 5-17: Residuals for the variables used in the multiple regression model with vertical stress as a variable.

Applying the coefficients found in Table 5-2, the tensile force in the reinforcement can be predicted using the equation

$$F=10\text{^}(0.02499-0.006041T+4.559x10^{-4}\sigma_v+0.02234P-0.006345\frac{S}{D} \\ -1.942x10^{-7}{\sigma_v}^2-6.026x10^{-5}T^2-1.843x10^{-4}P^2-3.934x10^{-6}T\sigma_v \\ -1.552x10^{-4}TP+0.001074T\frac{S}{D}+3.167x10^{-6}P\sigma_v-5.633x10^{-5}\sigma_v\frac{S}{D})-1 \quad (5\text{-}3)$$

where

F is the tensile force in the reinforcement in kips,

T is the transverse spacing of the reinforcement from the center of the pile in inches,

σ_v is the vertical stress on the reinforcement in psf,

P is the pile head load in kips, and

S/D is the normalized pile spacing with S being the distance from the center of the pile to the back face of the MSE wall and D being the pile diameter.

5.3.3 Model Parameter Range and Use

The range of values used for each variable in both regression models are presented in Table 5-3. Use of either regression model with values that are outside of the range of the variables presented in Table 5-3 is considered extrapolation and may cause the model results to be invalid. It is important to note that the effect of pile diameter was not able to be explored in the analysis because 12.75 in. diameter pipe piles were used exclusively in all of the tests performed. It is likely that the diameter of the pile could affect the transverse spacing and the load part of the equation. More testing to determine the effect of pile diameter will likely be needed in the future.

Table 5-3: Range of values for each variable applied in the multiple regression models

Parameter	Range
Transverse spacing, T	9 in. - 73 in.
Depth, Z	15 in. - 105 in.
Pile load, P	0.4 kip - 56.9 kip
Normalized spacing, S/D	1 - 6.8
Vertical stress, σ_v	272 psf - 1720 psf

5.4 Ground Displacement

The lateral load applied to the pile caused displacement of the ground surface between the pile and the MSE wall. The horizontal movement of the ground surface was monitored throughout testing using string potentiometers attached to steel stakes pounded into the ground between the pile and the wall. Vertical ground displacement was also measured using an optical surveying level and rod. Vertical ground displacement was measured at 3.0 in. pile head deflection but was not measured throughout the test for safety reasons.

Figure 5-18 shows the measured vertical ground displacement at 3.0 in. pile head deflection for all of the tests. In general, the heave at the wall tends to increase as the pile is loaded closer to the wall. In addition, the general trend is that vertical ground displacement is highest near the pile face and decreases with distance from the pile face. The 2.8D test is the exception. According to measurements taken, the soil displaced very little near the pile face and the greatest displacement was approximately 1 ft. from the pile face. There are several possible explanations for this. Because the pile was at 3 in. of displacement during the second measurement, the level rod may have been held at an angle while the second measurement was taken or perhaps the measurement was read from the rod incorrectly. Assuming the measurement is correct, this discrepancy could be due to the different panel configuration of the wall in front of the pile. A smaller 2.5x10 ft. panel is located

at the top of the wall for this test. Rotation of the top of the panel towards the pile was observed as lateral loading occurred. This may have caused additional compression of the soil between the pile and the wall and an increase in the soil heave further from the pile. Furthermore, it rained during this test increasing the uncertainty of the measurement.

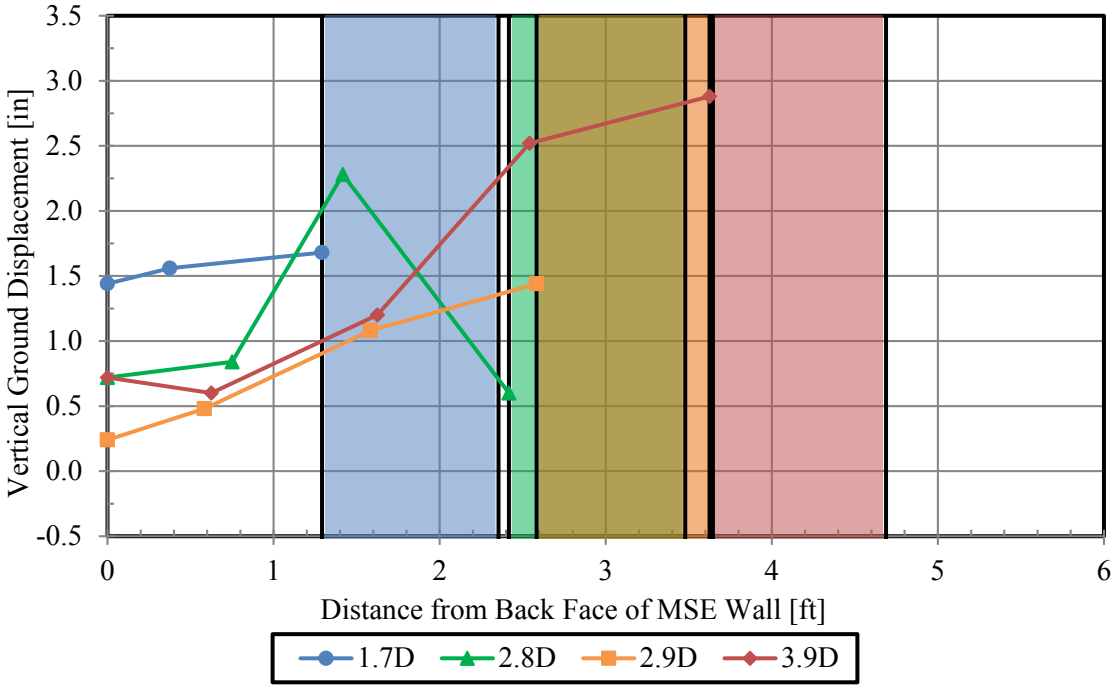

Figure 5-18: Vertical ground displacement for all test piles.

Horizontal ground displacement was greatest near the pile and decreased in a non-linear fashion with increased distance from the pile to relatively small values at the back face of the wall. Figure 5-19 is an example of the horizontal ground displacement between the pile and the back face of the MSE wall for the 2.9D test at several load levels. Horizontal ground displacement curves for the rest of the tests can be found in Appendix D. As expected, horizontal ground displacement tends to increase as the displacement of the pile increases. For each of the tests, the

distance from the pile where each measurement was taken was normalized by the pile diameter and the measured horizontal ground displacement was normalized by the pile displacement. Figure 5-20 is a plot showing these normalized curves at 3.0 in. of pile displacement. The curve for the pile at 3.9D suggests that a distance of 3.5 to 4 pile diameters might normally be required to reduce normalized horizontal displacements to near zero. However, at closer pile spacings, the reinforcing members appear to resist additional applied forces to reduce displacement at the wall.

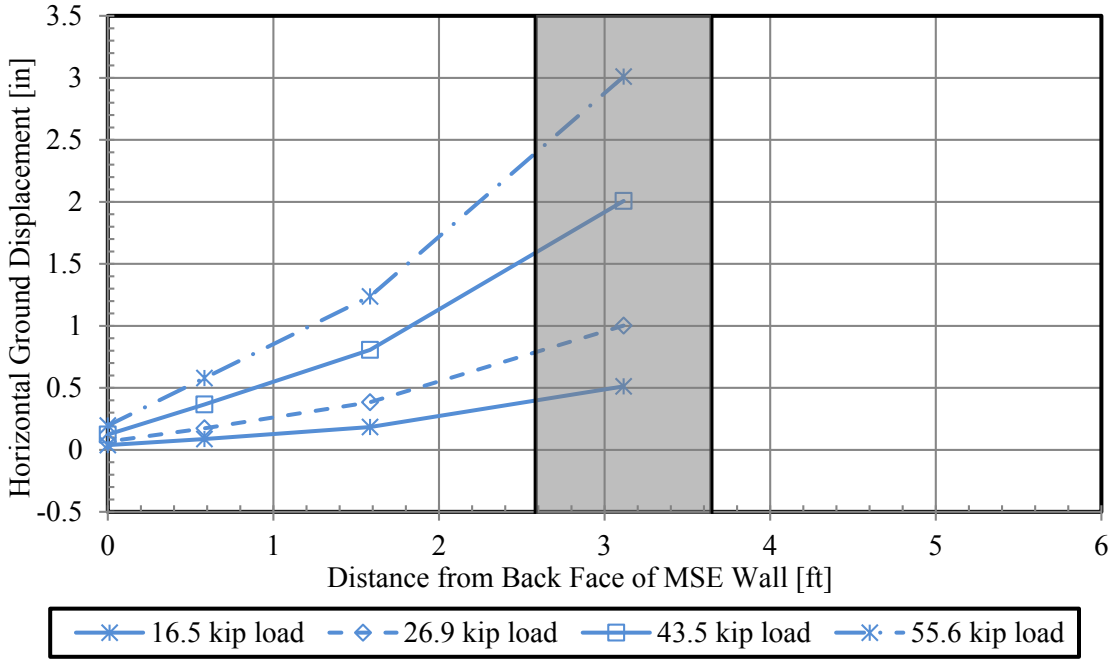

Figure 5-19: Horizontal ground displacement for 2.9D test at several pile head load levels.

Both the 2.8D and 3.9D curves show that normalized ground displacement dropped to near zero about one pile diameter (1 ft.) from the pile face, followed by a slight increase and then decrease to approximately zero at the back face of the wall. Both of these piles are located at the center of a wall panel while the other two are at a joint. A likely explanation is that the steel stakes that the string potentiometers were attached to rotated backwards slightly due to passive shear

plane development in front of the pile causing a decrease in measured displacement. The lines connecting the string potentiometers to the stakes could not be attached at ground level because space was needed to ensure string potentiometer function was not hindered by ground heave.

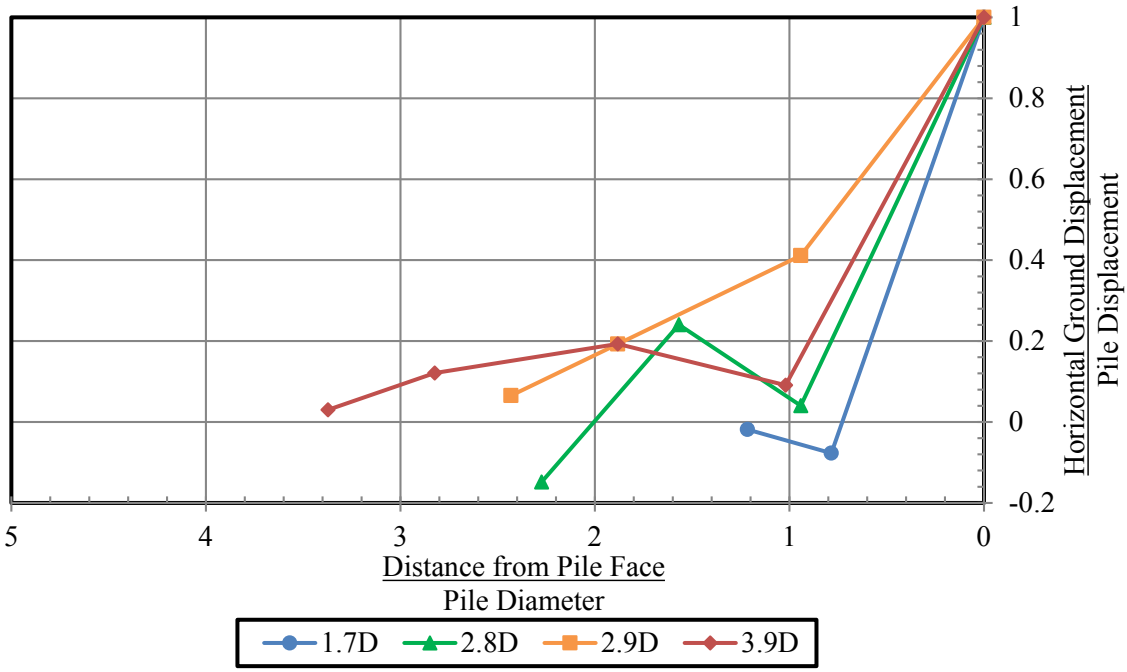

Figure 5-20: Normalized ground displacement.

5.5 Wall Panel Displacement

DIC was used as the primary method of monitoring wall panel displacement. Additionally, a string potentiometer was attached to the top of the wall to monitor the deflection of the top of the panel. Four shape arrays placed against the back side of the wall located at various transverse distances from the pile center were used as an additional method of measuring the deflection of the wall.

Figure 5-21 and Figure 5-22 show the respective results of the DIC analysis of wall panel displacement at 0.5 in. and 3.0 in. pile head deflection.

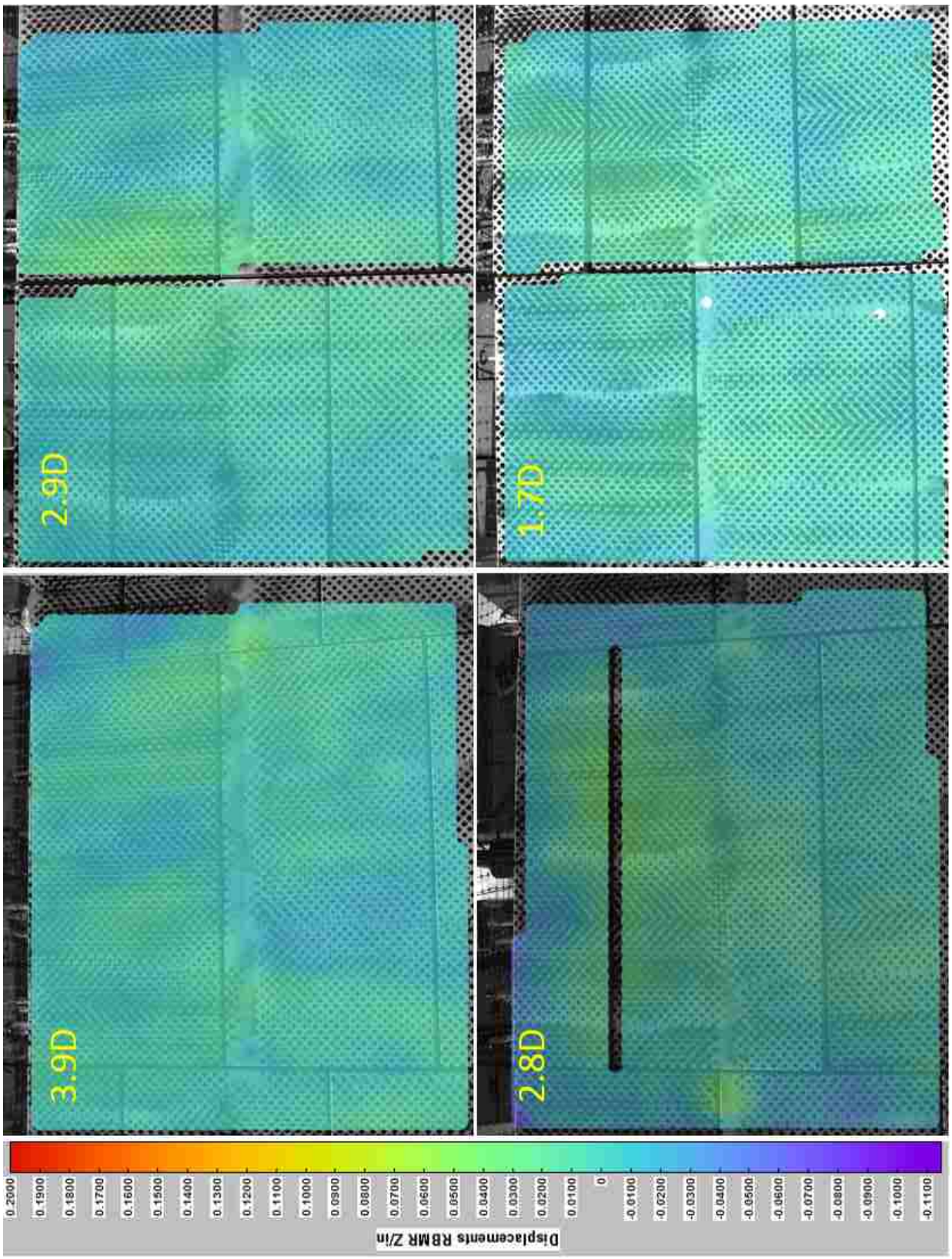

Figure 5-21: Wall panel displacement at 0.5 in. pile head displacement for all piles tested.

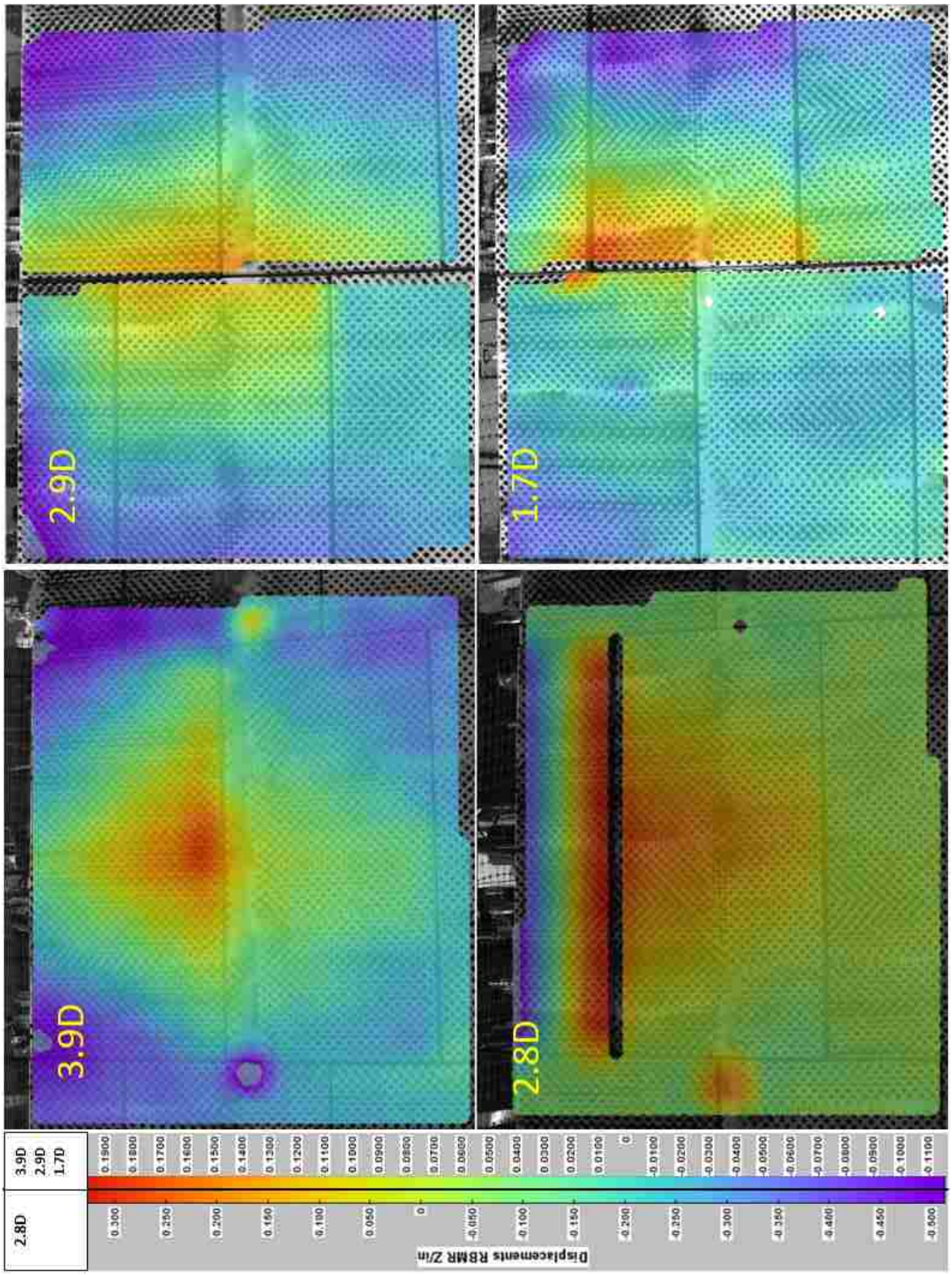

Figure 5-22: Wall panel displacement at 3.0 in. pile head deflection. Note different scale on 2.8D.

In both cases, the lateral load of the 2.8D test causes the greatest wall panel displacement. The higher displacement of the wall panels experienced by the 2.8D test is likely a result of the smaller 2.5 ft. tall by 10 ft. wide panel located at the top of the wall closest to this pile. This panel has only one layer of reinforcement located in the middle of the panel. The top of this panel rotated back towards the pile while the bottom rotated away from the pile, with the reinforcement acting as a horizontal neutral axis. At 0.5 in. pile head deflection, the maximum displacement observed for each of the four tests is approximately 0.050 in., and there is little evidence of any distinctive displacement pattern. This displacement level is likely near the threshold of the DIC system's ability to resolve displacement at the distance the cameras were placed from the wall. Based on the RBMR data, at 3.0 in. pile head deflection, the maximum panel displacement for the 3.9, 2.9, 2.8, and 1.7D tests was 0.18, 0.13, 0.35, and 0.19 in., respectively. The maximum wall deflection generally occurs near the second layer of soil reinforcement which also generally experienced the highest induced load.

With the data collected, it is difficult to determine the extent of the zone of influence on wall displacement caused by the lateral loading of the pile. The cameras for the DIC analysis were focused on an area of the wall approximately 10 ft. tall by 12 ft. wide. However, the results suggest that displacement is relatively insignificant beyond 5 to 6 ft. on either side of the loaded pile and below of depth of about 10 to 12 ft. A review of the displacement contours, suggests that displacement forms a narrower "columnar" horizontal band for piles loaded at a joint between panels, but is somewhat broader for the piles loaded in the center of a wall panel. In addition, for a pile loaded at a joint, the displacement pattern is not always uniform across the joint and one side will often experience greater displacement than the other. Similarly, the displacements do not always transfer uniformly with depth and offsets in displacement are also seen across horizontal

joints. The measurements indicate that the panels also rotated around a vertical axis but it is difficult to determine if part of the panel went backward or if it all came forward. There are different options in the software used to reduce the DIC images that allows different types of displacement to be calculated. One option is to calculate raw displacement in the x, y, or z-direction, with the z-direction being out-of-plane. It should be noted that when using this option, any movement relative to the initial position of the cameras is added to the total displacement, even if the movement is caused by the camera being moved. Another possibility is to use the Rigid Body Motion Removed (RBMR) option. This option only calculates displacements that are due to bending or distortion of an object. For example, if the camera were moved towards the wall but no bending or distortion of the wall occurred, this would show up as zero displacement. While this option seems like the best available option within the software to correct movement caused by wind or the camera settling, we observed that the cameras were not focused on a large enough area of the wall for the software to properly remove any rigid body motion and near the corners of the images negative deflections may be shown. These deflection are likely a result of the correction algorithm and not real. Hence, it is difficult to determine the extent of negative deflection that actually occurred when panels rotated. As shown in Figure 4-2, the DIC cameras were hooked to a tripod and there was wind blowing during most of the tests. Additionally, there was rain that caused some settlement of the tripod legs that were resting on the native soil. It would likely have been best to attach the camera to a more secure reference frame such as a concrete block that had been allowed to settle prior to testing so that the total z-displacement option could be used without the need of removing displacements caused by movement of the cameras. However, because some movement of the cameras did occur, a correction was determined for each time step. To determine the amount of deflection caused by movement of the camera versus actual deflection of the wall,

the z-displacement at each of the corners of the DIC images was analyzed. At a transverse distance of approximately 5.5 ft., very little movement of the wall should actually be occurring so any deflection measured by the DIC is probably due to the cameras moving rather than movement of the wall and could be used as a correction. Furthermore, the deflection should be similar at these locations if the movement is due to the cameras moving. This behavior was observed for all of the tests. Within the software used to compute the DIC deflections, there is no option available to apply this correction however so the RBMR option was used in computation of the wall deflections shown in Figure 5-21 and Figure 5-22. However, this correction is applied to other displacements calculated using the DIC data.

The displacement at the location of each instrumented soil reinforcement was extracted from the DIC data and corrected for any movement of the cameras caused by wind as outlined in the previous paragraph. Plots of pile head displacement versus the displacement at each of the instrumented reinforcement locations for the 1.7, 2.8, 2.9, and 3.9D tests are shown in Figure 5-23 through Figure 5-26, respectively. The displacement is shown for both the reinforcement which is located close to the pile and the one located further from the pile. Additionally, the displacement at the top of the wall measured by the attached string potentiometer is shown in these plots. The transverse distance from the center of the pile to the center of the reinforcement can be found in Table 4-2. The second and third layers of reinforcements generally experienced the highest displacement at the higher pile head deflections, rather than the top layer. In addition, the reinforcements closer to the pile deflected somewhat more than the reinforcements further away in the transverse direction.

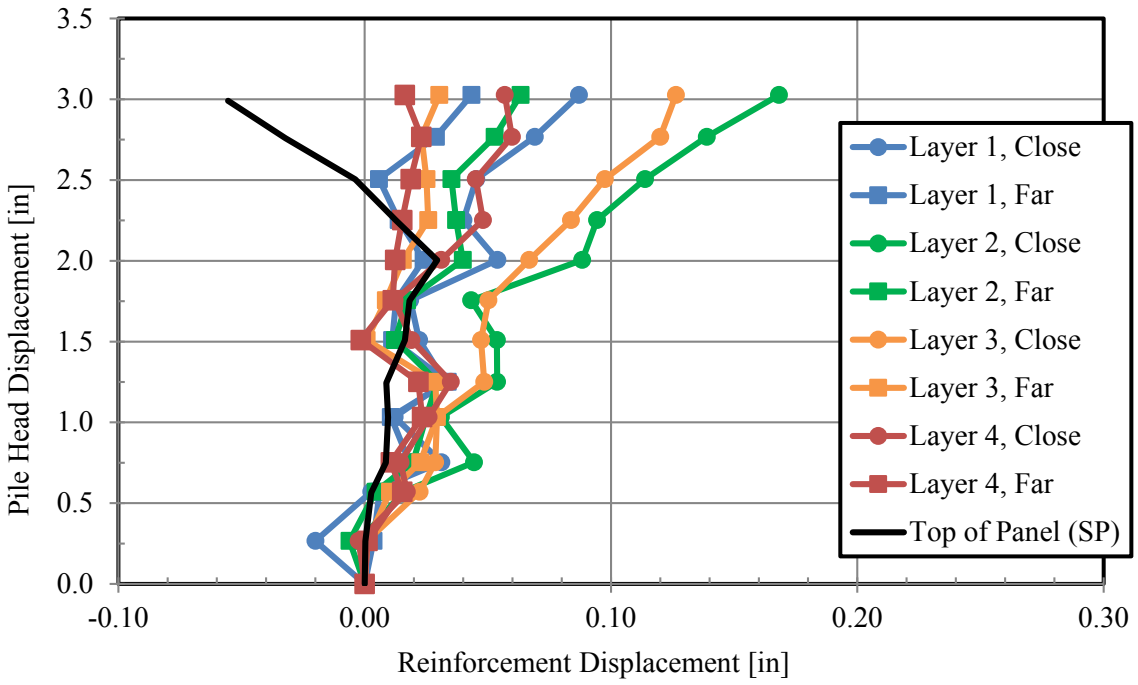

Figure 5-23: Panel displacement at the reinforcement connection location for the 1.7D test.

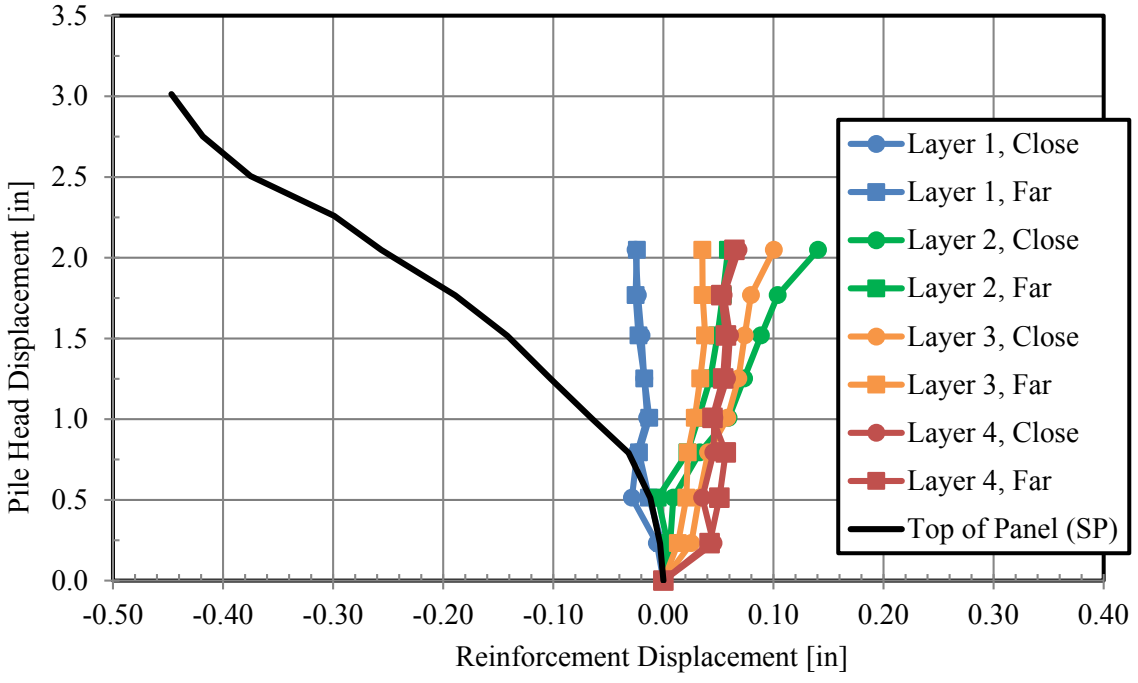

Figure 5-24: Panel displacement at the reinforcement connection location for the 2.8D test.

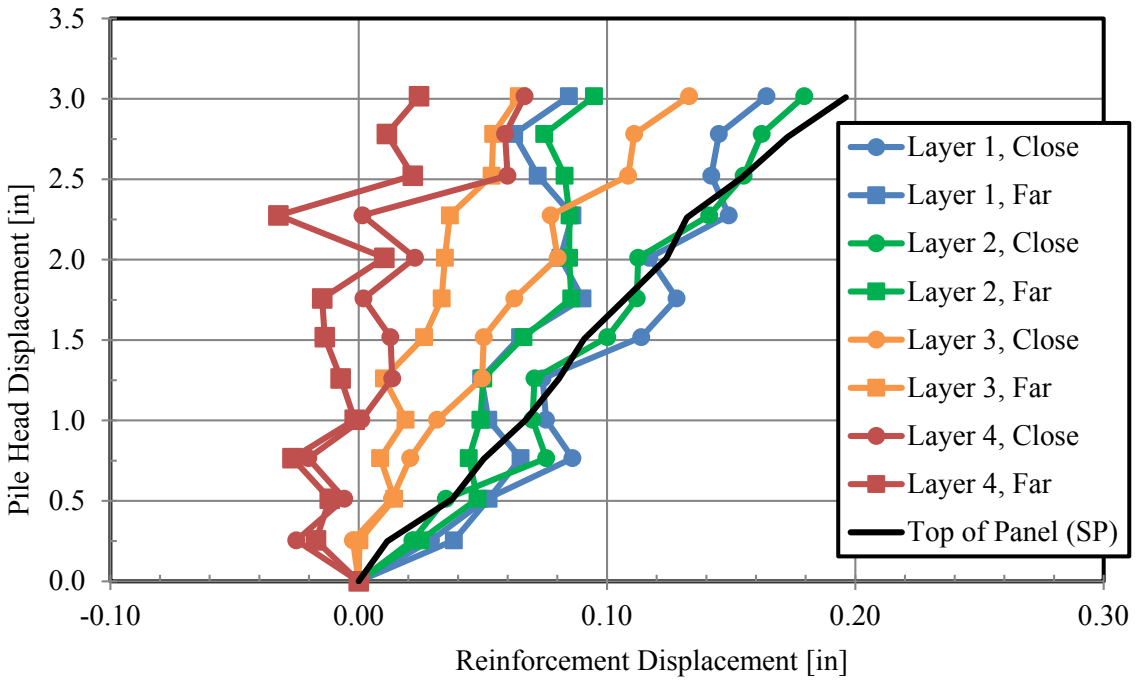

Figure 5-25: Panel displacement at the reinforcement connection location for the 2.9D test.

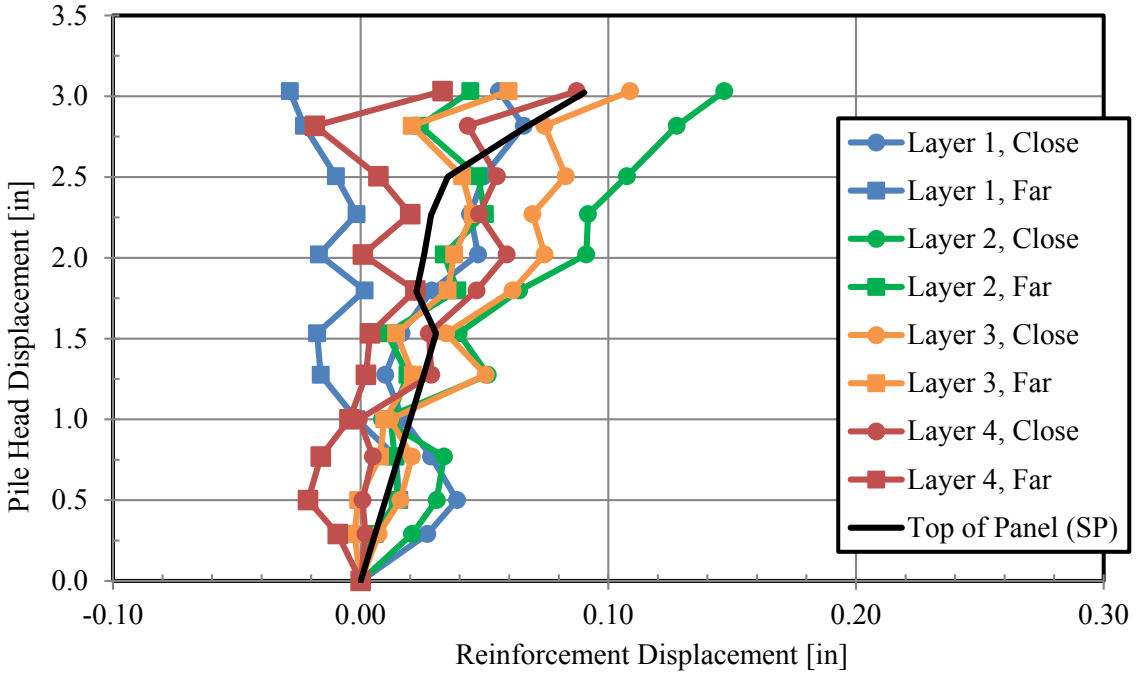

Figure 5-26: Panel displacement at the reinforcement connection location for the 3.9D test.

Although the curve shapes extracted from the DIC show some unexpected decreases in reinforcement deflection with increasing pile deflection the reinforcement deflection generally increases with increasing pile head deflection. The curve shapes do not appear to be flattening out at higher deflections as would be expected if the reinforcements were reaching their frictional capacity and pulling out. Despite the large lateral loads (and displacements) imposed on the piles, the reinforcement displacements were typically less than 0.25 in. in all cases and distress to the wall face was minimal even for the pile located 1.7D from the wall face.

Shape arrays were also used to monitor the deflection of the wall. Four shape arrays were placed in electrical conduit running vertically up the back face of the MSE wall at various transverse distances from the pile for each test. The conduit was secured against the back face of the MSE wall with duct tape during construction, but some separation of the conduit from the wall occurred during placement of the backfill. Additionally, the displacement of the top of the wall was measured by a string potentiometer that was attached to the top of the wall using an eye-bolt. The displacement measured by the shape array installed approximately in front of each pile being loaded is compared to the wall displacement at the same location calculated using the DIC data and to the displacement of the top of the wall measured by the string potentiometers. Figure 5-27 through Figure 5-30 shows this comparison for the 1.7, 2.8, 2.9, and 3.9D tests, respectively.

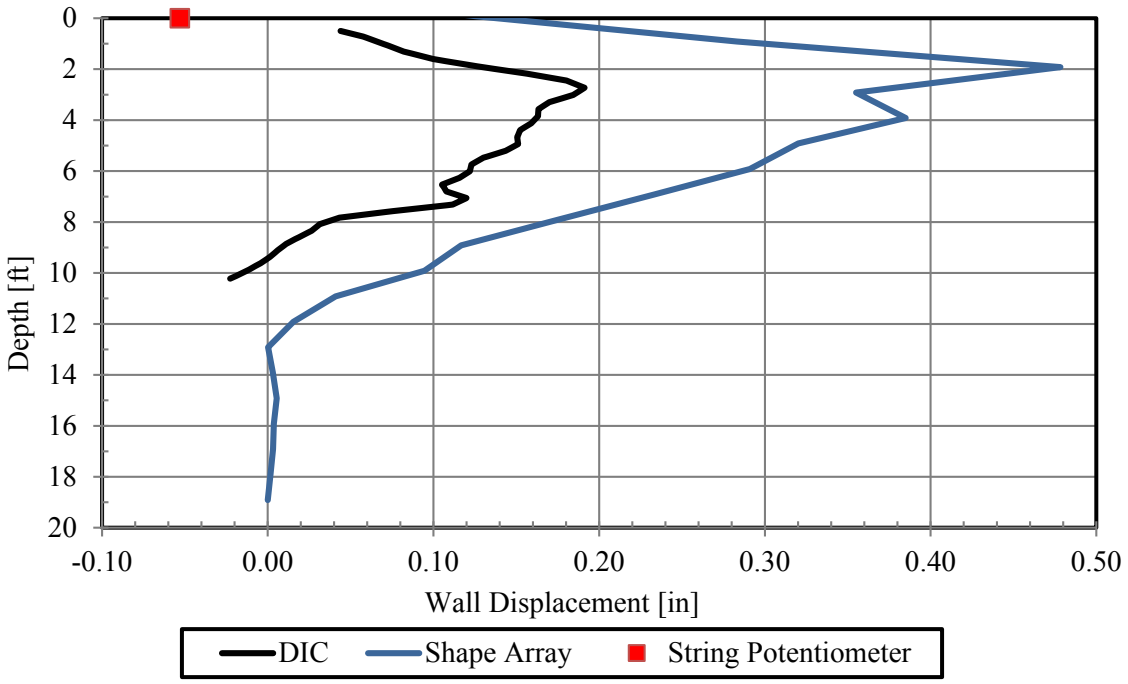

Figure 5-27: Comparison of wall displacement measured by the shape arrays to DIC and string potentiometer data for the 1.7D test at 3.0 in. pile head deflection.

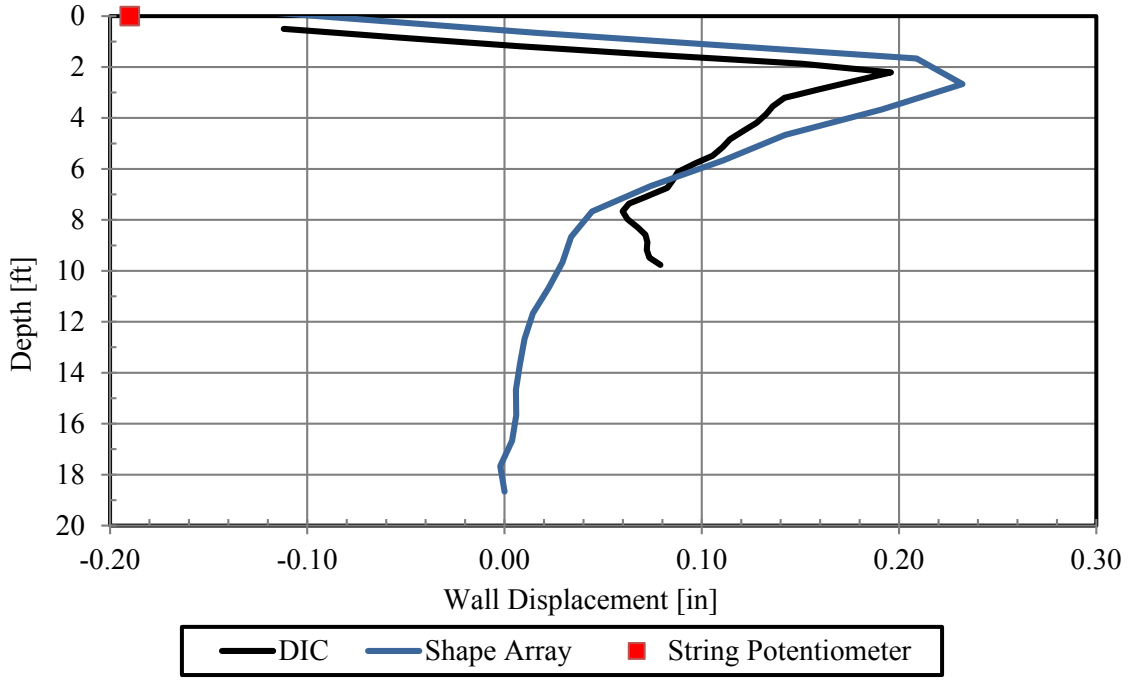

Figure 5-28: Comparison of wall displacement measured by the shape arrays to DIC and string potentiometer data for the 2.8D test at 1.75 in. pile head deflection.

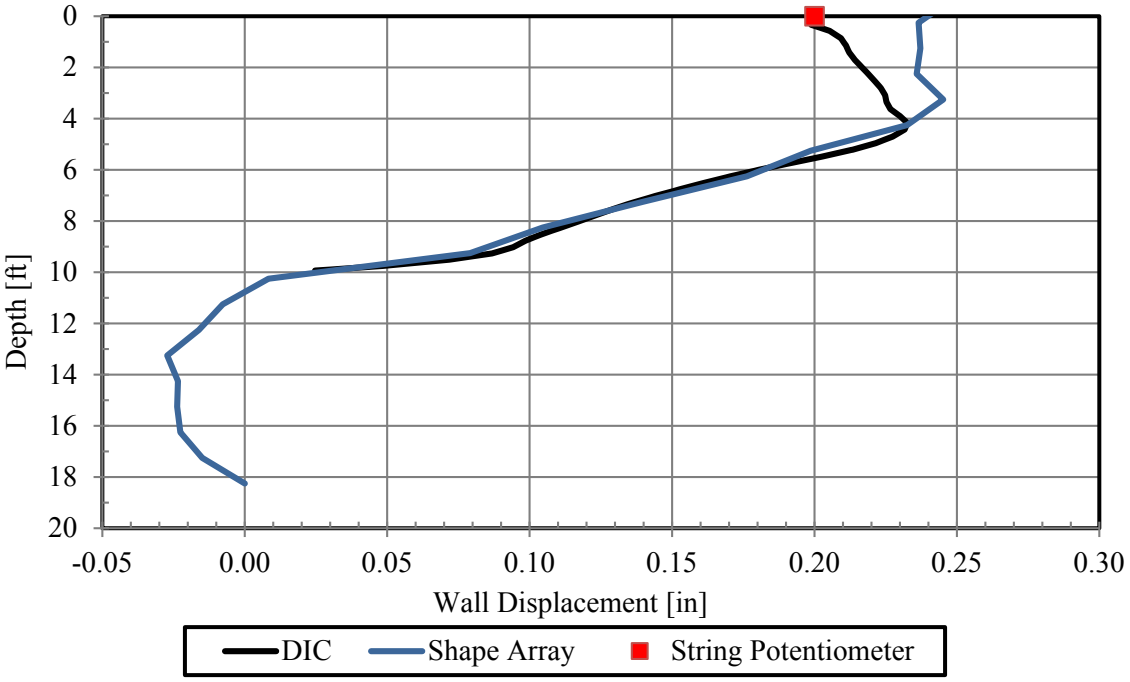

Figure 5-29: Comparison of wall displacement measured by the shape arrays to DIC and string potentiometer data for the 2.9D test at 3.0 in. pile head deflection.

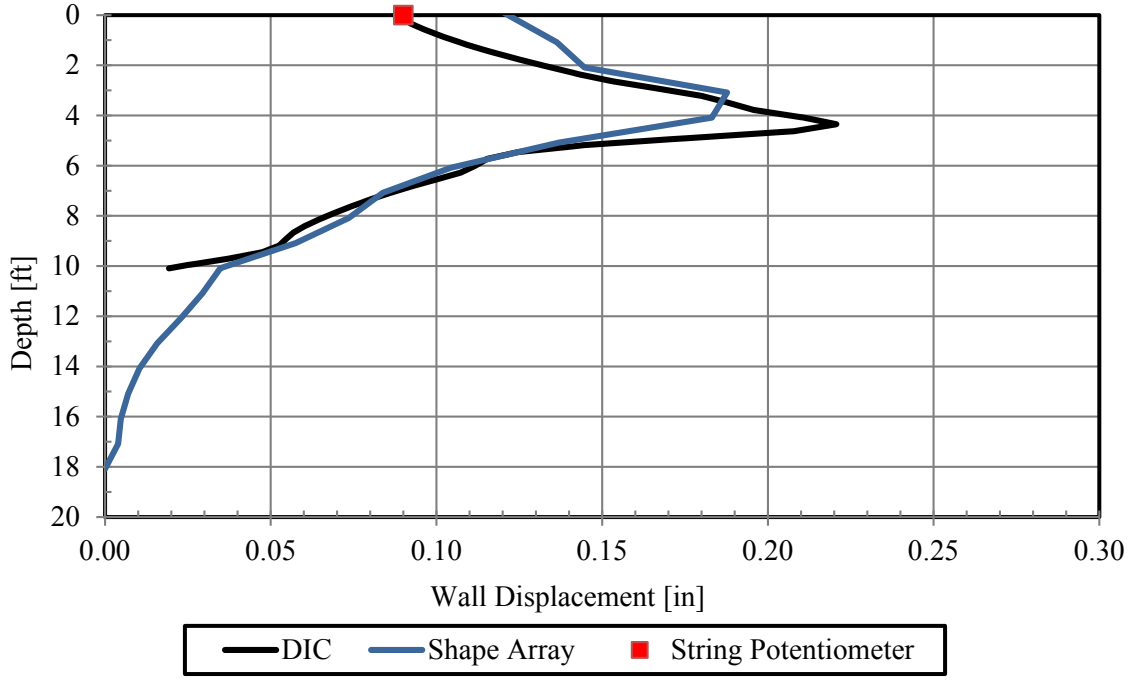

Figure 5-30: Comparison of wall displacement measured by the shape arrays to DIC and string potentiometer data for the 3.9D test at 3.0 in. pile head deflection.

Overall, the displacements are in good agreement and are likely within the accuracy of the respective systems. The DIC data has the correction applied as discussed previously in this section. The worst agreement was for the 1.7D test, with maximum wall displacement being measured as 0.48 in. using the shape arrays and 0.19 in. using DIC. This is likely due to separation of the PVC conduit from the wall in front of the pile, which allowed additional movement of the conduit with respect to the wall.

5.6 Pile Performance

Strain on the pile was measured at depths of 2, 4, 6, 9, 12, 15 and 18 ft. At these depths, gauges were applied to the side of the pile being loaded and the opposite side. The pile moment was estimated using the data. In the case where one of the gauges was damaged, the strain from the working gauge was used and in cases where both were damaged, the data point was omitted. The bending moment in the pile was calculated using the equation

$$M_i = \frac{EI}{2y}((\mu\varepsilon_{it} - \mu\varepsilon_{ot}) - (\mu\varepsilon_{ic} - \mu\varepsilon_{oc}))(10^{-6}) \qquad (5\text{-}4)$$

where

M_i is the bending moment in inch-kips for the pile at the i^{th} data point,

E is the modulus of elasticity of the pile (29,000 ksi),

I is the moment of inertia of the pile and the attached angle iron (314 in^4),

$\mu\varepsilon_{it}$ is the micro strain for the i^{th} data point, on the tension side of the pile,

$\mu\varepsilon_{io}$ is the initial micro strain for the tension side of the pile prior to loading,

$\mu\varepsilon_{it}$ is the micro strain for the i^{th} data point, on the compression side of the pile,

$\mu\varepsilon_{oc}$ is the initial micro strain for the compression side of the pile prior to loading, and

y is the distance separating the two strain gauges measured along the line of loading.

Several of the piles rotated during driving so the strain gauges were not directly in line with the load. As shown in Figure 5-31, the rotation of the pile was measured and the distance separating the gauges in line with the load was calculated and applied to y in Equation (5-4) to account for the reduced measured strain.

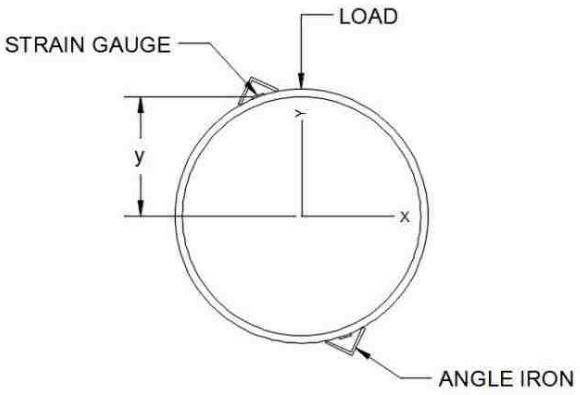

Figure 5-31: Measurement of y to correct strain measurement for pile rotation.

In spite of the angle iron covering the strain gauges and lead wires on the piles, some of the lead wires were cut during construction. This occurred for all of the strain gauges on one side of the 2.8D and 2.9D piles. For both of these piles, multiple wires were cut and it was not possible to determine their proper match through inspection of the wires. In this case, the strain of the gauges at unknown locations was compared to the strain measured by gauges at known depths and the gauges were assigned a location where opposing strains were approximately equal. There were several instances where both gauges at a given depth were not functioning properly and in this case, the moment at that depth was not calculated. When only one gauge was functioning, the strain at that location was doubled.

Figure 5-32 through Figure 5-35 are plots of bending moment in the pile versus depth below the ground surface for the four piles tested. The moment is given at several pile head loads for each test. The moment peaks at various depths ranging from 4 to 7 ft. The peak moment generally occurs at deeper depths as pile spacing decreases with the exception of the 1.7D test. This may be due to damaged strain gauges. Only one gauge was functioning at depths of 2, 6, and 9 ft., and neither gauge at 4 ft. was functioning. For a given load, the moment tends to be highest for the pile spaced furthest behind the wall and decreases as spacing of the piles decreases. This may be due to a softer response of the soil and wall as spacing decreases. The load applied to the pile may be distributed deeper in the profile rather than being focused at the top of the pile, causing less and a lower moment. This is also consistent with the observation that the observed moment tends to occur deeper as pile spacing decreases.

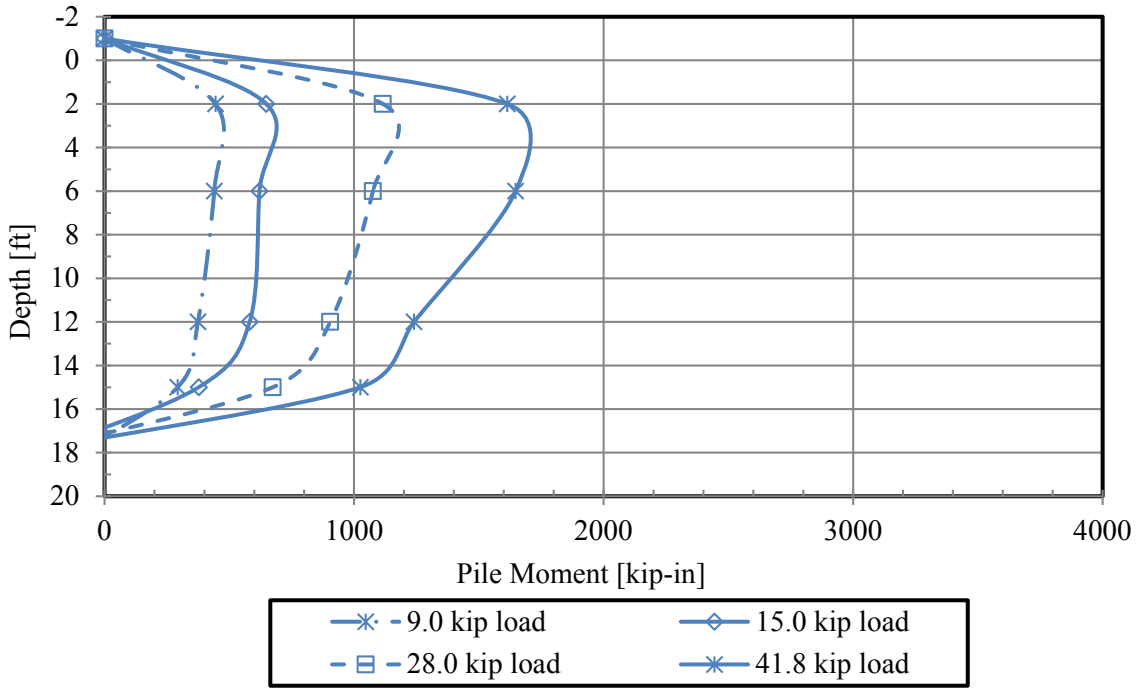

Figure 5-32: Moment versus depth for various loads on the 1.7D test.

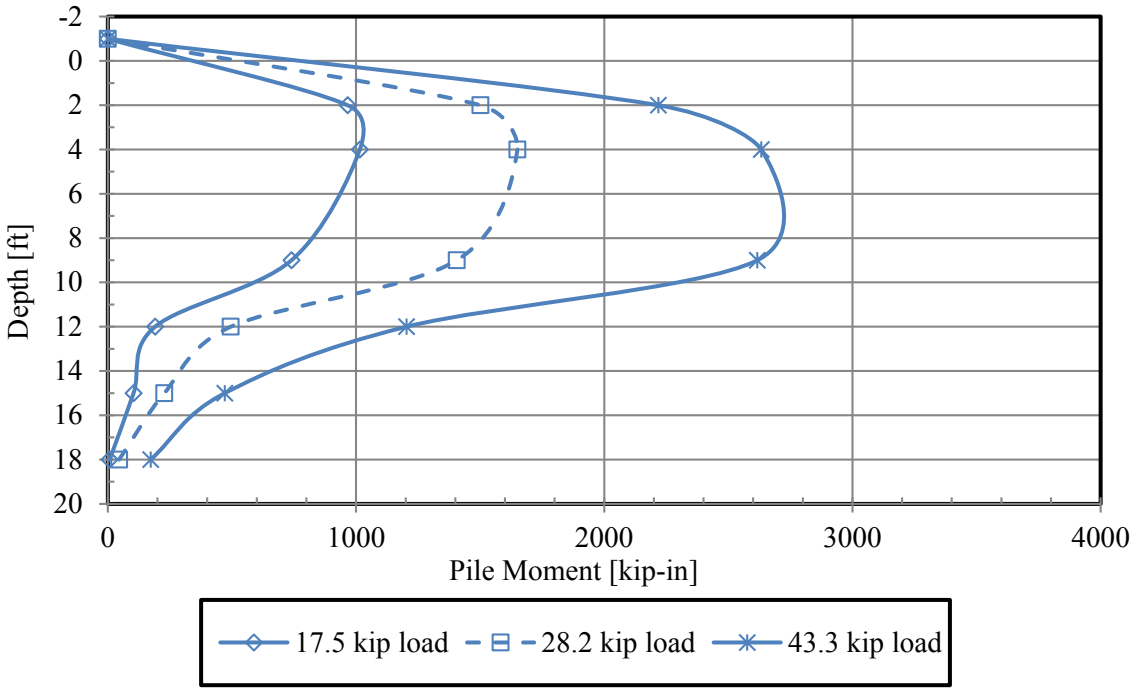

Figure 5-33: Moment versus depth for various loads on the 2.8D test.

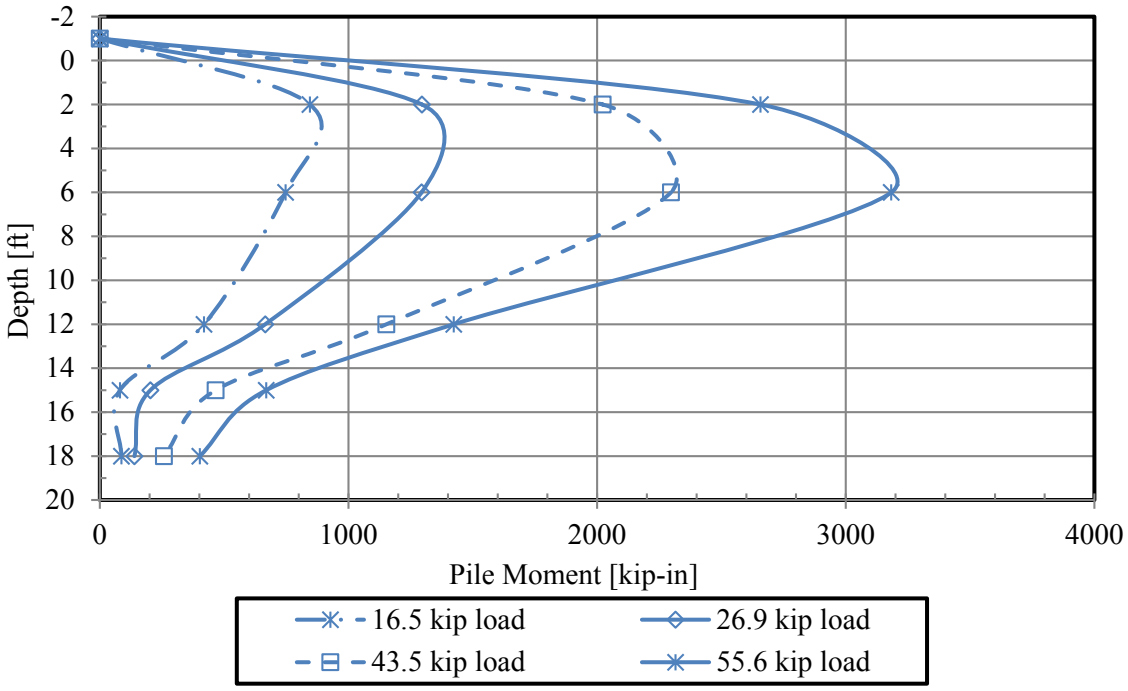

Figure 5-34: Moment versus depth for various loads on the 2.9D test.

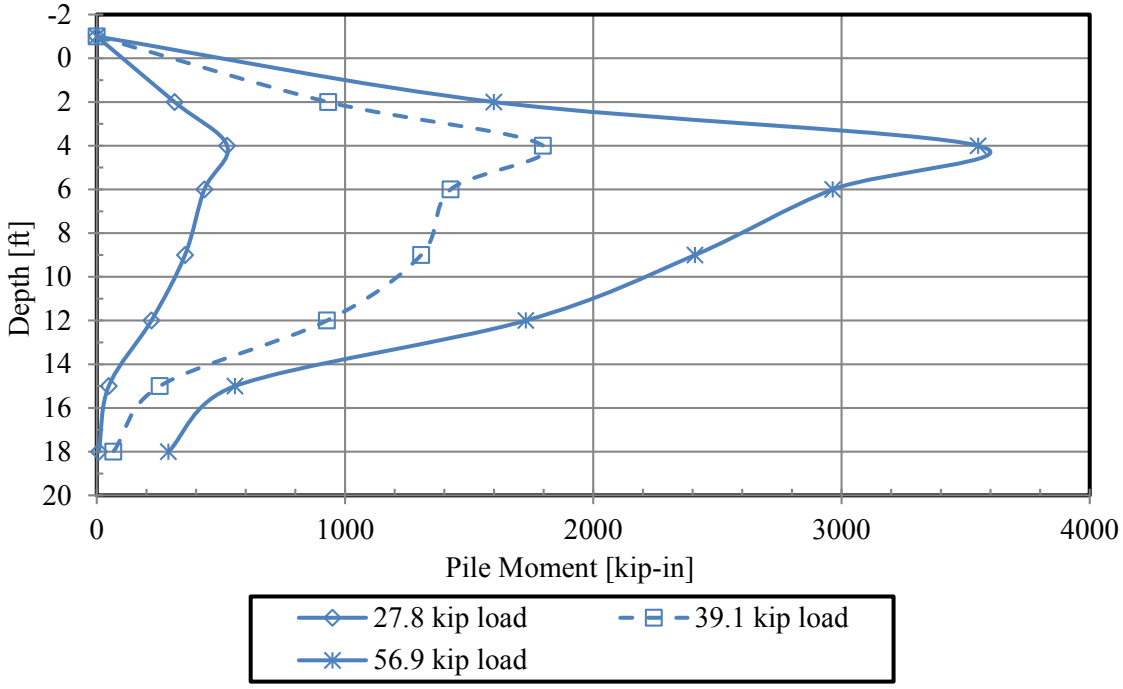

Figure 5-35: Moment versus depth for various loads on the 3.9D test.

Curves showing pile head load versus rotation of the tip of the pile for the four tests and the reaction pile are shown in Figure 5-36. The load for the curves is based on the hydraulic pressure gauge monitoring the pressure in the hydraulic jack line one minute after the target displacement was reached. The rotation of the pile head was calculated based on the string potentiometers at the load point and 3 ft. above the load point using the equation

$$\theta = \sin^{-1}\left(\frac{d_{3ft} - d_{lp}}{36in}\right) \qquad (5\text{-}5)$$

where

θ is the pile head rotation,

d_{3ft} is the pile displacement 3 ft. above the load point, and

d_{lp} is the pile displacement at the load point.

The rotation of the pile tended to increase as the load increases for all of the tests. The pile head load versus pile head rotation curves are all very similar for the 3.9, 2.9, and 2.8D tests, just as the load displacement curves are for these tests. At a given load, the rotation of the pile tends to be lower for the 1.7D test indicating that less bending of this pile is occurring than it is for the other tests which is also consistent with the lower observed pile moment.

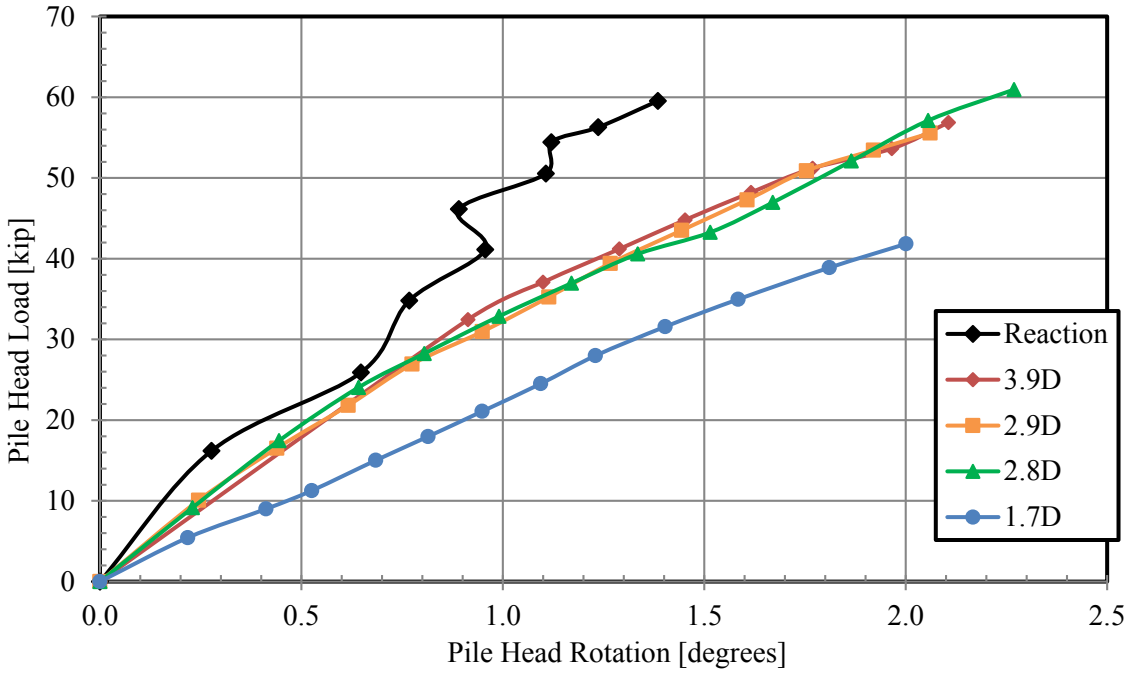

Figure 5-36: Pile head load versus rotation of the tip of the four test piles and the reaction pile.

6 LATERAL PILE LOAD ANALYSIS

To be more useful for a broad range of applications, the results of these tests were modeled in LPILE, a computer program commonly used to analyze laterally loaded piles. LPILE is a finite difference program that uses the p-y method. With the p-y method, the soil surrounding the pile is modeled as a series of springs at various depths along the pile. The spring stiffness varies nonlinearly with displacement. The displacement of a pile at any depth at a given lateral load can be determined through an iterative approach using this method. Soil type and state, pile geometry, and loading method can all cause variation of the pile displacement at any given lateral pile load. Hence, various p-y curves are necessary for different types of soil. LPILE computes deflection, bending moment, shear force, and soil response over the length of the pile. Various options are available within the program for determining p-y curves based on different soil types. The accuracy of the analysis depends on how accurately the reaction of the soil is modeled by the p-y curve. The API Sand (1982) method built into LPILE seems to model the backfill used for the wall reasonably well and is used for lateral load analysis of the piles in these tests. The API method was also the method used by Price (2012), Nelson (2013), Hatch (2014), and Han (2014) in their analyses so this approach is consistent with their work.

The pile located 3.9 pile diameters from the wall was assumed to have no interaction with the wall based on previous research performed by Price (2012) and Nelson (2013). This pile was used to calibrate the soil parameters used in the LPILE model. The displacement of the pile head

at any given load is dependent on the soil moist unit weight, γ; friction angle, ϕ; and the modulus of subgrade reaction, k; all of which are assumed to be the same for all tests. The unit weight was known from field testing described previously. Initial estimates of friction angle and subgrade reaction were made based on relative density estimated from the relative compaction. The friction angle and subgrade reaction were then varied until the predicted load versus displacement of the pile head matched the measured load versus displacement. After the soil friction angle and subgrade reaction which modeled the soil correctly were determined, a p-multiplier (less than 1) was applied to the p-y curve to account for the reduced resistance of the piles closer to the wall.

This analysis allows the results of these tests to be more useful for a broad range of applications. Designers can create an LPILE model based on their soil and pile type and use the reduction curves to determine proper multipliers to use based on the distance of the pile behind the wall. The use of this approach is based on the assumption that a similar reduction in lateral resistance is expected for other pile sizes and types, soil types, wall panel types, and so on. Additional tests with larger diameter piles will likely be necessary to confirm this assumption in the future.

6.1 Material Properties

Table 6-1 is a list of input parameters for the pile and their respective values used in the LPILE analysis. The pile was modeled as a linear elastic material. After running the analysis, this assumption was checked and it was found that the stress on the piles reached the yield point from 2.5 to 3.0 in. pile head deflection depending on the pile. However, after updating the model for the 3.9D pile, the analysis showed that the predicted deflection changes less than 2% at 3.0 in. pile head deflection so the linear elastic model of the pile was still used. The pile moment of inertia and cross-sectional area were calculated for the pile including the angle iron tack welded to the

pile to protect the strain gauges. A pinned head load condition was used in the analysis consistent with the field loading condition. Loads were applied 12 in. above the ground surface and were the measured loads from the analysis. The piles were modeled as hollow sections despite being driven open ended. The piles eventually plugged with soil; however, the soil plugs were generally limited to a zone about 12 ft. from the pile tip leaving the upper 28 ft. of the pile hollow. Therefore, for practical purposes, the section of the pile interacting with soil was acting as a hollow section and the plugged section was deep enough to have no effect on the results.

Table 6-1: Pile properties for LPILE analysis

Pile Shape	Total Length[ft]	Number of Increments	Distance from top of pile to top of ground surface [in]	Outside diameter [in]	Wall thickness [in]	Moment of inertia [in^4]	Cross-sectional Area [in^2]	Modulus of elasticity [psi]	Yield stress [psi]
Circular pipe	40	100	12	12.75	0.375	314	15.3	29000000	Elastic (57,000)

The soil friction angle, modulus of subgrade reaction, and soil effective unit weight are the required inputs for the API Sand method in LPILE. Figure 6-1 shows the API soil subgrade reaction correlated to relative density or to soil friction angle. Curves are provided for sand above and below the water table. The backfill was above the water table so the curve representing sand above the water table was used. To determine the correct friction angle and subgrade reaction to represent the soil, a friction angle was initially estimated and the corresponding subgrade reaction was read from Figure 6-1. If the displacements were too high for a known pile load based on measured load deflection curves, a higher friction angle and subgrade reaction were chosen and vice versa. This process was repeated until the predicted deflection at measured loads matched the measured deflection.

As described in section 3.1.2, a 600 psf surcharge was applied behind each pile using concrete blocks to simulate a 5-ft. high bridge abutment behind the wall. LPILE does not have the option to apply an asymmetric soil profile, so there was no way to model the surcharge as it was applied during the testing. Although the surcharge was not in front of the pile during loading, the spreading of the load with depth is likely to have caused additional resistance deeper in the profile. In an attempt to model the surcharge, a layer of soil with a 2400 pcf unit weight, 3 in. thick, was applied to the top of the profile. The user defined p-y option was applied to this layer in a manner that the layer would provide no lateral resistance but only additional vertical stress on the underlying layers. The reinforced backfill was modeled using the API Sand approach, and the friction angle was found to be 31 degrees with a modulus of subgrade reaction of approximately 60 pci. The underlying native soil was also modeled using the API sand approach with a friction angle of 34 degrees, however, the analysis is unaffected by the soil properties at this depth. Table 6-2 summarizes the soil properties used in the analysis when the surcharge was modeled in LPILE. Two LPILE models of each of the piles were created, one attempting to simulate the 600 psf applied surcharge and one in which no attempt to simulate the surcharge was made. Table 6-3 summarizes the soil properties used in the analysis when no attempt was made to model the surcharge. The same analysis was performed as described previously and the back-calculated friction angle for the reinforced soil was found to be 39 degrees with a subgrade reaction of 260 pci. In reality, the actual stress in the soil profile caused by the 600 psf surcharge would be somewhere between these two cases so the friction angle is somewhere between 31 and 39 degrees and the subgrade reaction is between 60 and 260 pci. This range of friction angles is reasonable for the backfill material based on the backfill estimated relative density of 50% (See section 3.1.1) and the friction angles corresponding to various relative density shown in Figure 6-1.

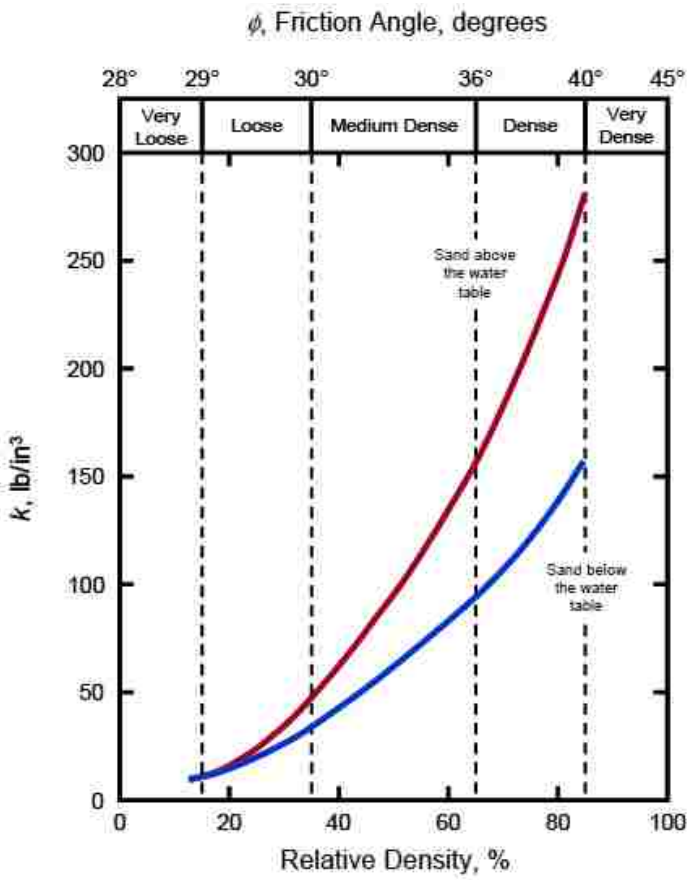

Figure 6-1: Soil modulus reaction based on soil friction angle or relative density (API, 1982).

Table 6-2: Soil properties used in LPILE analysis with simulated surcharge

Depth [ft]	Description	Soil type (p-y model)	Eff. Unit weight, γ [pcf]	Friction angle, ϕ [deg]	p-y modulus, k [pci]
0.75 - 1	Surcharge	User defined	2400	0	0
1 - 21	Reinforced fill	API Sand (O'Neil)	127.8	31	60
21 - 40	Underlying native soil	API Sand (O'Neil)	125	34	100

Table 6-3: Soil properties used in LPILE analysis with surcharge not simulated

Depth [ft]	Description	Soil type (p-y model)	Eff. Unit weight, γ [pcf]	Friction angle, ϕ [deg]	p-y modulus, k [pci]
1 - 21	Reinforced Fill	API Sand (O'Neil)	127.8	39	260
21 - 40	Underlying native soil	API Sand (O'Neil)	125	34	100

6.2 Results of LPILE Analysis

The computed load-deflection curves were compared to measured load-deflection curves for each pile and used to calibrate an LPILE model for each pile tested and determine appropriate p-multipliers for the piles spaced closer to the wall than approximately 3.8D. LPILE also computes pile bending moment and rotation, both of which are compared to measured results as another check to ensure that the LPILE model is correct.

6.2.1 Load-Deflection Curves

Figure 6-2 shows the final load-deflection curves computed by LPILE compared to the measured load-deflection curves. Two LPILE predicted curves are shown, one for the case without the surcharge modeled (q=0 psf) and one for the case when the surcharge is modeled (q=600 psf). The measured load-deflection curves are based on the average of 30 seconds of data starting one minute after the peak load was reached for each target deflection. Table 6-4 gives the back-calculated p-multiplier determined for each test based on the LPILE model without the surcharge modeled, as has been done in previous research. It was found that a p-multiplier of 1 was most appropriate for the 3.9, 2.9 and 2.8D tests and a p-multiplier of 0.5 was used for the 1.7D test. Although the load deflection curve predicted by LPILE does not fit the measured curve very well,

the R^2 value was lowest using a p-multiplier of 0.5 (R^2=0.86). Only one computed curve is shown for the 3.9 through 2.8D tests because the p-multiplier is 1 and the load-deflection curves are all approximately identical. For all four of the piles tested, the LPILE model with the surcharge simulated matches the measured results slightly better than the model without the surcharge. Overall, the predicted and measured load-deflection curves match very well. For the 1.7D test, the predicted LPILE curve with the simulated surcharge only matches for the first 0.25 in. of pile displacement. After that, LPILE predicts a stiffer response out to approximately 1.5 in. of pile displacement, after which the response softens and the curve begins to level out. The measured curve shows that the response is approximately linear, at least to the extent of the displacements measured. This may be an indication that the actual response is governed by the resistance the soil reinforcement is providing rather than by the resistance of the soil. This would indicate that the full resistance of the soil reinforcement has not been mobilized at the peak measured displacement. Another possibility is that the soil around the pile was loose and compacted due to the pressure applied from the lateral pile load causing the soil to become progressively stronger which could also lead to the more linear curve shape.

Table 6-4: P-Multipliers for each test

Pile	P-multiplier
1.7D	0.5
2.8D	1.0
2.9D	1.0
3.9D	1.0

.

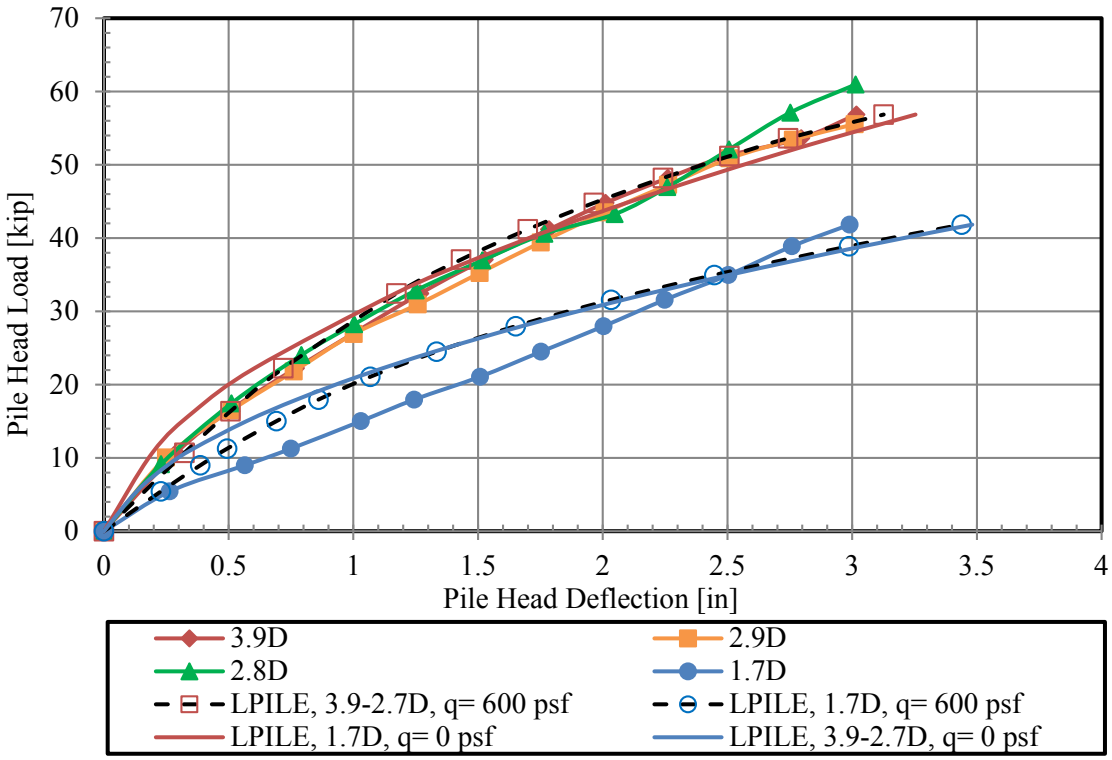

Figure 6-2: Comparison of load versus deflection curves computed by LPILE to measured load-deflection curves.

The reason why the load deflection curves are nearly identical for the 3.9, 2.9, and 2.8D tests is unknown. The spacing of the 2.9 and 2.8D piles behind the wall is similar enough that similar load deflection curves are expected. However, according to previous research, the p-multiplier for a pile spaced at these distances should be approximately 0.9 compared to the pile spaced at 3.9D (See Figure 2-19). The p-multiplier for the 1.7D test is also higher than expected. A p-multiplier of 0.5 provided the best overall calibration of the model while a multiplier of 0.3 is expected based on previous research. If the lateral resistance of the 3.9D pile had been higher, the p-multipliers for the other tests would have been reduced. A comparison of all the pipe piles tested during this research indicates that the strength of the 3.9D test is similar to the other pipe piles at similar distances behind the wall as shown in Figure 6-3 while the three piles spaced at 2.9, 2.8,

and 1.7 diameters have a higher lateral resistance than other pipe piles tested at similar spacing as shown in Figure 6-4 and Figure 6-5. The reason for the higher resistance of the 2.9, 2.8, and 1.7D may be the soil compaction was higher for these piles. Compaction between the piles and the wall was performed using a vibratory plate compactor. The path of compaction generally was around the pile, next to the wall, and then in-between piles. Assuming the same number of passes of the plate compactor occurred between each pile and the wall, the soil between the wall and piles on the 1.7, 2.8, and 2.9D piles would have received more compaction effort than the soil around the 3.9D pile. Although nuclear density testing was performed throughout construction as outlined in the section 3.1.1 of this report, the exact location of all tests is not known. In addition, as indicated in section 3.1.1, the scatter in the relative compaction data for the zone between the piles and the wall exhibited considerable variation. Another possible reason for the higher resistance of these piles is the night before the 2.8 and 2.9D piles were tested, a significant rainstorm occurred at the site. The USCS material classification of SP-SM indicates that there are some fines in the soil, (See Appendix B. Geneva Rock Laboratory Test Reports) so perhaps the resistance of the 2.8 and 2.9D tests was increased due to cohesion that added to the strength of the soil. Both of the tests were performed on the day following the rainstorm. Furthermore, the water that infiltrated the soil would increase the unit weight of the soil and may have caused some natural compaction.

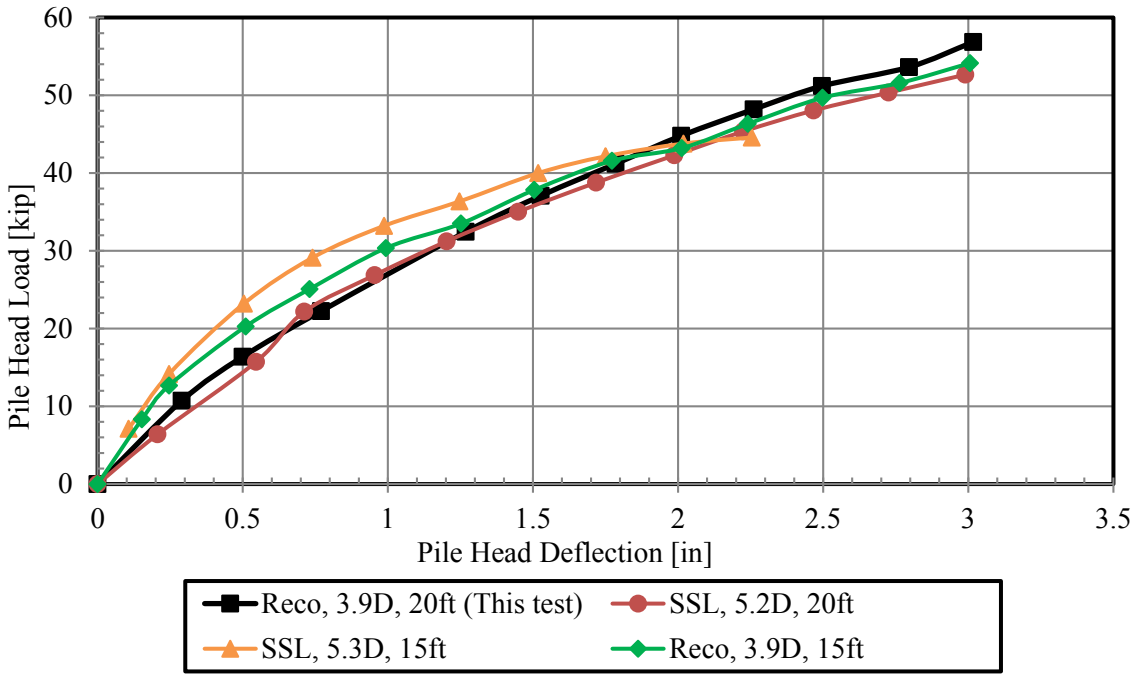

Figure 6-3: Comparison of load versus displacement curves for the 3.9D pile to other piles at similar spacings tested during this study.

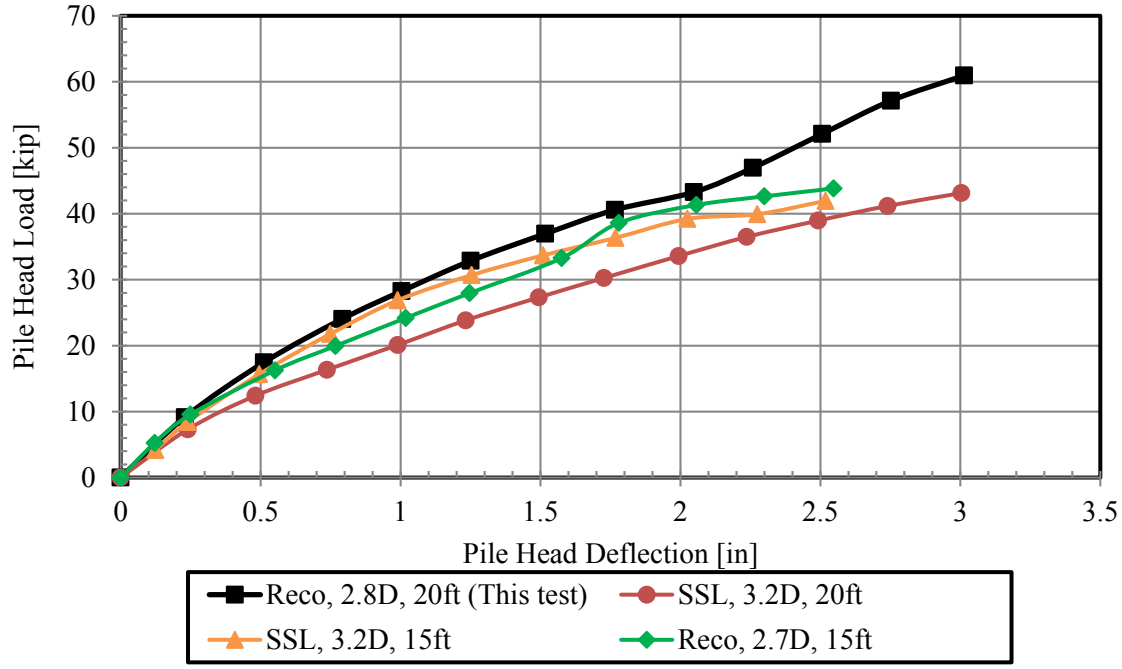

Figure 6-4: Comparison of load versus displacement curves for the 2.8D pile to other piles at similar spacings tested during this study.

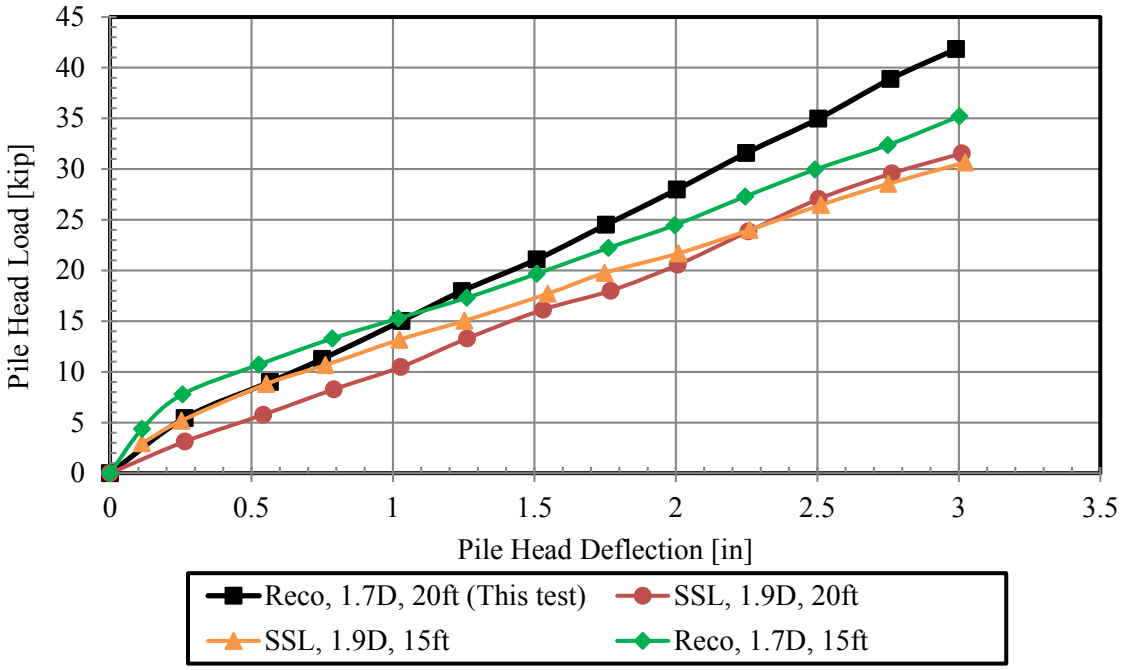

Figure 6-5: Comparison of load versus displacement curves for the 1.7D pile to other piles at similar spacings tested during this study.

6.2.2 P-Multipliers versus Pile Spacing Curves

Figure 6-6 is a plot of the p-multipliers for this test and also all other p-multipliers to date for steel pipe piles near MSE walls with metallic reinforcing. The distance from the back face of the MSE wall to the center of the pile has been normalized by the pile diameter allowing the curve to be used for a broad range of pile sizes at various spacings. The diameter of piles for these tests ranged from 12.75 to 16.0 inches. The soil reinforcing used by Hatch (2014) and Price (2012) was galvanized welded wire grids and the soil reinforcing used by Han (2014), Nelson (2013), and in this test was galvanized ribbed steel strips. The L/H ratio varied between 0.72 for this test to 1.2 for some of the tests done by Nelson (2013). A p-multiplier of 1.0 indicates that there is no interaction between the pile and the MSE wall and a p-multiplier lower than 1.0 is used to account for reduced resistance of piles located closer to the wall.

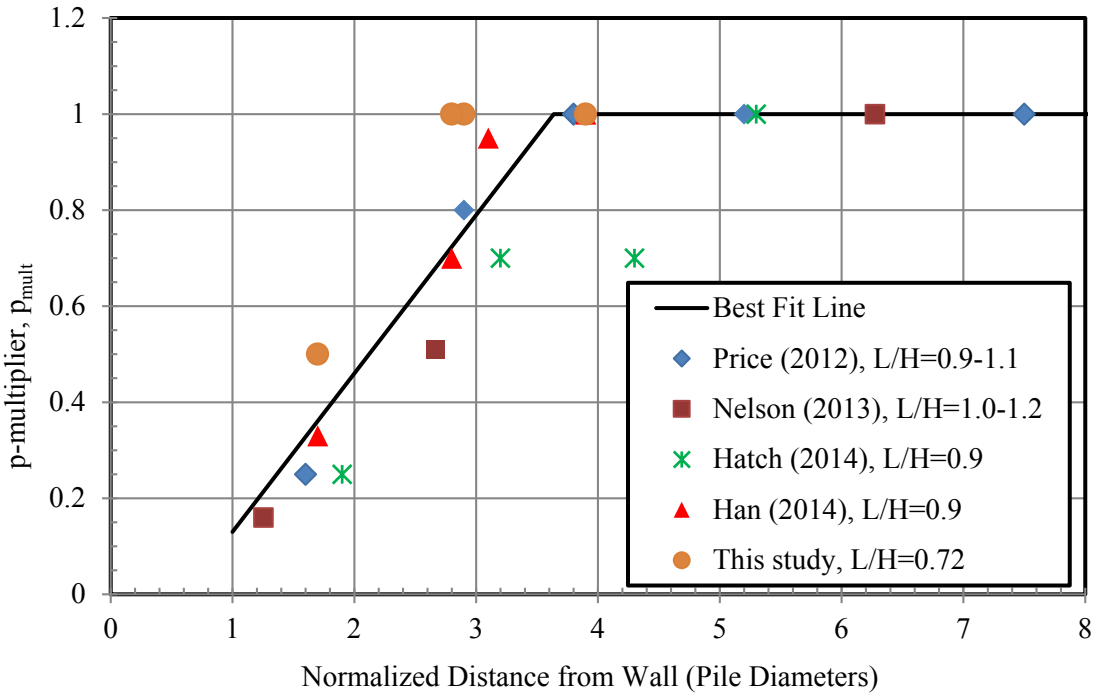

Figure 6-6: P-multiplier curve versus normalized distance from the wall from this study in comparison with previous test results.

As part of this study, a linear regression analysis was performed to develop a relationship between the back-calculated p-multipliers from available tests and the normalized pile spacing (S/D) behind the wall. Only data with an S/D value less than four were used in the regression analysis. The data suggest that piles with normalized spacings greater than four typically had p-multipliers of 1.0 indicating that there was no adverse effect arising from the presence of the wall. A total of 15 data points with an S/D less than four were available for developing the correlation. The best-fit relationship for the p-multiplier, p_{mult}, was given by the linear equation

$$p_{mult} = 0.33\frac{S}{D} - 0.20 \qquad \text{for } S/D < 3.6 \text{ and} \qquad (6\text{-}1a)$$

$$p_{mult} = 1.0 \qquad \text{for } S/D > 3.6 \qquad (6\text{-}1b)$$

where

p_{mult} is the p-multiplier,

S is the distance from the center of the pile to the back face of the MSE wall, and

D is the pile diameter.

Equation (6-1) has a R^2 value of 0.80 indicating that about 80% of the variation in the p-multiplier is accounted for by the equation.

The bi-linear equation predicted by Equation (6-1a) is plotted along with the data points in Figure 6-6. The p-multipliers from this study and the previous studies generally scatter about the best fit line, although the results from this study are somewhat higher than other results. Nevertheless, the results are not unreasonable considering the variation in relative compaction that apparently develops with low levels of compactive energy near the MSE wall face. These results suggest that the p-multiplier versus S/D curve is relatively insensitive to the L/H ratio for the various MSE walls as well as the reinforcing type (strip versus welded wire grid). This result indicates that a single p-multiplier equation (Equation 6-1) may provide reasonable predictive power for a range of MSE wall types and geometries.

6.2.3 Pile Head Load versus Rotation Curves

The rotation of the pile was measured using data from string potentiometers attached to the pile as described in section 4.2. Figure 6-7 and Figure 6-8 show the measured values compared to those predicted by LPILE for the 1.7 and 2.9D tests. The results are shown for the LPILE model with and without the simulated surcharge. The results of the pile head rotation predicted by LPILE are very close to measured values. The worst agreement is for the 1.7D test. This is expected because the predicted load-displacement curve was also the worst for the 1.7D pile. The agreement between the 2.8 and 3.9D tests is very similar to that of the 2.9D test.

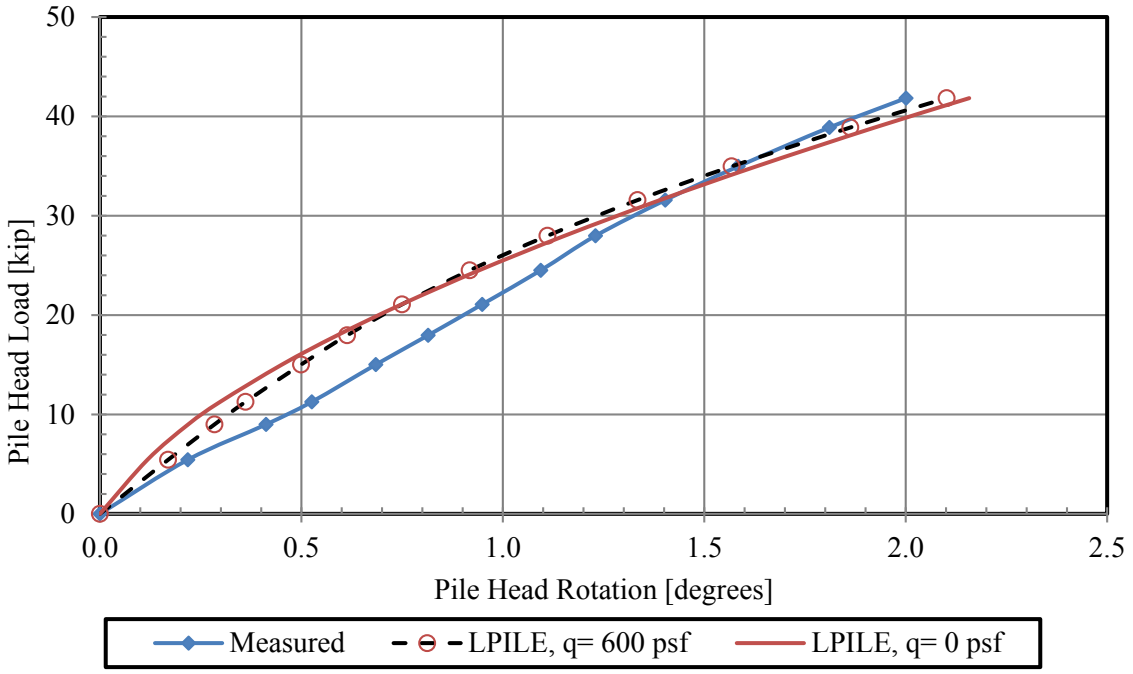

Figure 6-7: Comparison of pile head load versus rotation curves computed by LPILE to measured pile head load versus rotation curves for the 1.7D test.

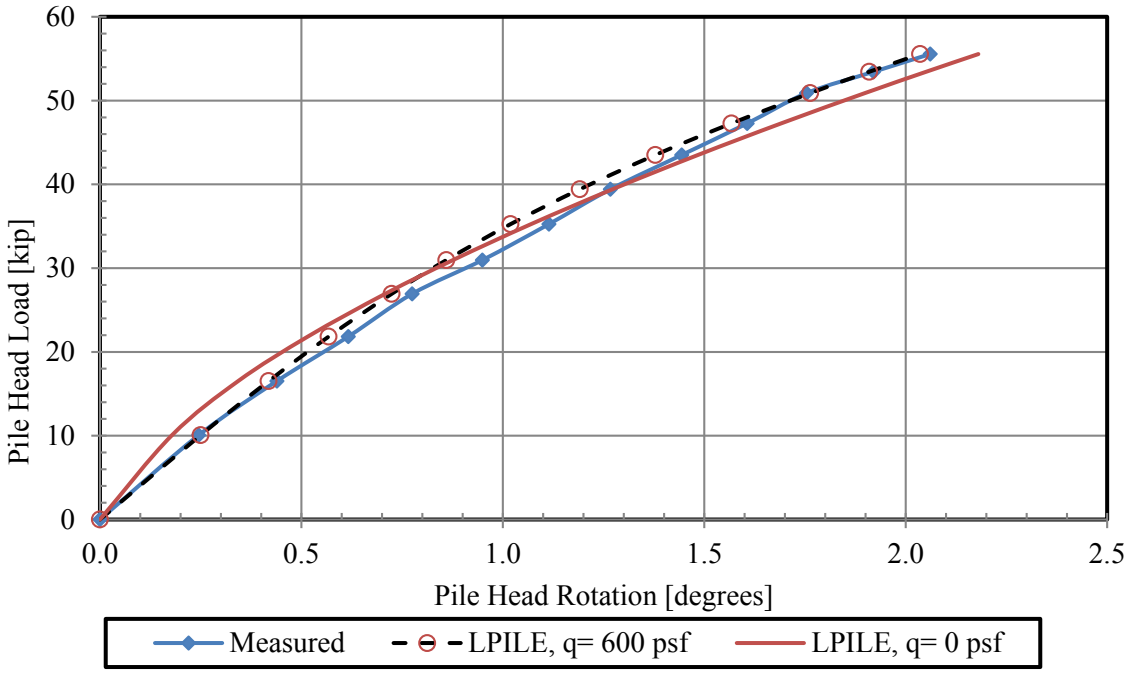

Figure 6-8: Comparison of pile head load versus rotation curves computed by LPILE to measured pile head load versus rotation curves for the 2.9D test.

6.2.4 Bending Moment versus Depth Curves

Bending moment versus depth curves for each of the piles was computed using strain gauge data as described previously. The measured bending moment is compared to the bending moment computed by the LPILE model with and without the simulated surcharge, q, for each of the test piles. Figure 5-32 through Figure 5-35 show this comparison at two different pile head loads for each test. The same soil profiles were used in LPILE as discussed in section 6.1.

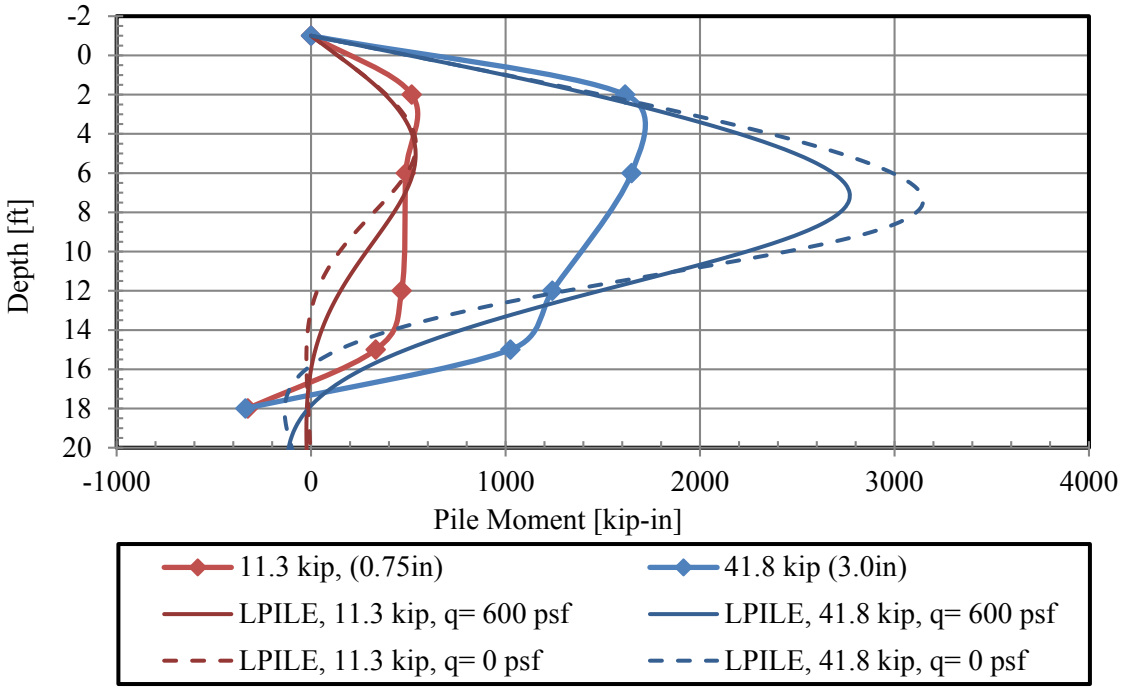

Figure 6-9: Measured and computed pile bending moment at multiple pile head load levels for the 1.7D test.

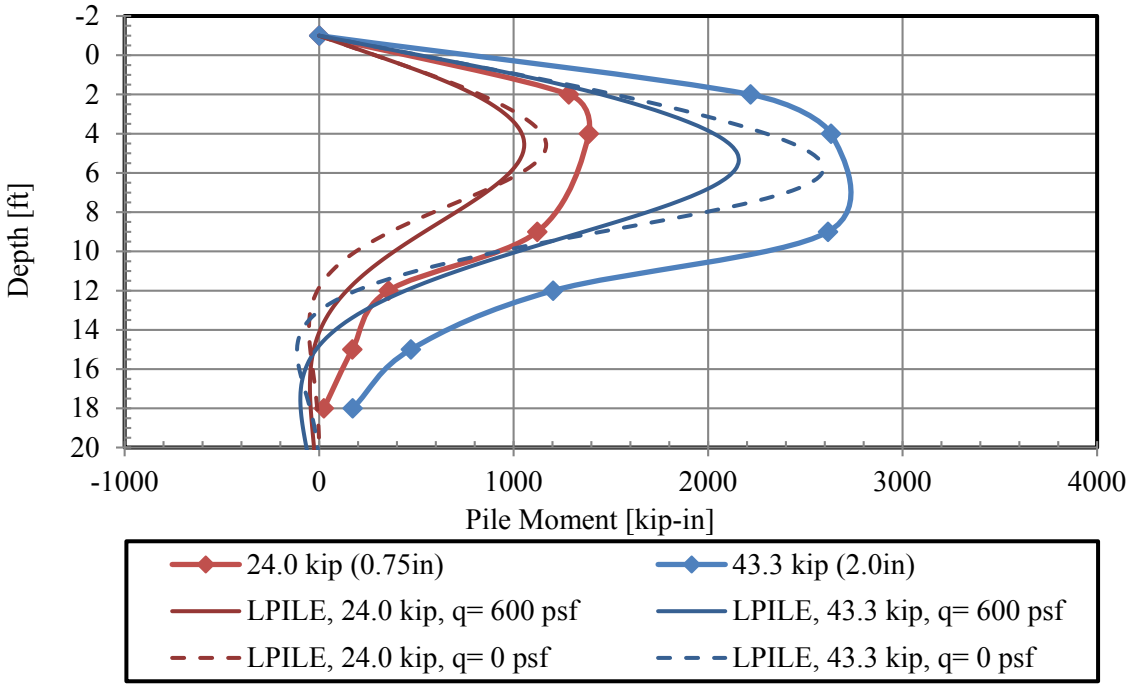

Figure 6-10: Measured and computed pile bending moment at multiple pile head load levels for the 2.8D test.

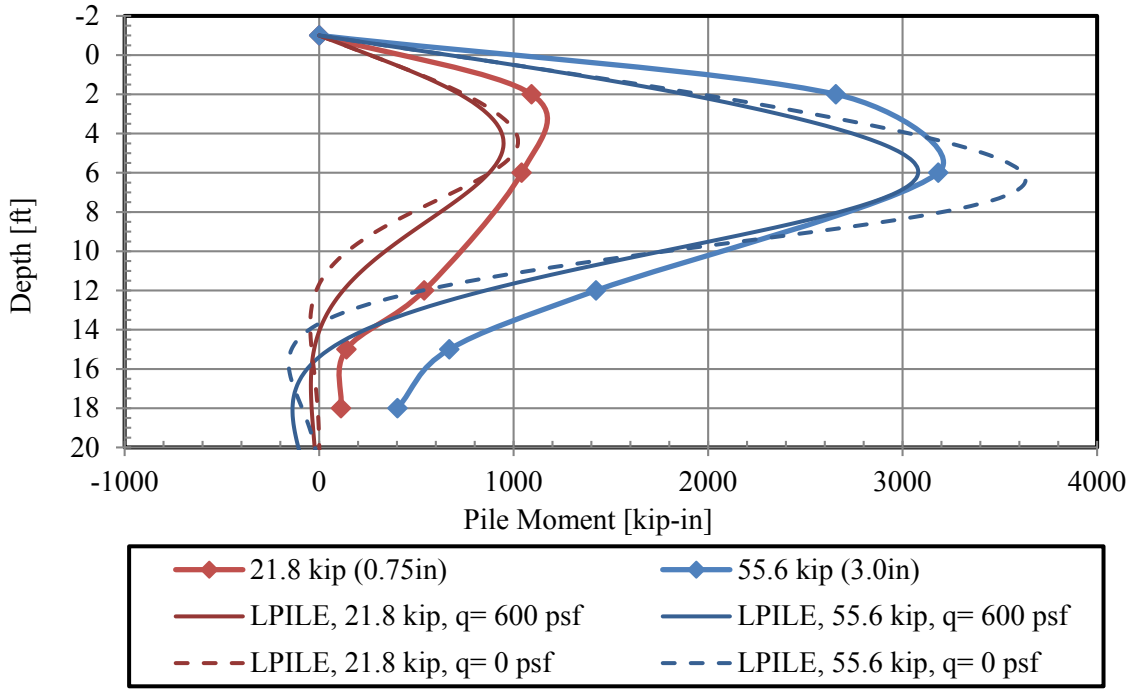

Figure 6-11: Measured and computed pile bending moment at multiple pile head load levels for the 2.9D test.

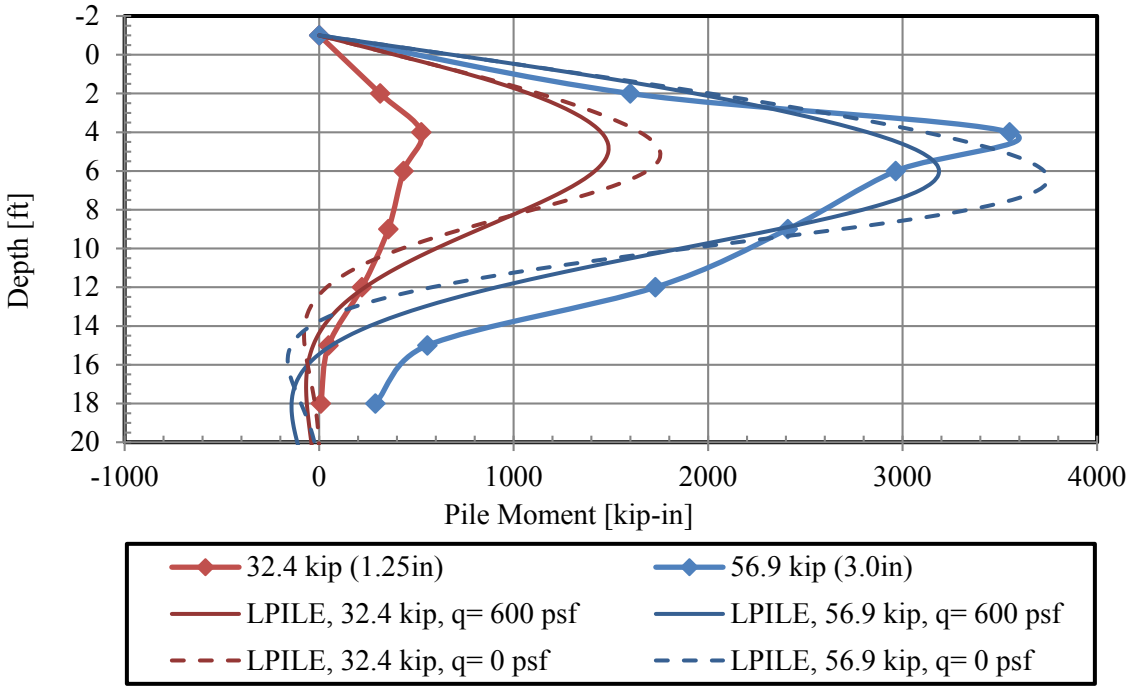

Figure 6-12: Measured and computed pile bending moment at multiple pile head load levels for the 3.9D test.

The agreement of the results varies between each test and pile head load. The depth of the maximum moment predicted by LPILE is within 2 ft. of the measured for all the tests except the 1.7D test and the predicted maximum moment is within 25% of the computed maximum moment for the 2.8, 2.9, and 3.9D tests and within 40% of 1.7D test. The relatively poor prediction of maximum moment is consistent with the fact that the load-deflection curve for this case was not well predicted in comparison with the other test piles. Overall, the LPILE model with the simulated surcharge does not seem to clearly match the measured curve better than the model without the applied surcharge in this case.

7 CONCLUSION

Piles used to support bridge abutments are commonly located within the reinforced zone of MSE walls and are subject to lateral loading from earthquakes and thermal expansion and contraction. Full scale lateral load testing was performed on 12.75x0.375 pipe piles spaced at 3.9, 2.9, 2.8, and 1.7 pile diameters behind an MSE wall which was constructed for this research to determine appropriate reduction factors for lateral pile resistance based on pile spacing behind the back face of the wall. Galvanized ribbed steel strips were used as the reinforcement for the MSE wall in the vicinity of the four piles discussed in this report. The relationship between lateral pile load and induced load on the soil reinforcement was also investigated through instrumentation of four layers of soil reinforcement located near the laterally loaded piles. Based on data gathered in this research in combination with previous testing and research the following conclusions can be made. The conclusions are primarily limited to the type of wall tested but may be applied to other situations using engineering judgment.

7.1 Conclusions Relative to Lateral Pile Resistance

1. Lateral pile resistance tends to decrease as spacing from the back of the MSE wall decreases.
2. In general, piles spaced further than 3.8D behind the MSE wall can be assumed to have no reduction in lateral resistance because of interaction with the wall. However, the

resistance of piles spaced closer to the wall than 3.8D can be modeled in LPILE using a p-multiplier less than 1.0 that varies linearly with spacing from the wall.

3. P-multipliers for the 3.9D, 2.9D, 2.8D, and 1.7D tests are 1.0, 1.0, 1.0, and 0.5, respectively. These multipliers are higher than expected based on previous testing and research and are likely a result of increased compactive effort near the 2.9D and 2.8D piles. These results indicate the importance of consistent compactive effort for the soil between the pile and the wall in evaluating lateral pile resistance.
4. The p-multiplier versus normalized spacing relationships were relatively unaffected by the reinforcement length to height (L/H) ratio or the reinforcement type (ribbed strip versus welded wire).
5. The reinforced backfill can be modeled in LPILE using the API Sand (1982) method with a friction angle of 31 degrees and a subgrade modulus of approximately 60 pci when a uniform surcharge of 600 psf is applied. If no surcharge is applied, a friction angle of 39 degrees and subgrade modulus of 260 pci is more appropriate.

7.2 Conclusions Relative to Force Induced in the Reinforcements

1. Induced load in reinforcement tends to increase with depth to the 2nd or 3rd layer of reinforcement after which it decreases.
2. Induced load in the reinforcement tends to increase as pile spacing decreases.
3. Induced load in the reinforcement decreases rapidly with increased transverse distance from the pile.
4. The tensile force induced in the reinforcement can be estimate using a regression equation which considers the influence of pile load, pile spacing behind the wall, reinforcement depth or vertical stress on the reinforcement, and transverse spacing of

the reinforcement. The R^2 value for the model is approximately 0.70, indicating that about 70% of the observed variation is accounted for by the equation.

5. Despite the relatively high applied lateral loads and pile displacements, the reinforcements were successful in reducing lateral wall displacements to acceptable levels for all of the tests. Max wall panel displacement was highest for the 2.8D test and reached 0.35 in. at 3.0 in. of pile head displacement. The max wall displacement at 3.0 in. of pile head displacement was similar for all of the other tests but was only approximately 0.15 to 0.20 inches.

7.3 Recommendations for Further Research

A pinned head loading condition was used for all lateral load tests. In reality, piles supporting a bridge abutment generally have a concrete pile cap which prevents rotation of the pile head. It seems likely that lateral loads the pile can sustain and loads induced in the reinforcement at various depths would be affected by the amount the pile head is able to rotate. Furthermore, the pile cap causes all of the piles to be loaded simultaneously. Studies have shown that the resistance of piles loaded as a group have reduced resistance (Rollins et al. 2006), but it is not known if the same reduced resistance can be applied to piles near a wall face. All tests completed for this research consisted of static loading conditions and only one cycle was used. In an earthquake, loading would be applied more quickly and would be cyclic. Also, loading from thermal expansion and contraction is cyclic. Hence, it would be beneficial to establish the response of pile lateral resistance when subject to cyclic loading conditions.

Nelson (2013) found that the presence of a lightly compacted free drainage gravel layer near the wall reduced the lateral resistance of piles. A similar conclusion can be reached assuming that the higher resistance of the 2.8 and 2.9D tests from this research was caused by higher

compaction of the soil between the wall and the piles. Hence, soil compaction appears to play a very important role in the lateral resistance and should be studied further.

It is likely that wall panel configuration near the pile being tested has an effect on the pile lateral resistance and on total panel displacement, especially for piles spaced closer than about 4D. It is difficult to determine the relationship from this research because the panel configuration was different for each test as well as the pile spacing. Additional research could be performed to determine if additional reduction factors are necessary based on panel configuration.

REFERENCES

American Petroleum Institute (API) (1982). "API recommended practice for planning, designing and constructing fixed offshore platforms" API RP 2A, 13th Edition.

Berg, R.R., Christopher, B.R., and Samtani, N.C. (2009). "Design of Mechanically Stabilized Earth Walls and Reinforced Soil Slopes" FHWA, Washington, D.C., Report No. FHWA-NHI-10-024.

Han, J. (2014). "Lateral Resistance of Piles Near 15 Foot Vertical MSE Abutment Walls Reinforced with Ribbed Steel Strips" MS Thesis, Department of Civil and Environmental Engineering, Brigham Young University, Provo, UT

Hatch, C. (2014). "Lateral Resistance of Piles Near Vertical MSE Abutment Walls" MS Thesis, Department of Civil and Environmental Engineering, Brigham Young University, Provo, UT.

Huang, J., et al. (2011). "Numerical analysis of a laterally loaded shaft constructed within an MSE wall" Geotextiles and Geomembranes 29.3 (2011): 233-241.

Lee, K.L., and Singh, A. (1971). "Compaction of granular soils" Engineering Geology and Soils Engineering Symposium, Proceedings of the 6th Annual. No. pp 63-64.

Nelson, K.R. (2013). "Lateral Resistance of Piles Near Vertical MSE Abutment Walls at Provo Center Street" MS Thesis, Department of Civil and Environmental Engineering, Brigham Young University, Provo, UT.

Pierson, M.C., et al. (2009). "Capacity of laterally loaded shafts constructed behind the face of a mechanically stabilized earth block wall" *No. K-TRAN: Ku-07-6.*

Price, J.S. (2012). "Lateral Resistance of Piles Near Vertical MSE Abutment Walls" MS Thesis, Department of Civil and Environmental Engineering, Brigham Young University, Provo, UT.

Reese, L.C., et al. (2004). “User’s manual of LPILE plus 5.0 for windows”, Ensoft Inc., Austin, TX.

Rollins, K.M., Price, J.S., and Nelson, K.R. (2013). “Lateral Resistance of Piles Near Vertical MSE Abutment Walls” No. UT-13.04. 2013.

Rollins, K.M., et al. (2006). “Pile Spacing Effects on Lateral Pile Group Behavior: Analysis” Journal Of Geotechnical & Geoenvironmental Engineering 132, no. 10 (October 2006): 1272-1283.

APPENDIX A. FACTOR OF SAFETY AGAINST PULLOUT CALCUALTIONS

Depth below top of wall, Z (ft)	K_r/K_a	F*
0	1.7	20
20	1.2	10

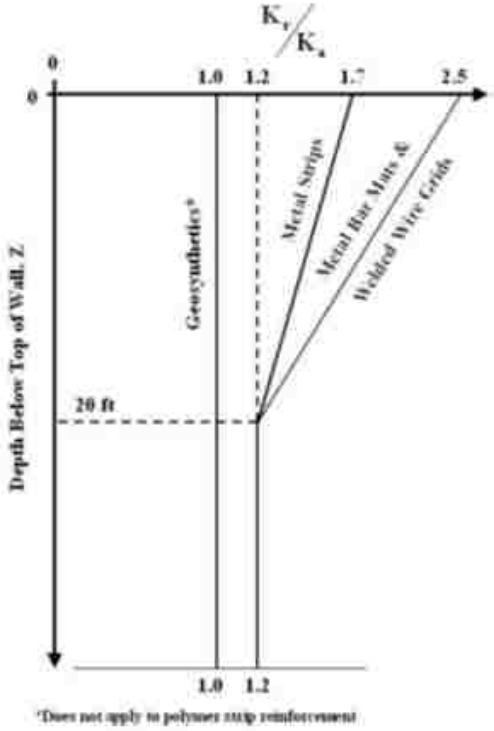

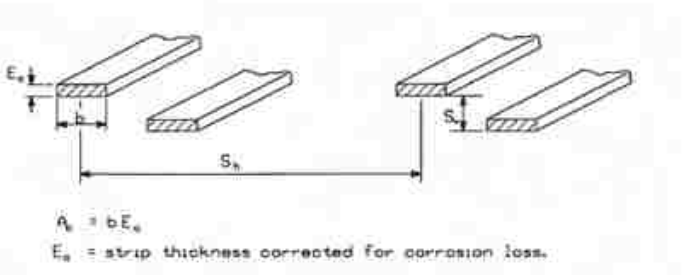

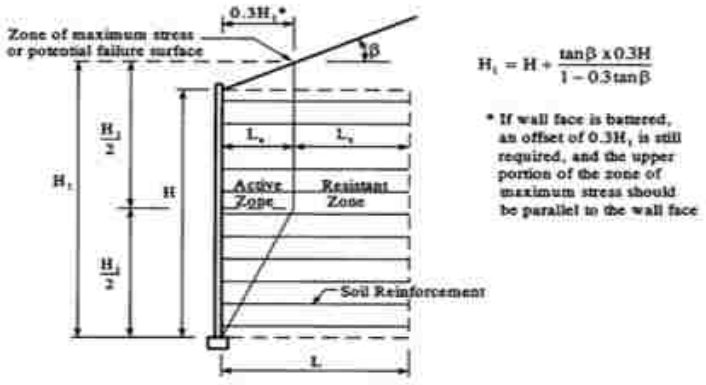

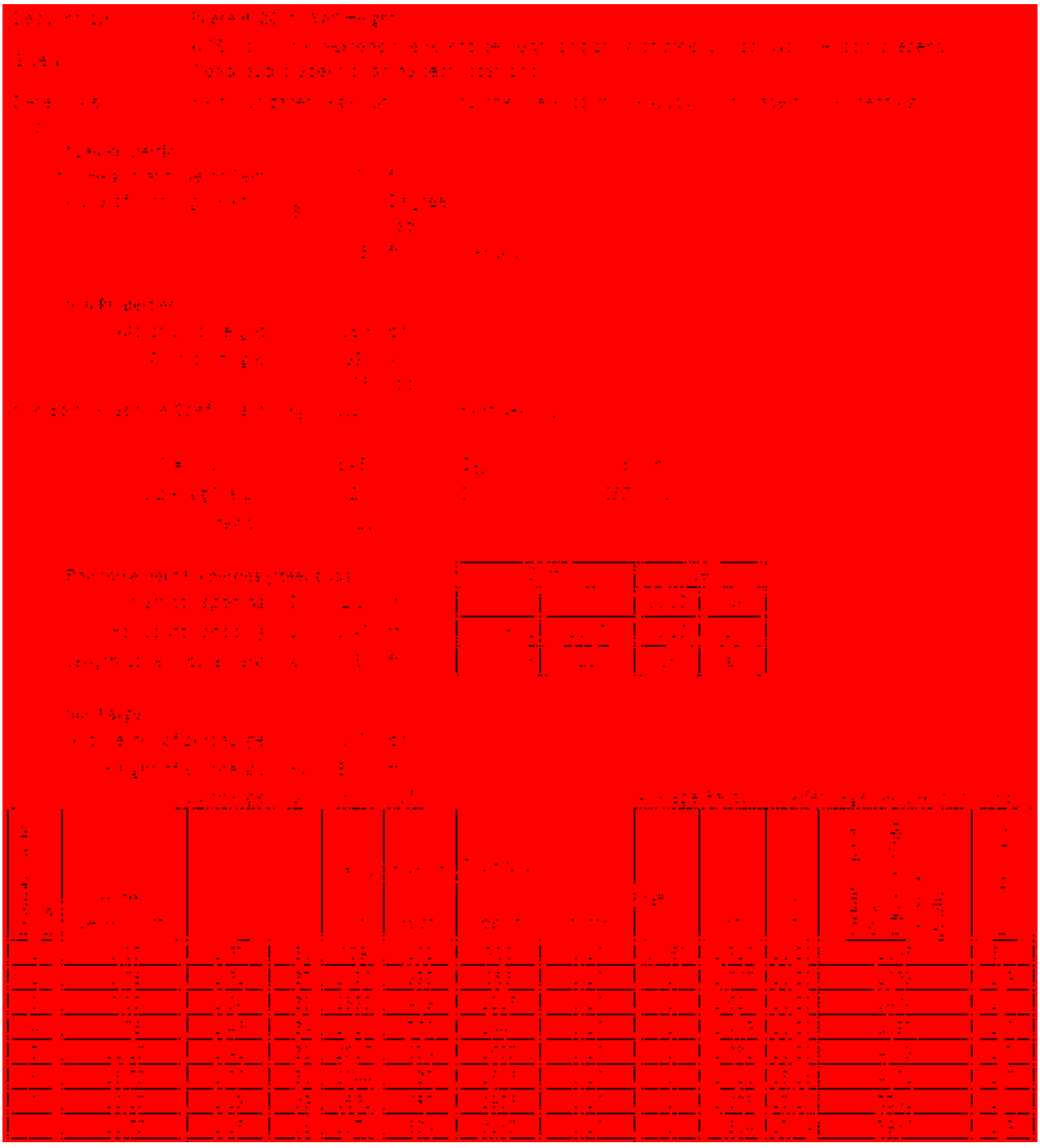

APPENDIX B. GENEVA ROCK LABORATORY TEST REPORTS

Phase 1

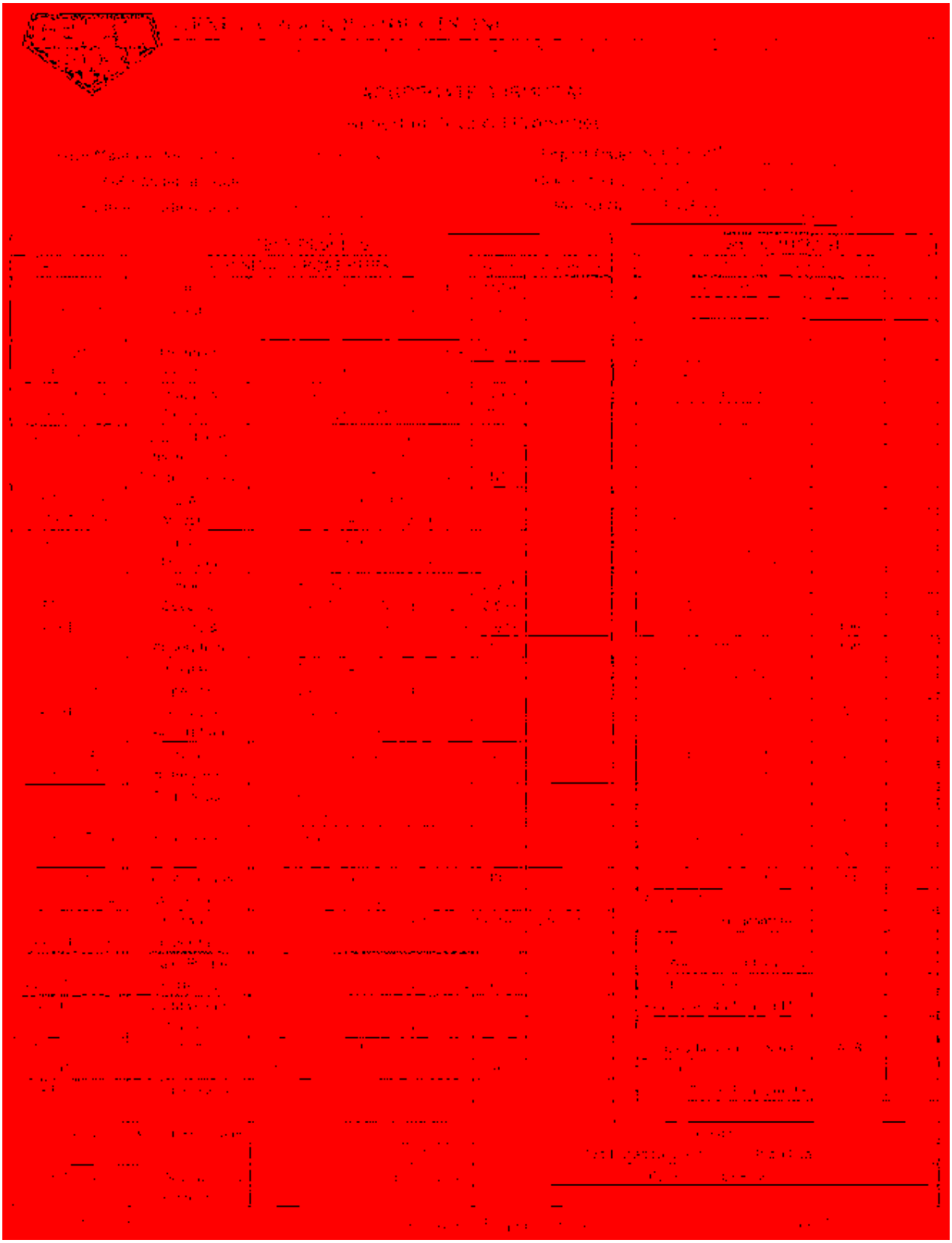

Phase 2

APPENDIX C. LOAD DISPLACEMENT CURVES

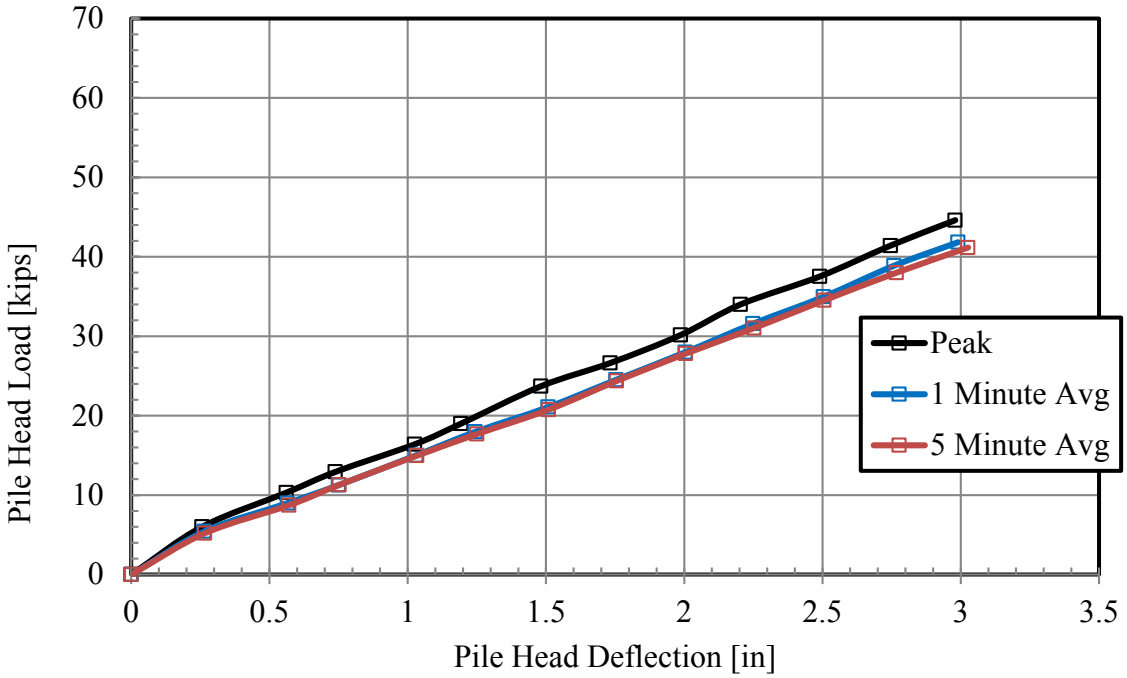

Figure C-1: Load-deflection curves for 1.7D test.

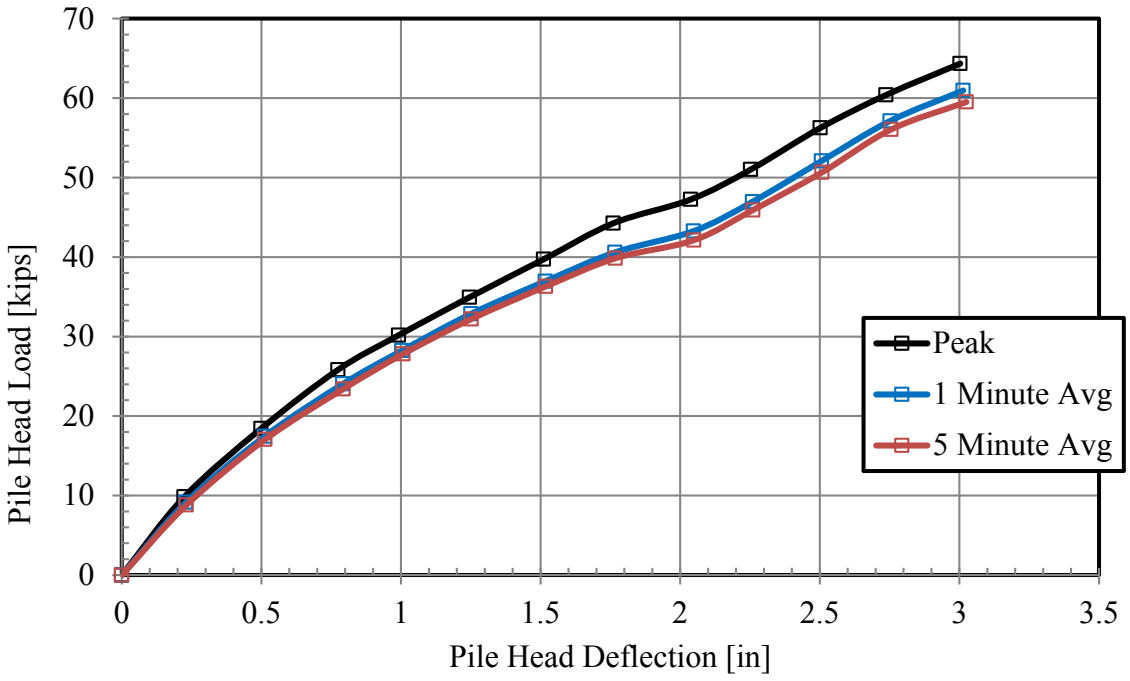

Figure C-2: Load-deflection curves for 2.8D test.

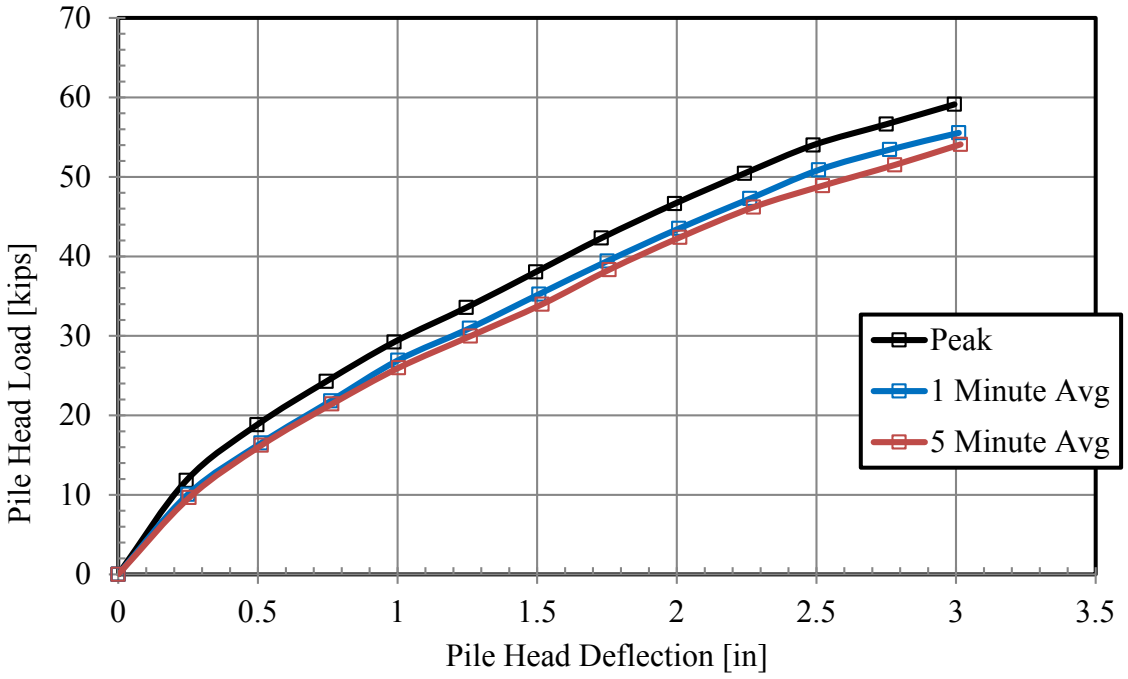

Figure C-3: Load-deflection curves for 2.9D test.

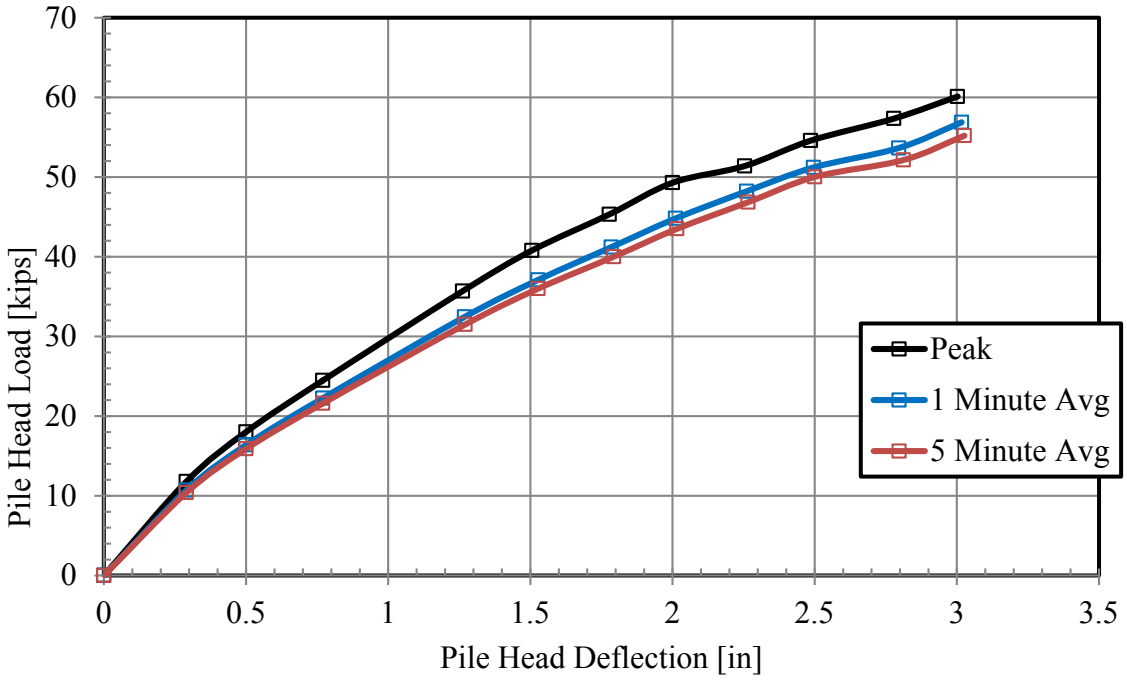

Figure C-4: Load-deflection curves for 3.9D test.

APPENDIX D. GROUND DISPLACEMENT CURVES

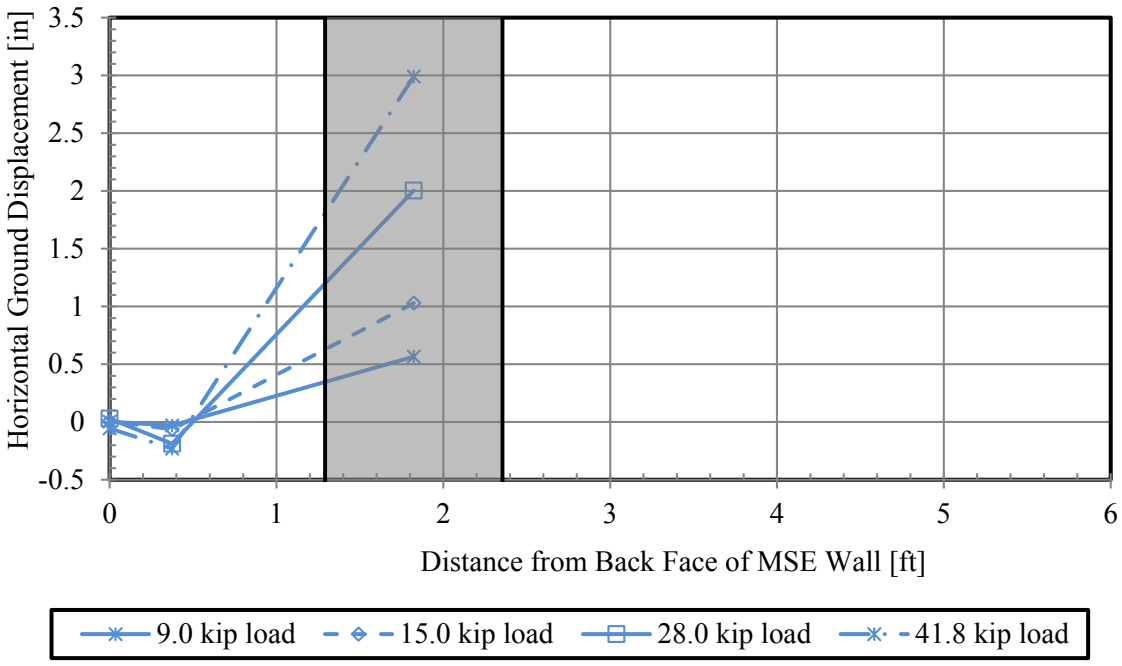

Figure D-1: Horizontal ground displacement at several load levels for 1.7D test.

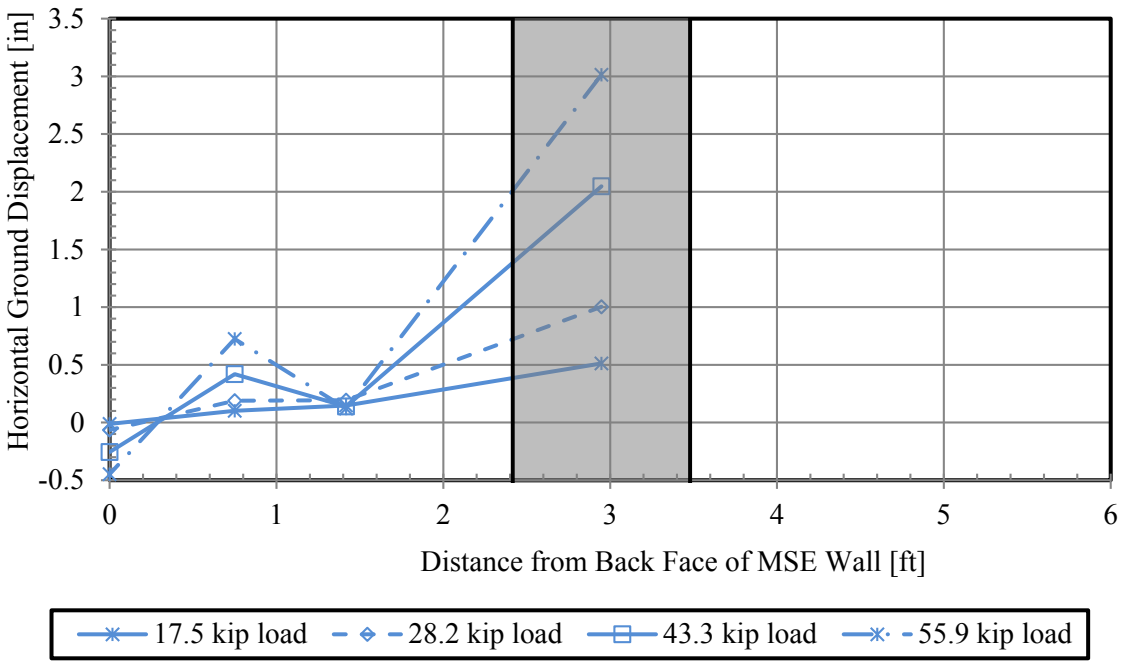

Figure D-2: Horizontal ground displacement at several load levels for 2.8D test.

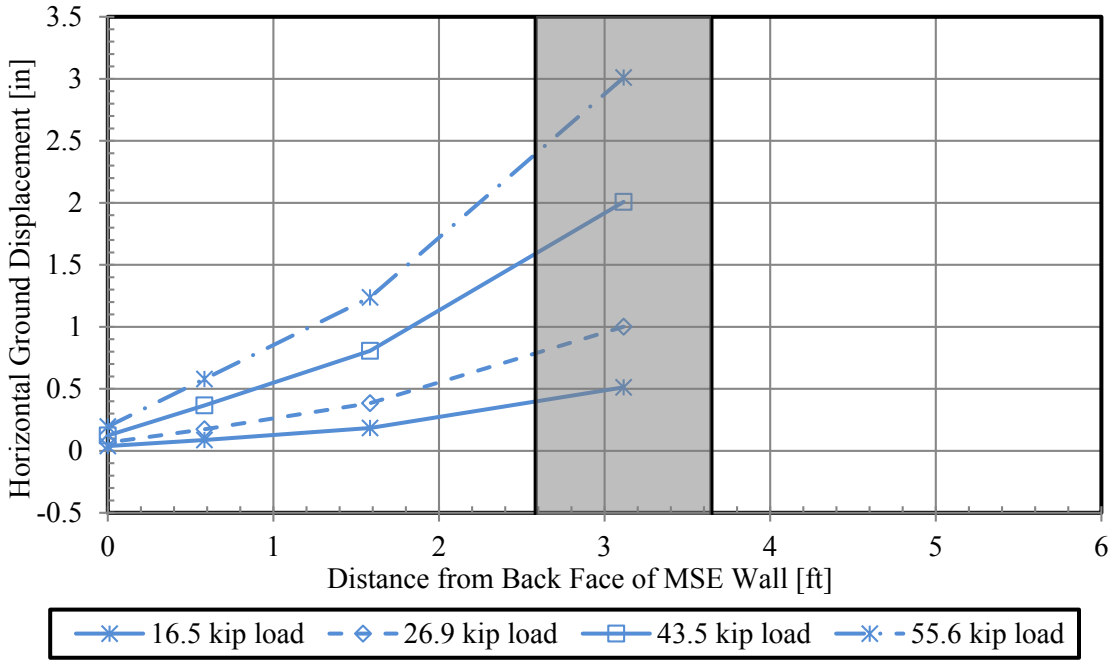

Figure D-3: Horizontal ground displacement at several load levels for 2.9D test.

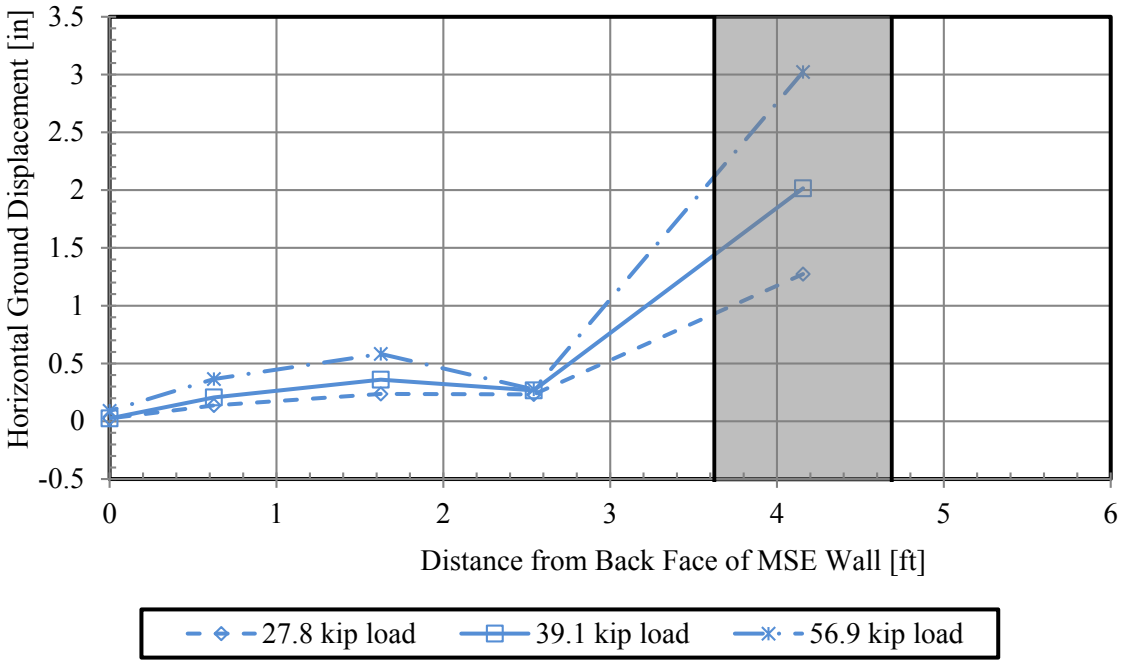

Figure D-4: Horizontal ground displacement at several load levels for 3.9D test.

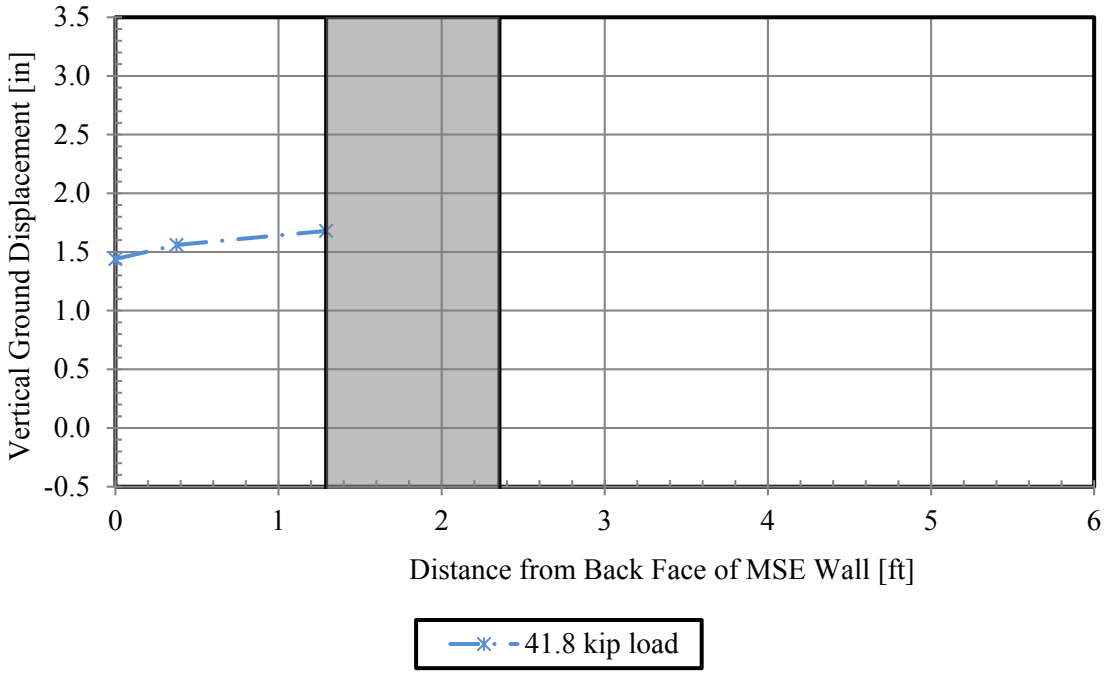

Figure D-5: Vertical ground displacement at peak pile load for 1.7D test.

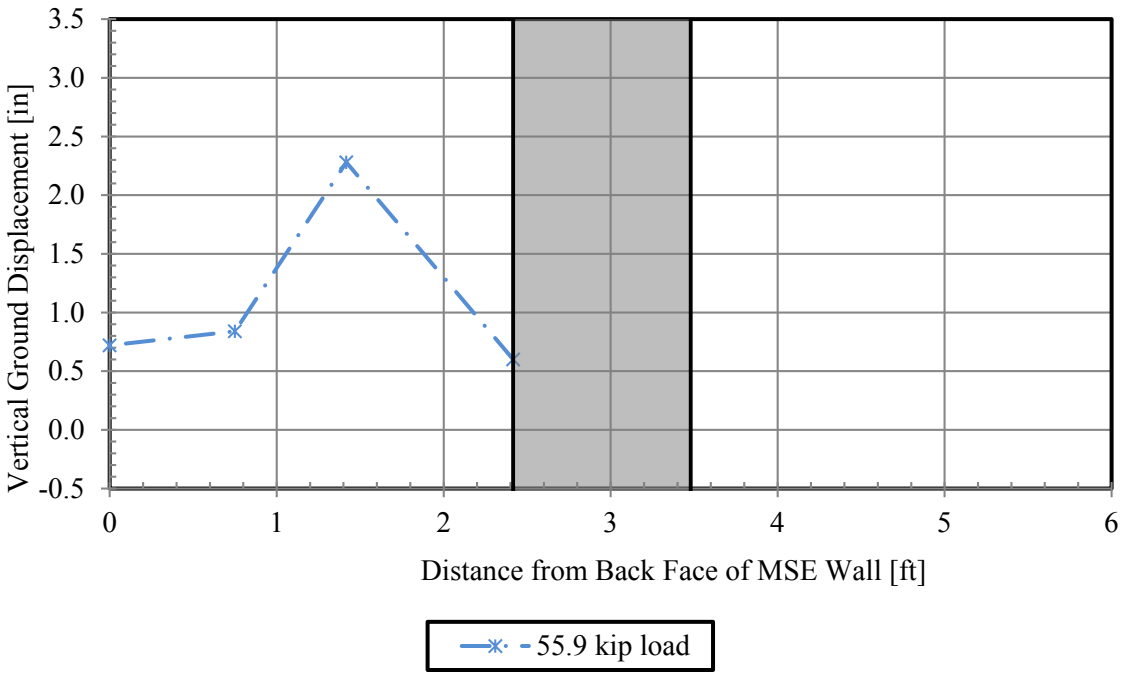

Figure D-6: Vertical ground displacement at peak pile load for 2.8D test.

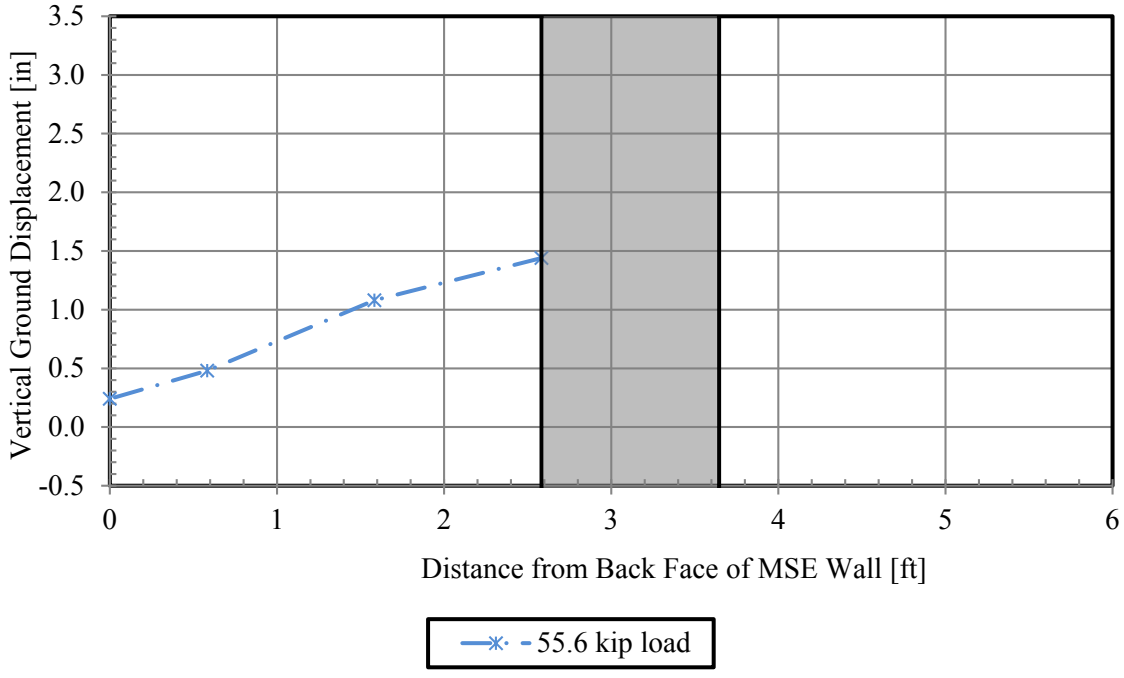

Figure D-7: Vertical ground displacement at peak pile load for 2.9D test.

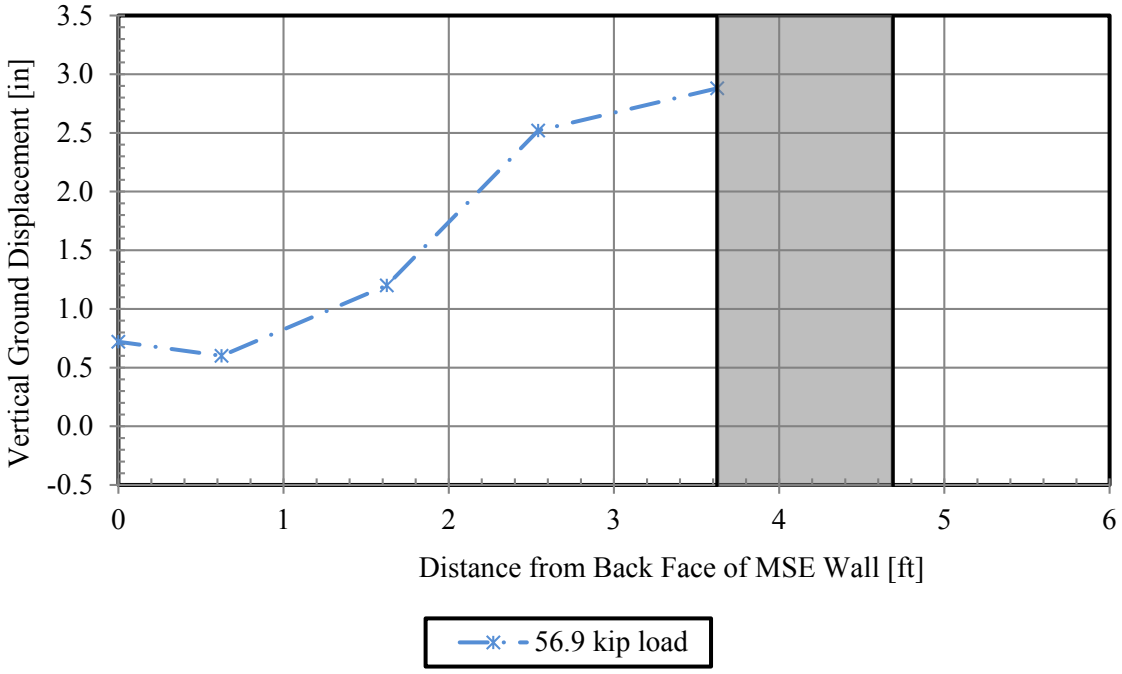

Figure D-8: Vertical ground displacement at peak pile load for 3.9D test.

APPENDIX E. INDUCED FORCE IN THE REINFORCEMENT CURVES

1.7D Soil Reinforcement Curves

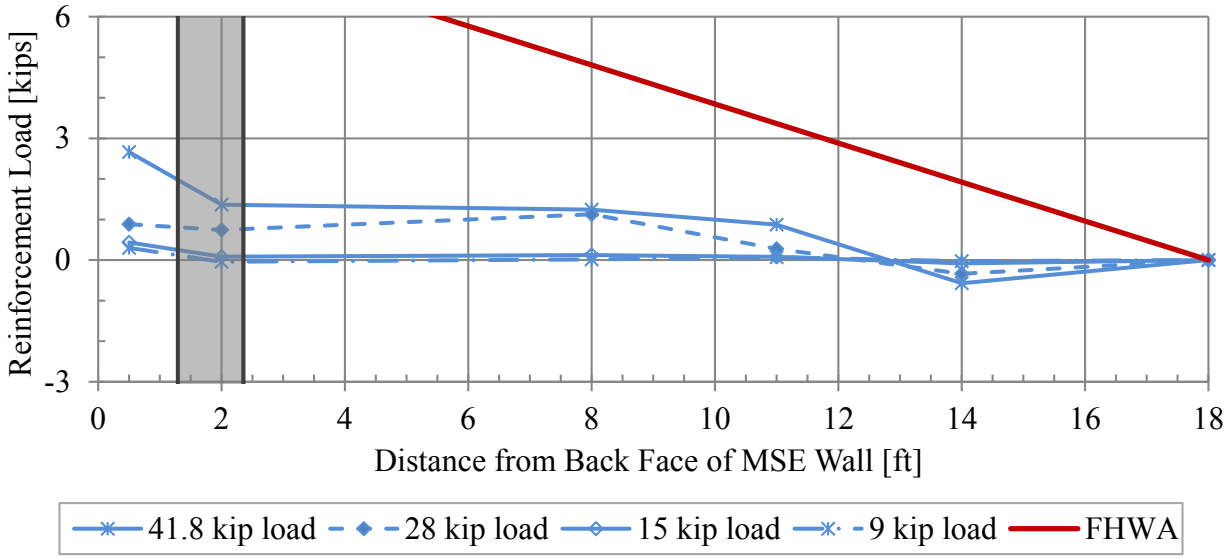

Figure E-1: Induced force in soil reinforcement at varying pile head loads and distances from the back face of the MSE wall for the 1.7D test; 15 in. depth and 9.5 in. transverse spacing from center of pile.

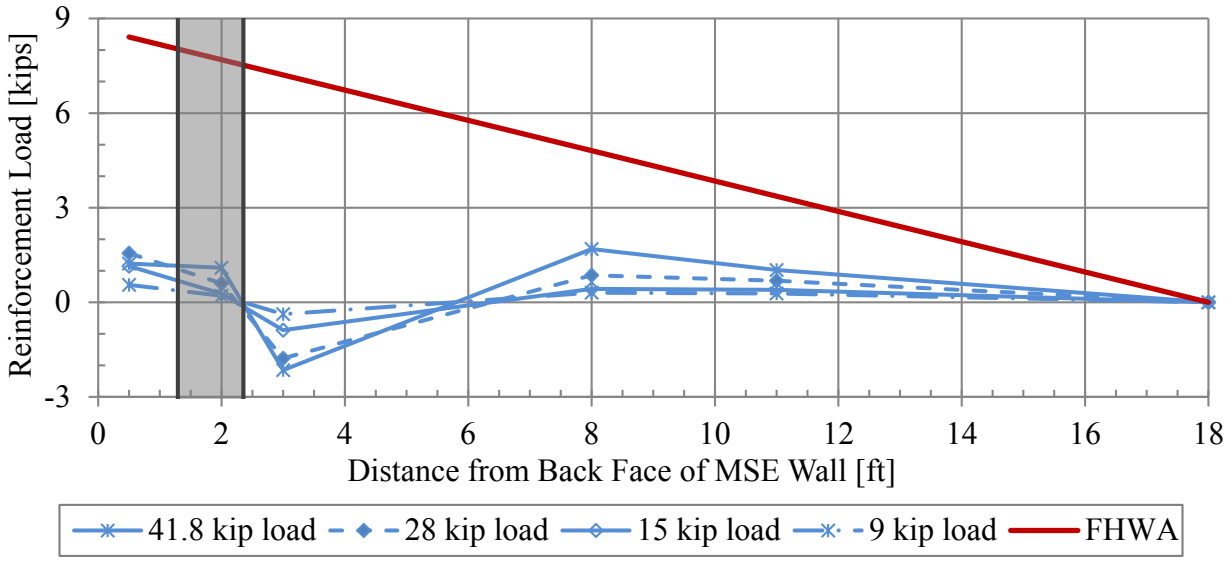

Figure E-2: Induced force in soil reinforcement at varying pile head loads and distances from the back face of the MSE wall for the 1.7D test; 15 in. depth and 35 in. transverse spacing from center of pile.

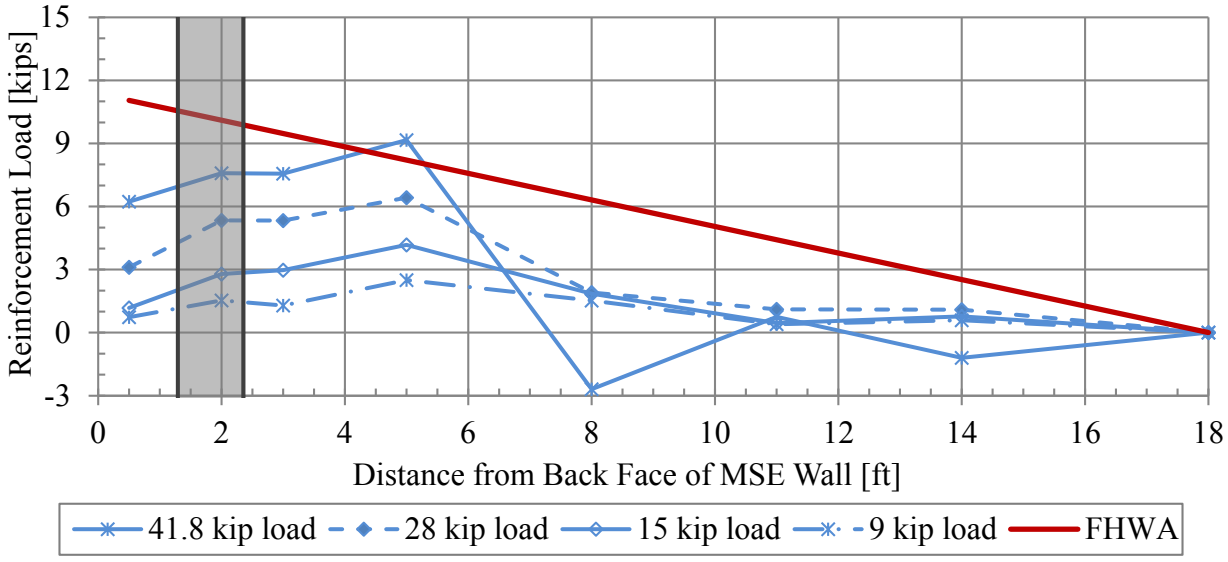

Figure E-3: Induced force in soil reinforcement at varying pile head loads and distances from the back face of the MSE wall for the 1.7D test; 45 in. depth and 11 in. transverse spacing from center of pile.

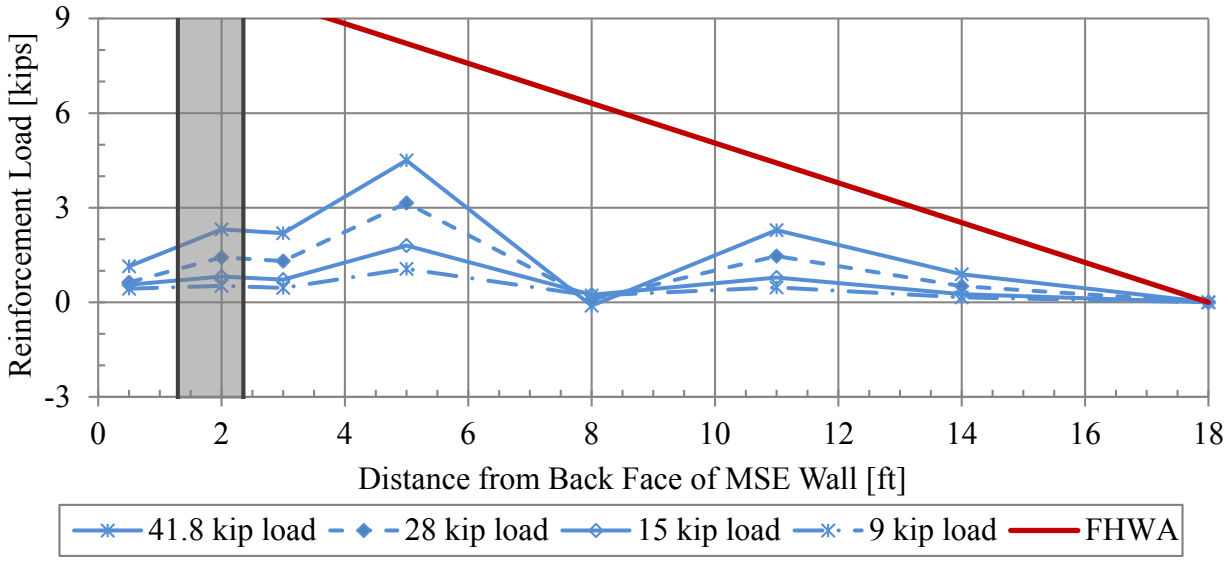

Figure E-4: Induced force in soil reinforcement at varying pile head loads and distances from the back face of the MSE wall for the 1.7D test; 45 in. depth and 37.5 in. transverse spacing from center of pile.

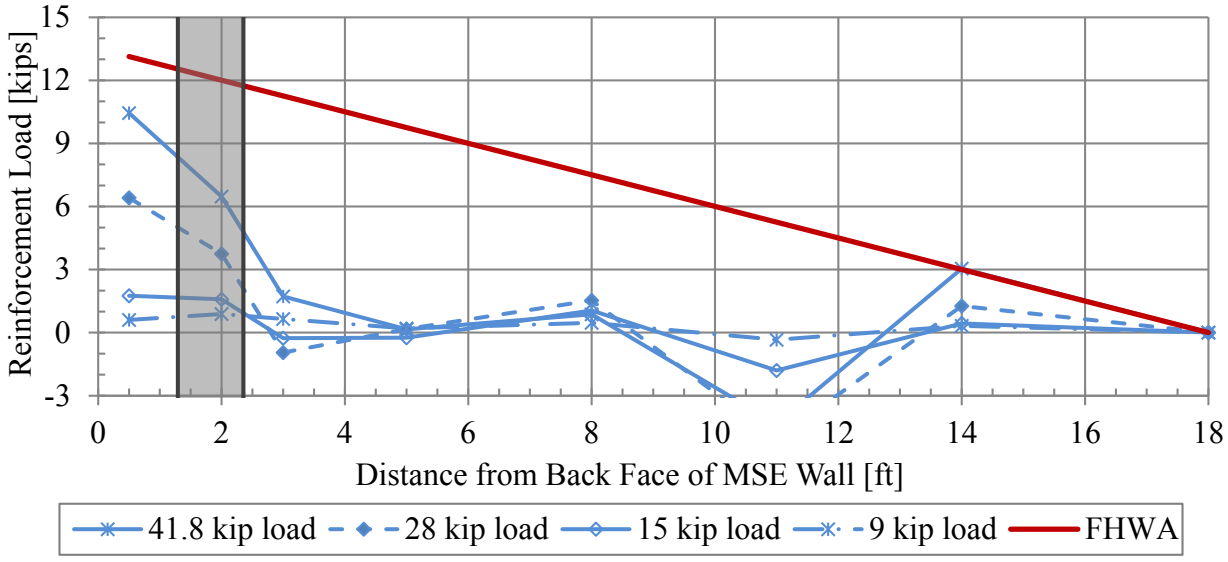

Figure E-5: Induced force in soil reinforcement at varying pile head loads and distances from the back face of the MSE wall for the 1.7D test; 75 in. depth and 9 in. transverse spacing from center of pile.

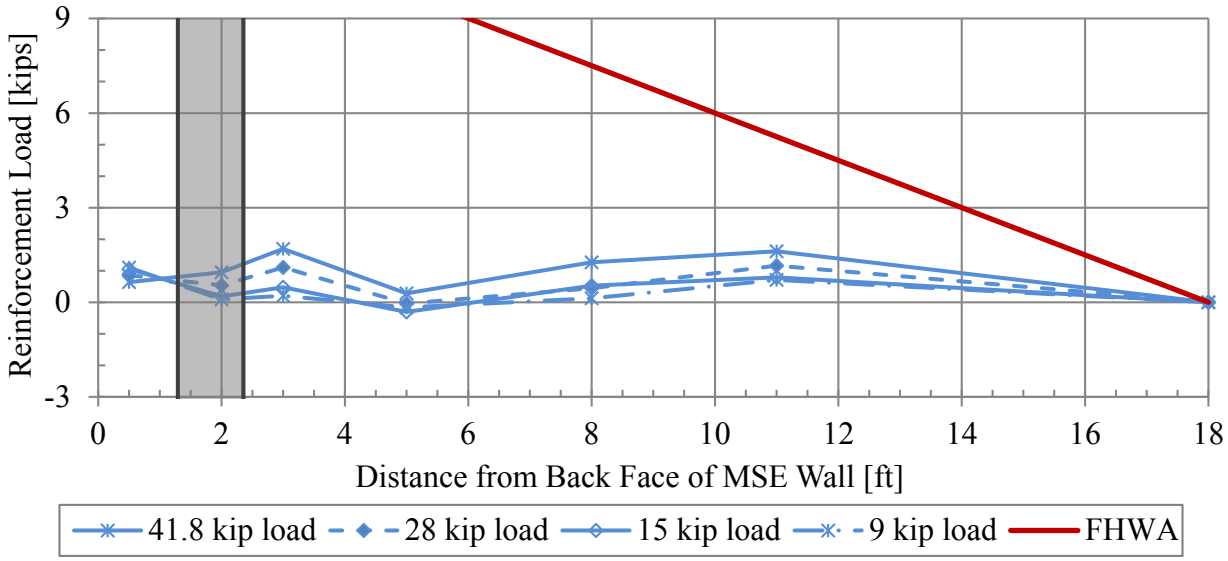

Figure E-6: Induced force in soil reinforcement at varying pile head loads and distances from the back face of the MSE wall for the 1.7D test; 75 in. depth and 36 in. transverse spacing from center of pile.

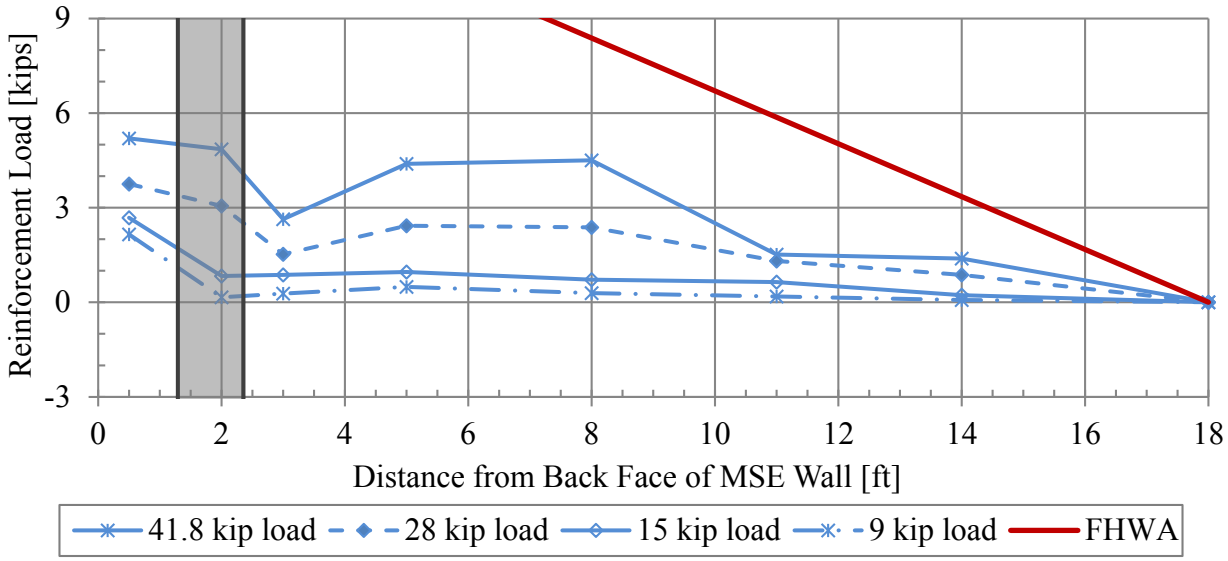

Figure E-7: Induced force in soil reinforcement at varying pile head loads and distances from the back face of the MSE wall for the 1.7D test; 105 in. depth and 9 in. transverse spacing from center of pile.

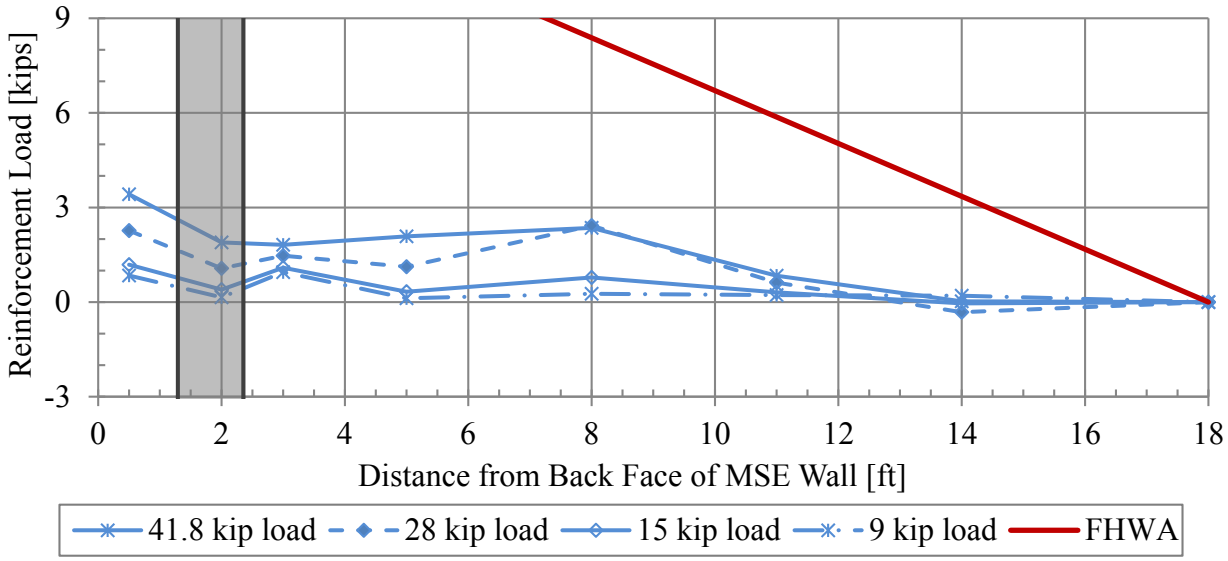

Figure E-8: Induced force in soil reinforcement at varying pile head loads and distances from the back face of the MSE wall for the 1.7D test; 105 in. depth and 35 in. transverse spacing from center of pile.

2.8D Soil Reinforcement Curves

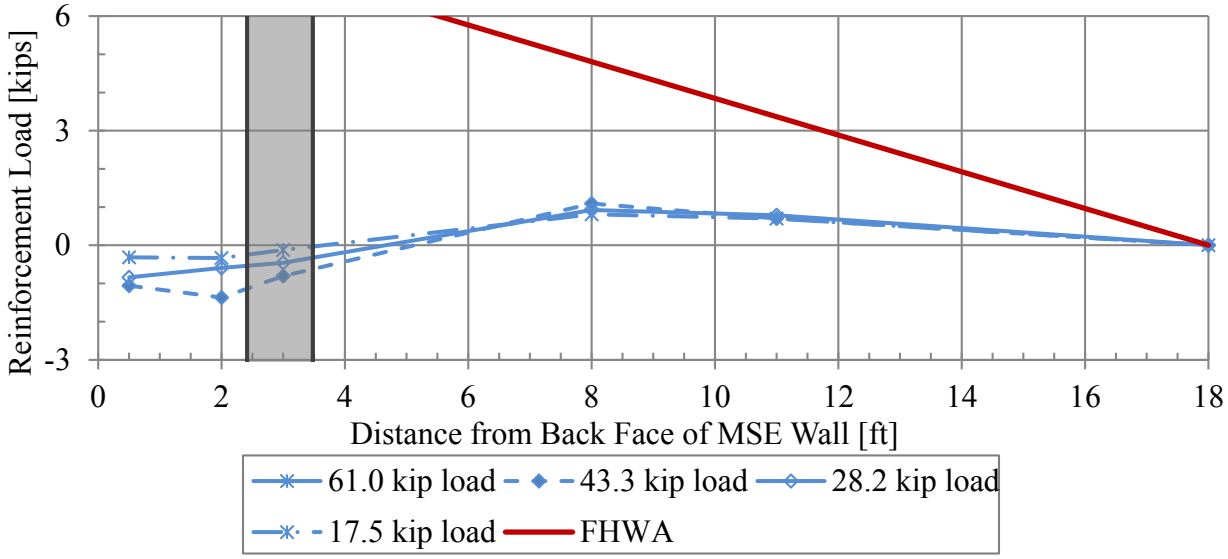

Figure E-9: Induced force in soil reinforcement at varying pile head loads and distances from the back face of the MSE wall for the 2.8D test; 15 in. depth and 24.5 in. transverse spacing from center of pile.

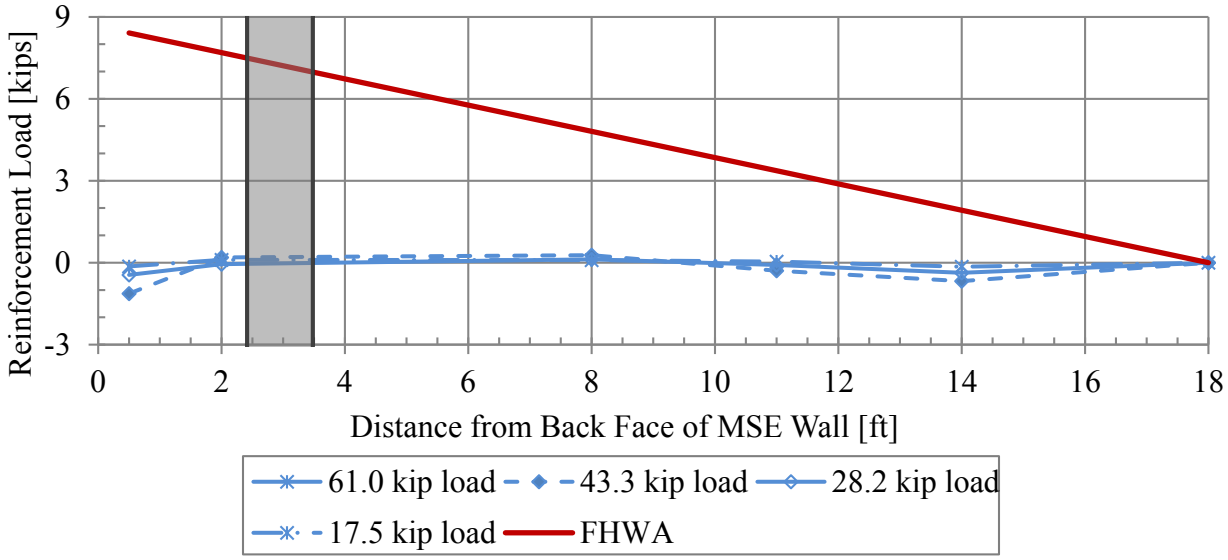

Figure E-10: Induced force in soil reinforcement at varying pile head loads and distances from the back face of the MSE wall for the 2.8D test; 15 in. depth and 50 in. transverse spacing from center of pile.

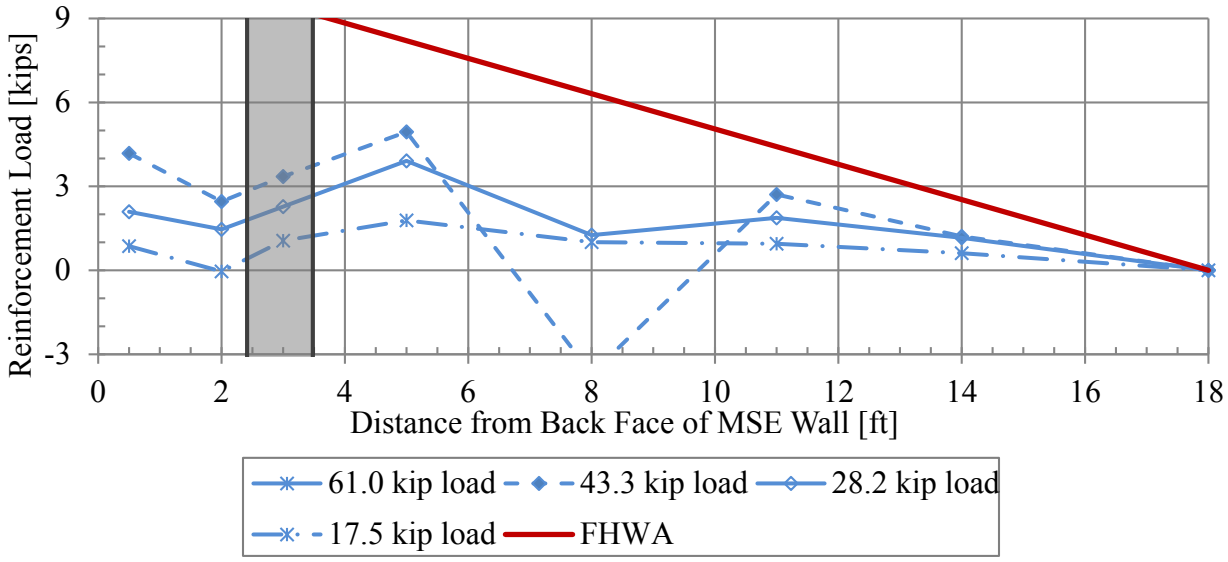

Figure E-11: Induced force in soil reinforcement at varying pile head loads and distances from the back face of the MSE wall for the 2.8D test; 45 in. depth and 20.5 in. transverse spacing from center of pile.

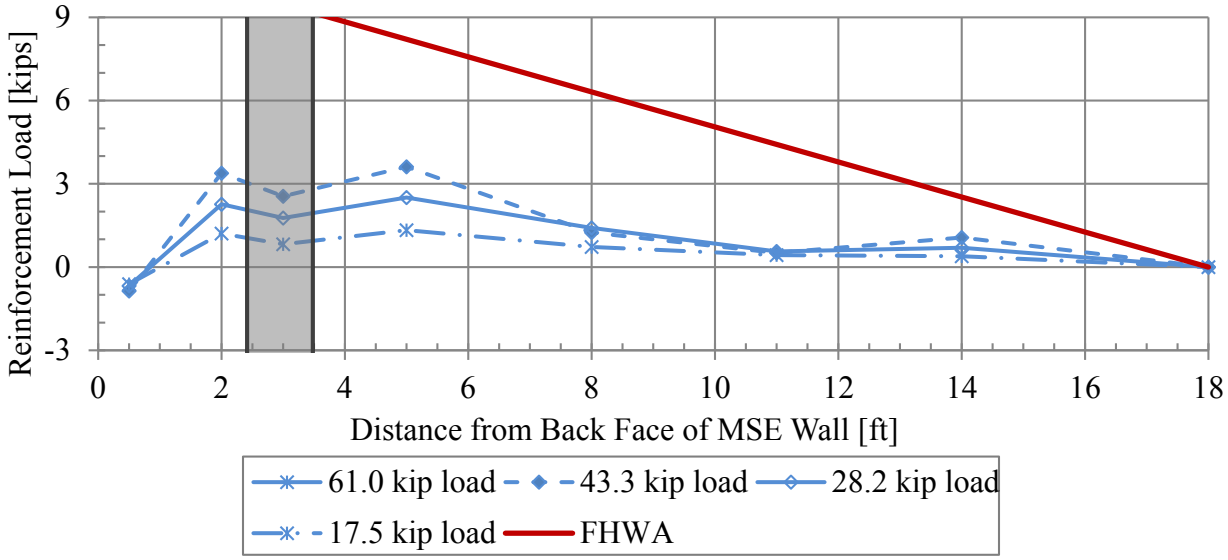

Figure E-12: Induced force in soil reinforcement at varying pile head loads and distances from the back face of the MSE wall for the 2.8D test; 45 in. depth and 47 in. transverse spacing from center of pile.

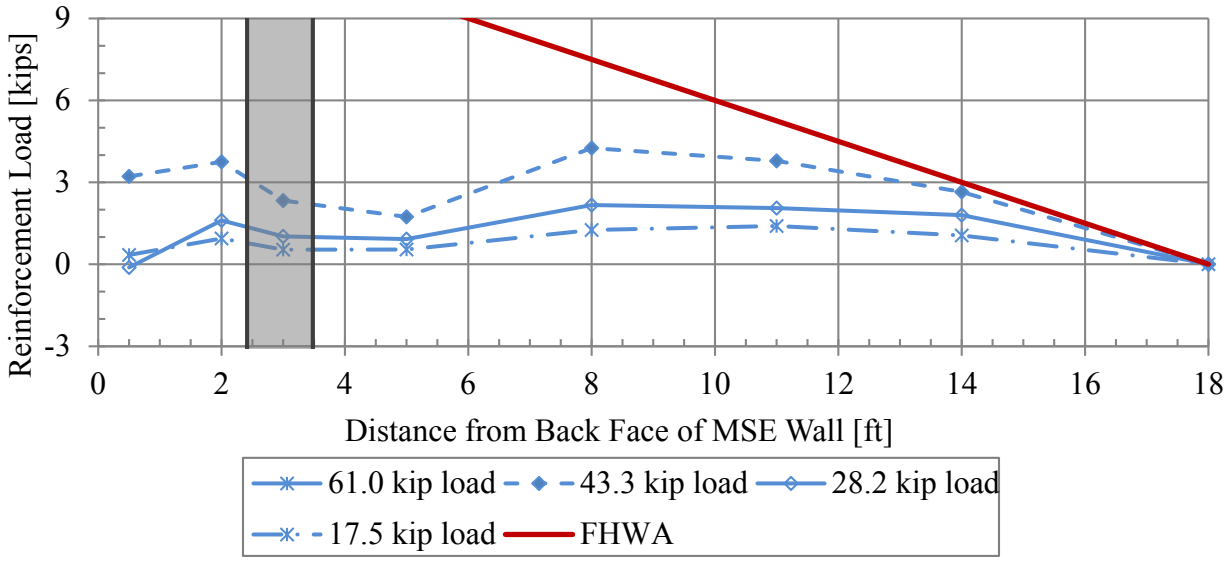

Figure E-13: Induced force in soil reinforcement at varying pile head loads and distances from the back face of the MSE wall for the 2.8D test; 75 in. depth and 22.5 in. transverse spacing from center of pile.

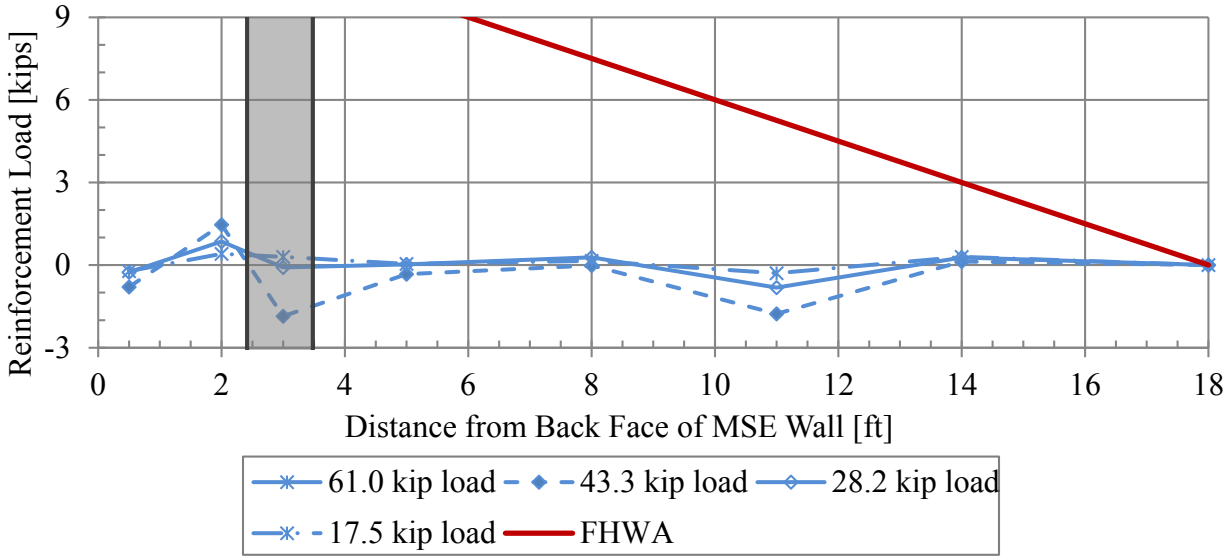

Figure E-14: Induced force in soil reinforcement at varying pile head loads and distances from the back face of the MSE wall for the 2.8D test; 75 in. depth and 49.5 in. transverse spacing from center of pile.

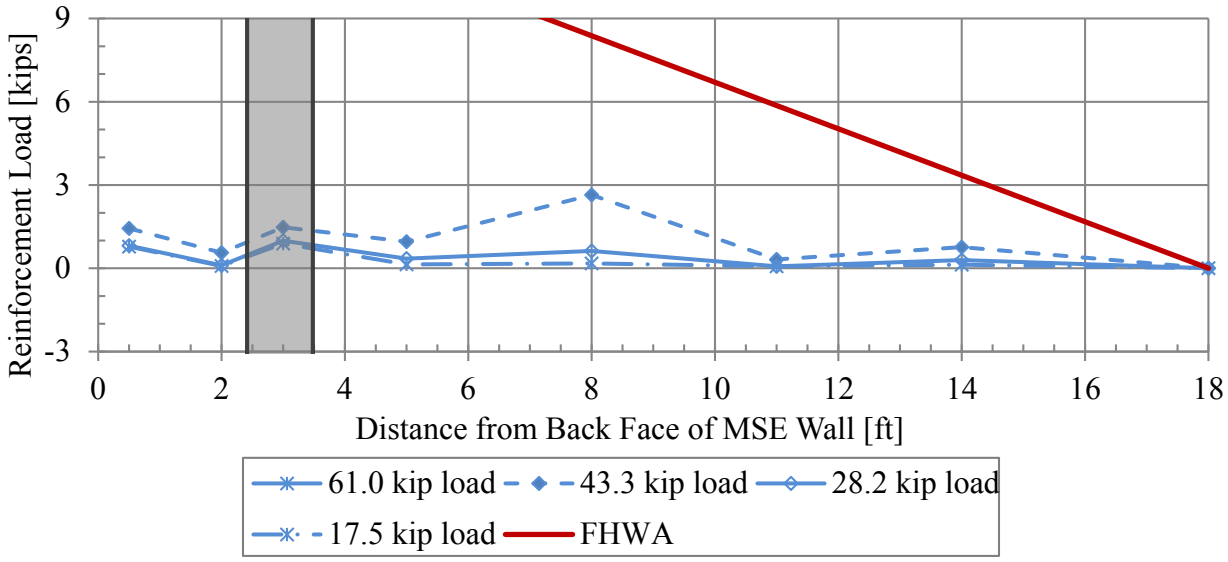

Figure E-15: Induced force in soil reinforcement at varying pile head loads and distances from the back face of the MSE wall for the 2.8D test; 105 in. depth and 23.5 in. transverse spacing from center of pile.

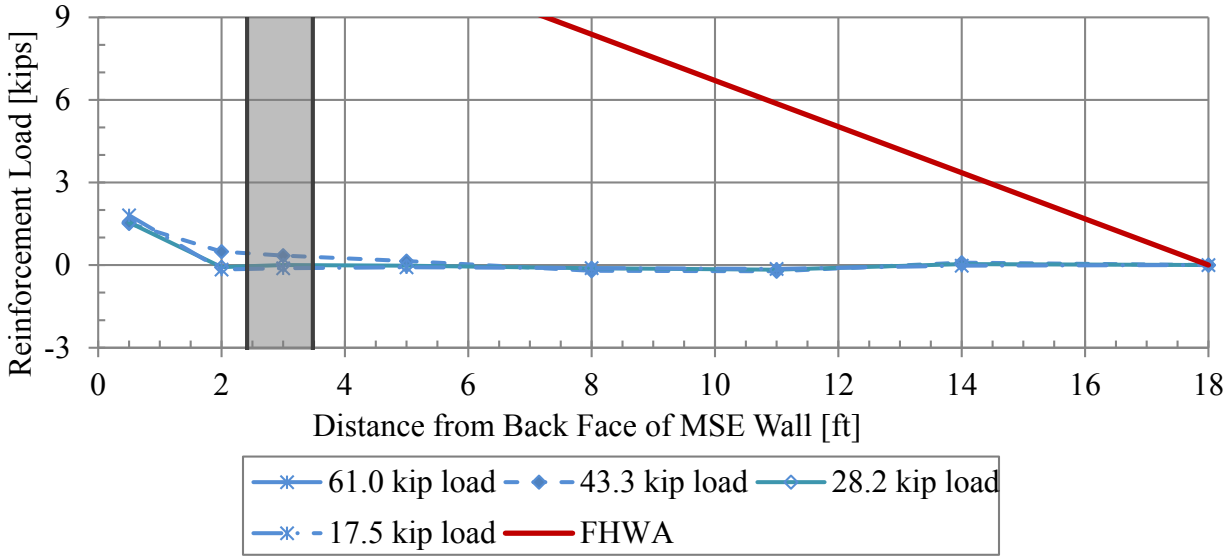

Figure E-16: Induced force in soil reinforcement at varying pile head loads and distances from the back face of the MSE wall for the 2.8D test; 105 in. depth and 50 in. transverse spacing from center of pile.

2.9D Soil Reinforcement Curves

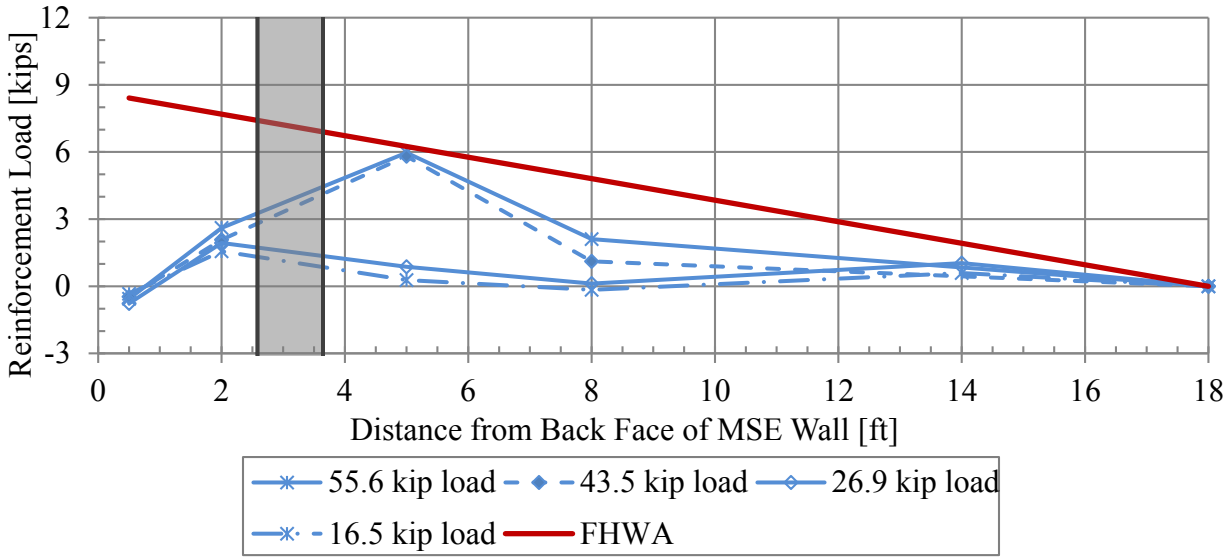

Figure E-17: Induced force in soil reinforcement at varying pile head loads and distances from the back face of the MSE wall for the 2.9D test; 15 in. depth and 10 in. transverse spacing from center of pile.

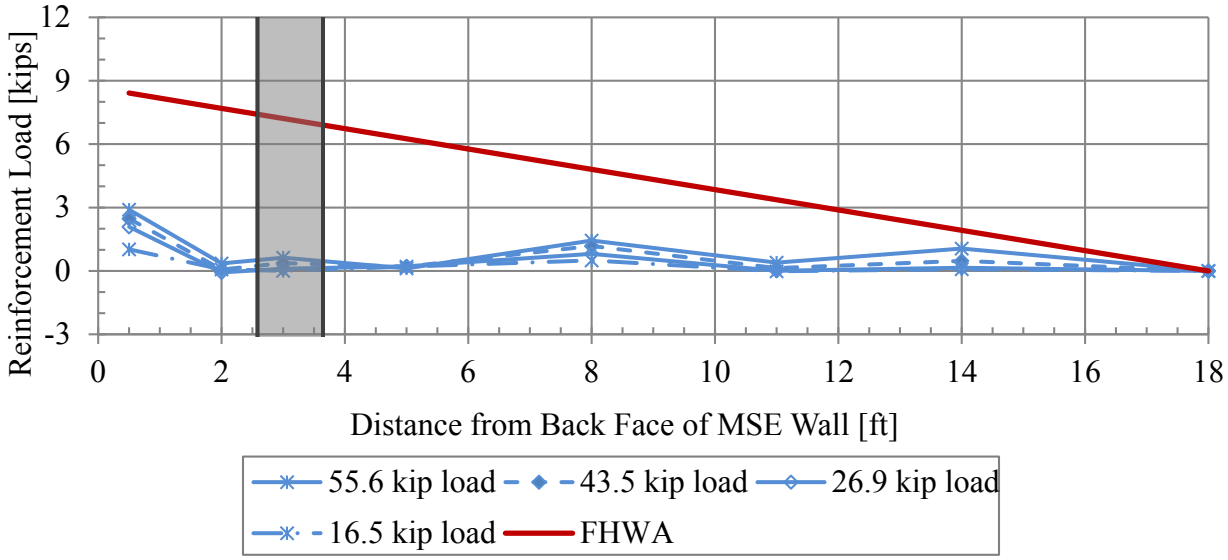

Figure E-18: Induced force in soil reinforcement at varying pile head loads and distances from the back face of the MSE wall for the 2.9D test; 15 in. depth and 35.5 in. transverse spacing from center of pile.

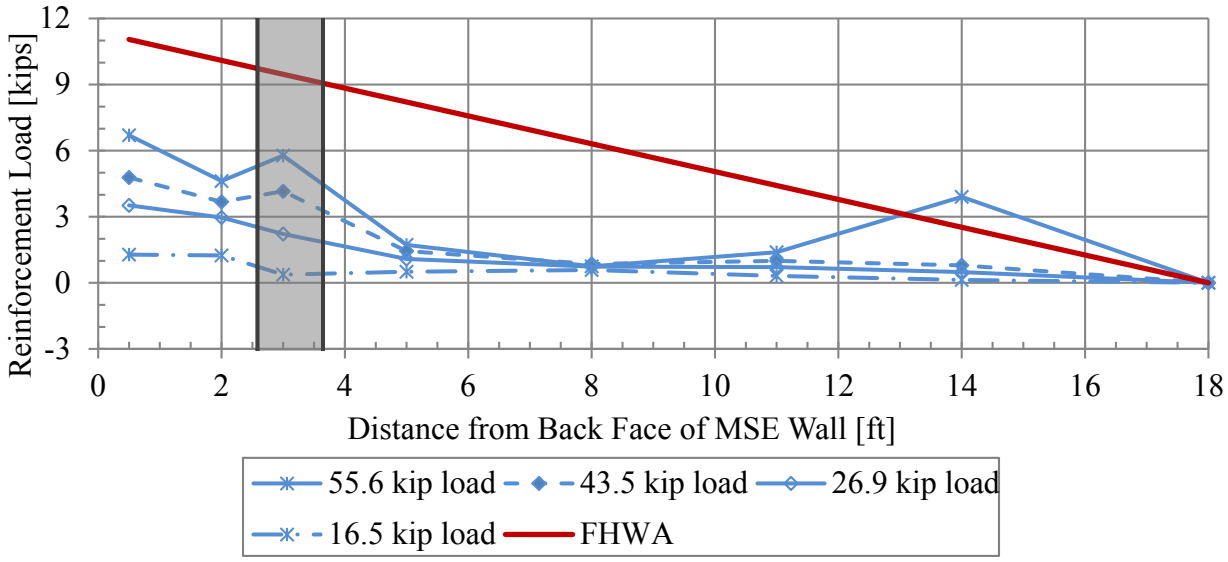

Figure E-19: Induced force in soil reinforcement at varying pile head loads and distances from the back face of the MSE wall for the 2.9D test; 45 in. depth and 12 in. transverse spacing from center of pile.

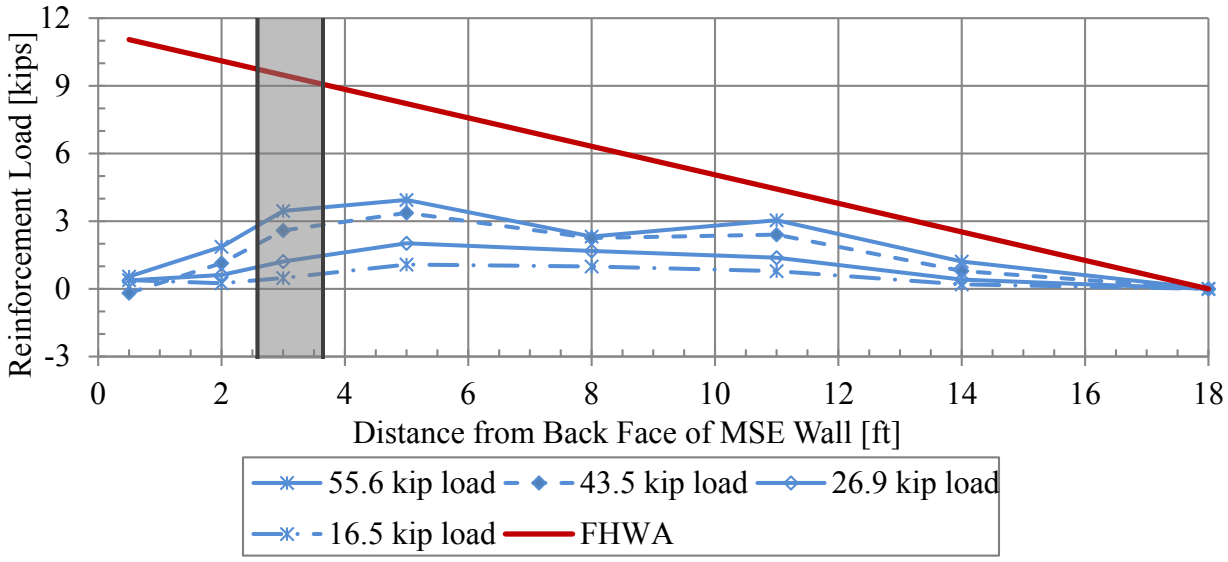

Figure E-20: Induced force in soil reinforcement at varying pile head loads and distances from the back face of the MSE wall for the 2.9D test; 45 in. depth and 38 in. transverse spacing from center of pile.

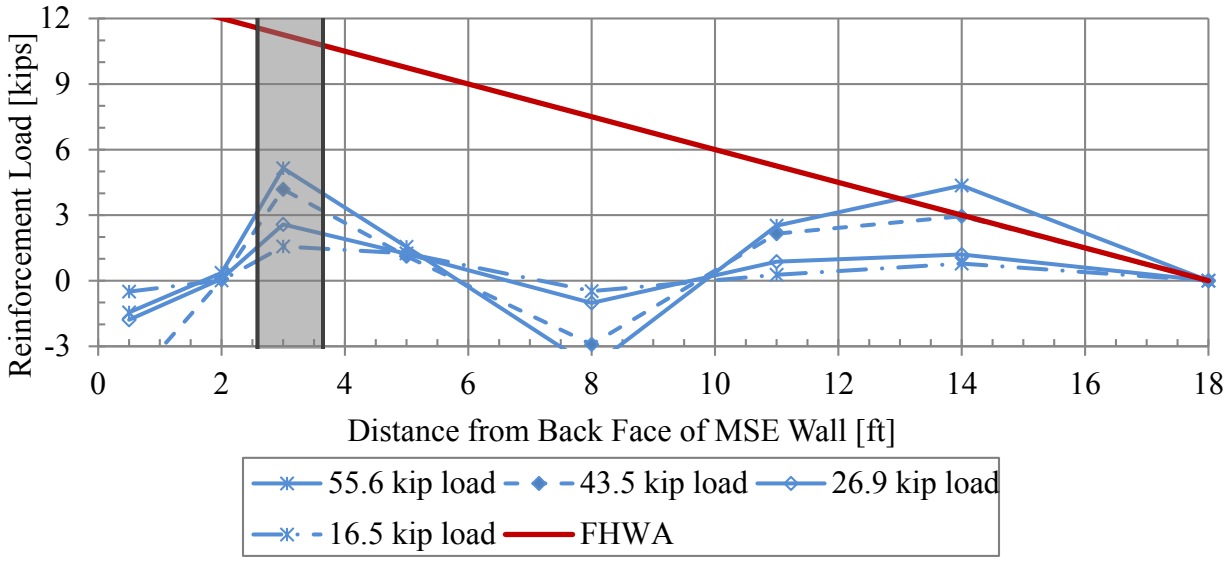

Figure E-21: Induced force in soil reinforcement at varying pile head loads and distances from the back face of the MSE wall for the 2.9D test; 75 in. depth and 11.5 in. transverse spacing from center of pile.

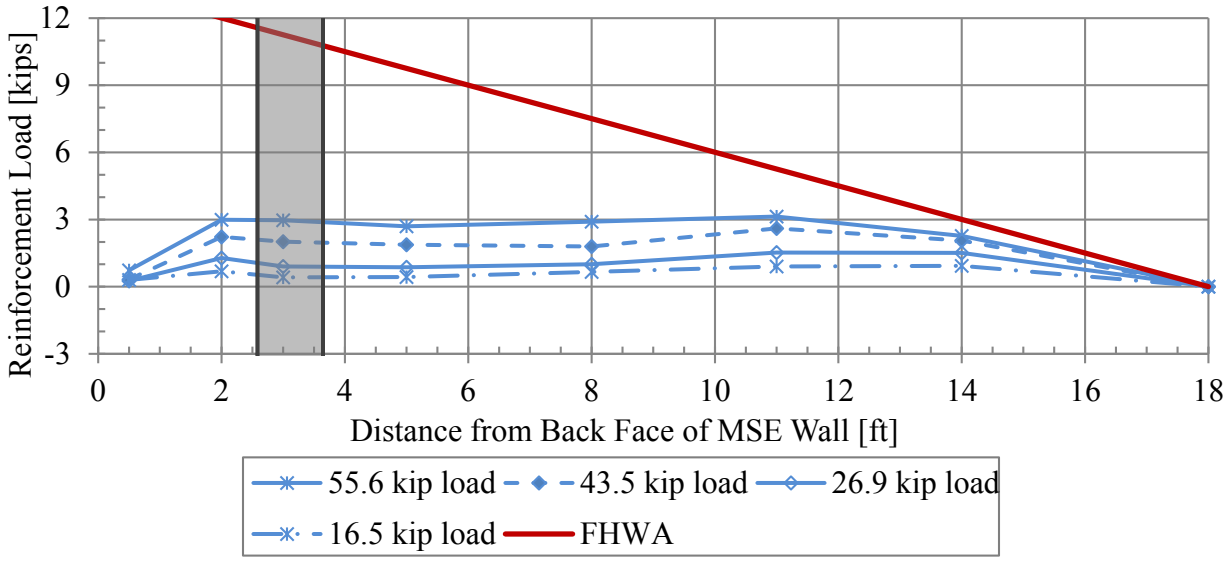

Figure E-22: Induced force in soil reinforcement at varying pile head loads and distances from the back face of the MSE wall for the 2.9D test; 75 in. depth and 37 in. transverse spacing from center of pile.

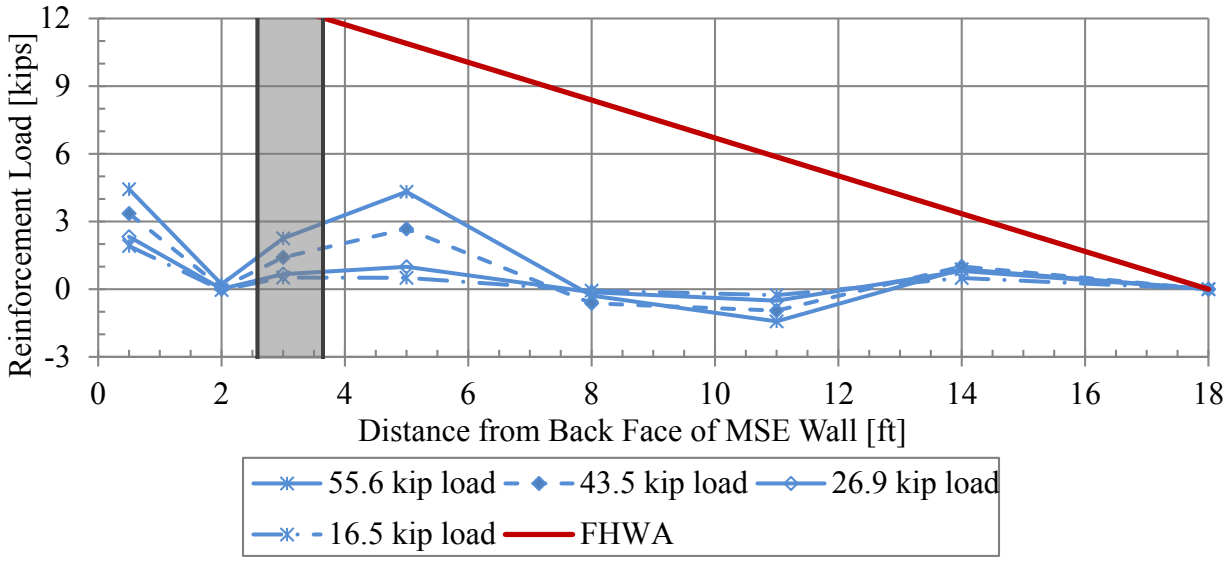

Figure E-23: Induced force in soil reinforcement at varying pile head loads and distances from the back face of the MSE wall for the 2.9D test; 105 in. depth and 10.5 in. transverse spacing from center of pile.

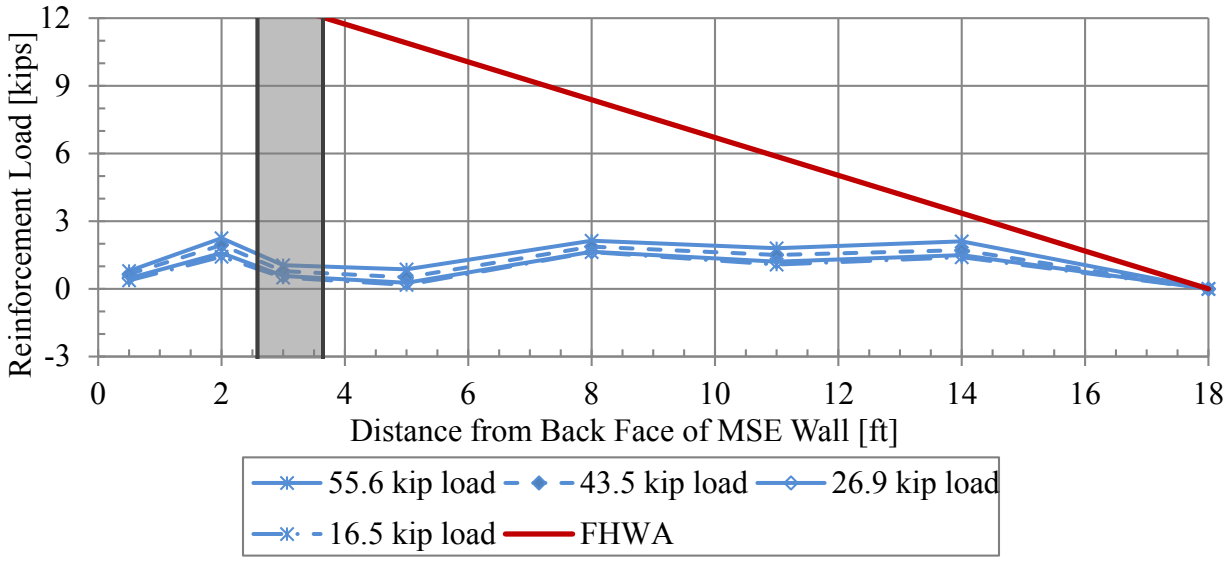

Figure E-24: Induced force in soil reinforcement at varying pile head loads and distances from the back face of the MSE wall for the 2.9D test; 105 in. depth and 38 in. transverse spacing from center of pile.

3.9D Soil Reinforcement Curves

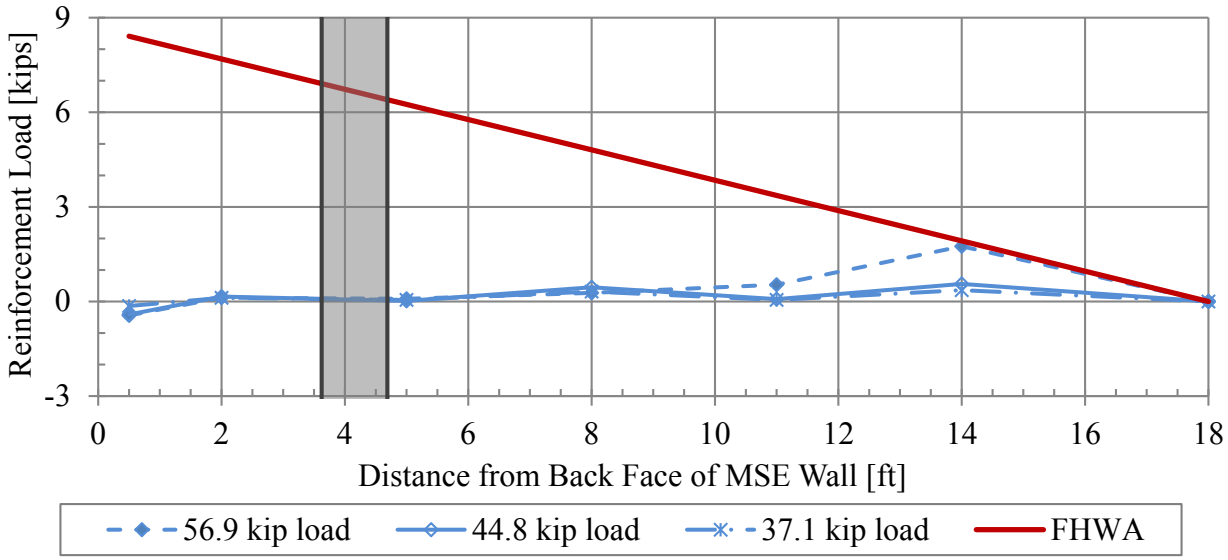

Figure E-25: Induced force in soil reinforcement at varying pile head loads and distances from the back face of the MSE wall for the 3.9D test; 15 in. depth and 26 in. transverse spacing from center of pile.

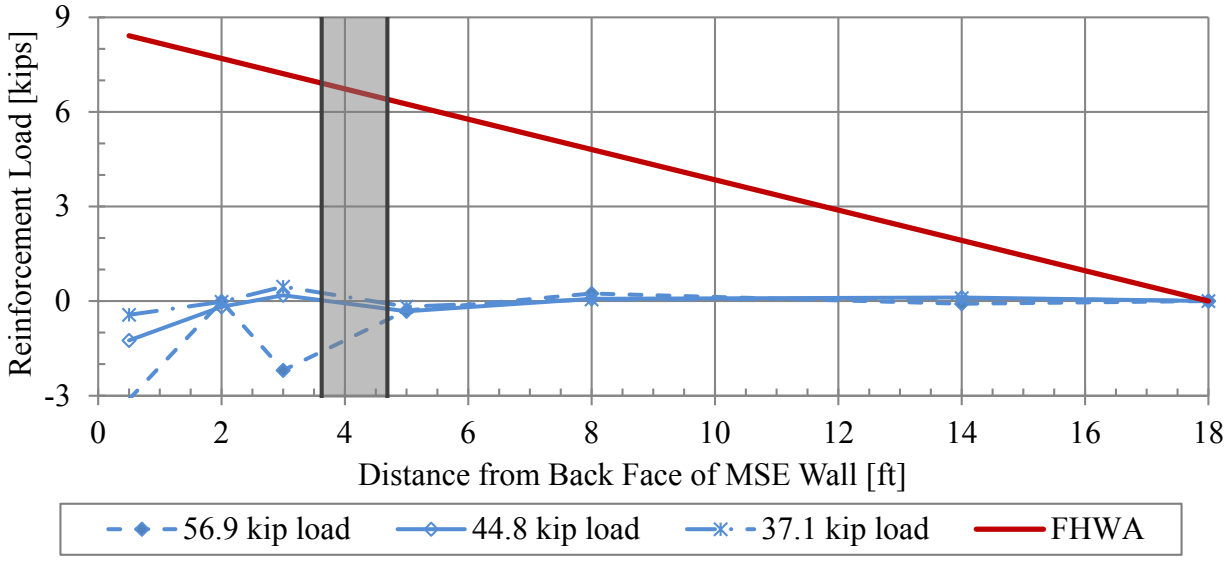

Figure E-26: Induced force in soil reinforcement at varying pile head loads and distances from the back face of the MSE wall for the 3.9D test; 15 in. depth and 51 in. transverse spacing from center of pile.

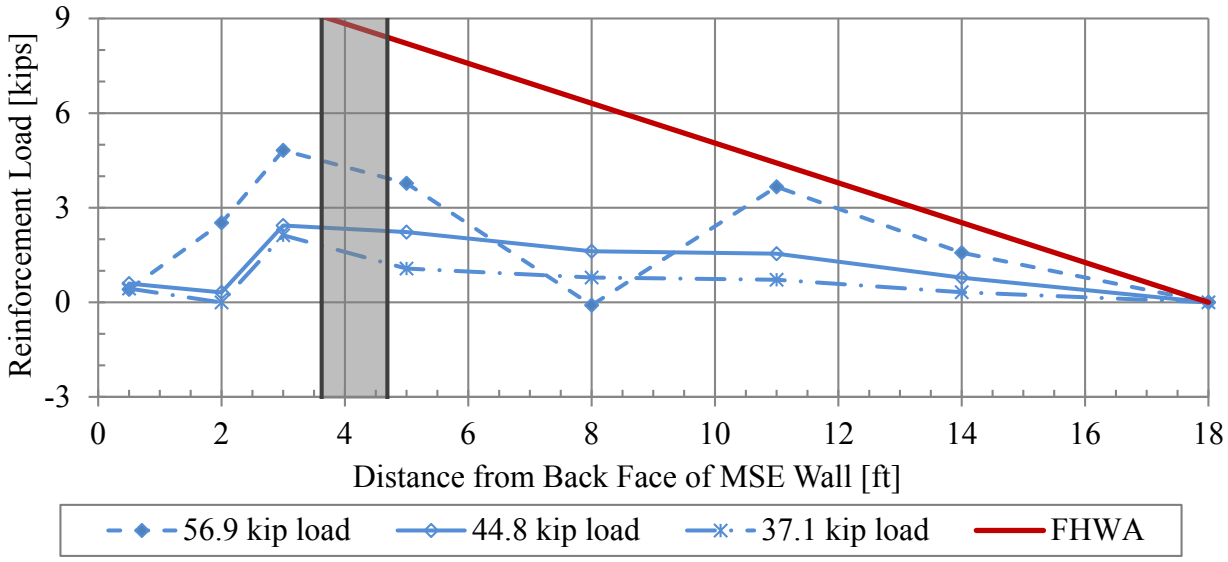

Figure E-27: Induced force in soil reinforcement at varying pile head loads and distances from the back face of the MSE wall for the 3.9D test; 45 in. depth and 22.5 in. transverse spacing from center of pile.

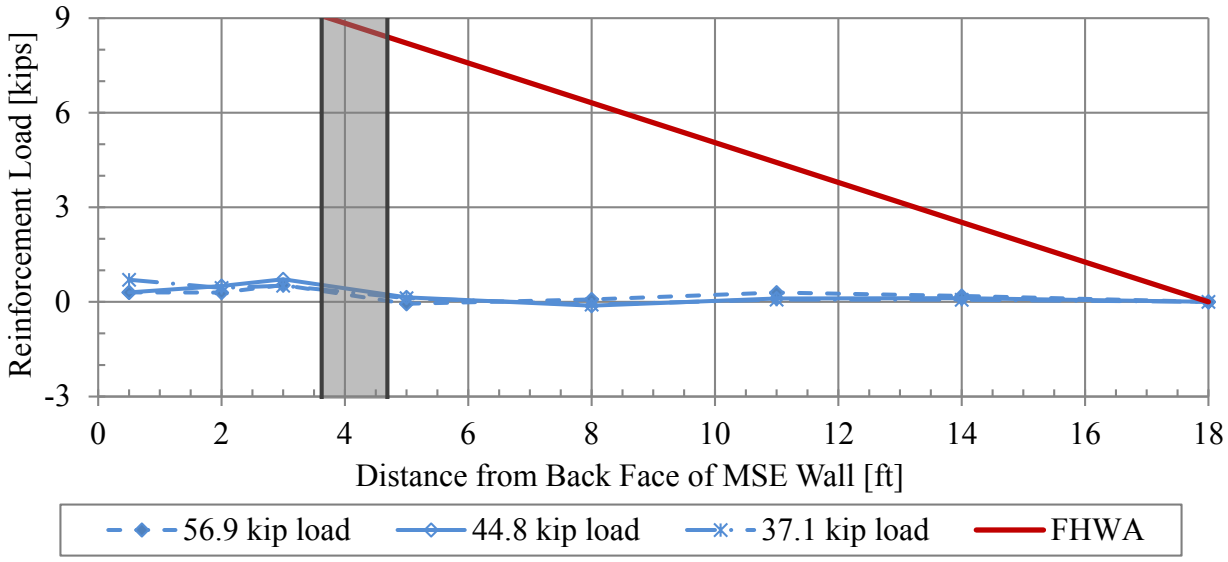

Figure E-28: Induced force in soil reinforcement at varying pile head loads and distances from the back face of the MSE wall for the 3.9D test; 45 in. depth and 49 in. transverse spacing from center of pile.

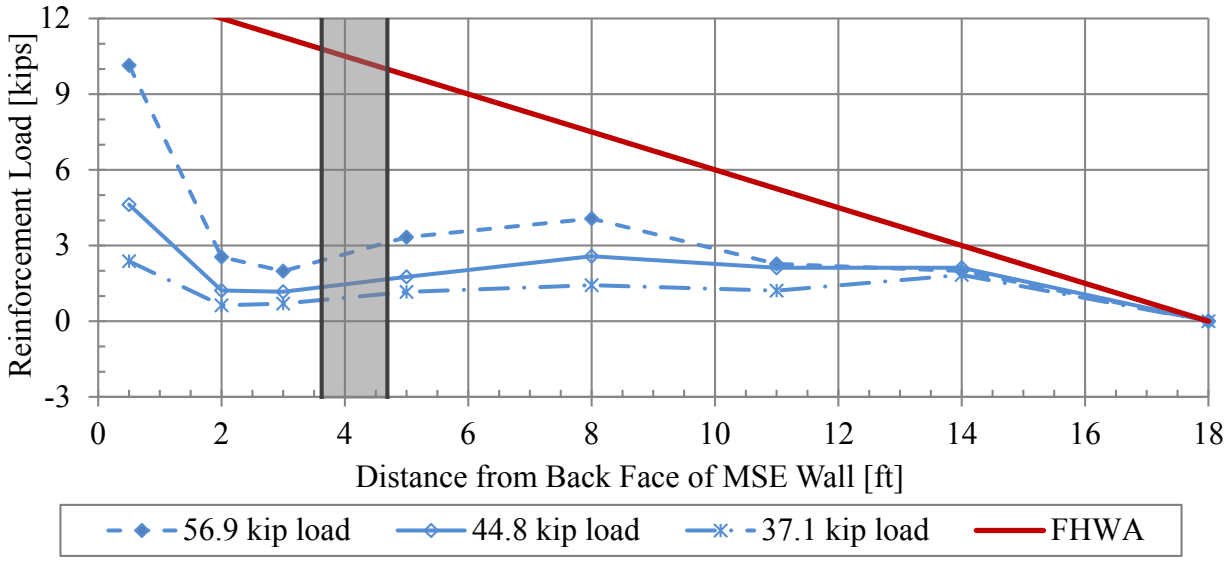

Figure E-29: Induced force in soil reinforcement at varying pile head loads and distances from the back face of the MSE wall for the 3.9D test; 75 in. depth and 24.5 in. transverse spacing from center of pile.

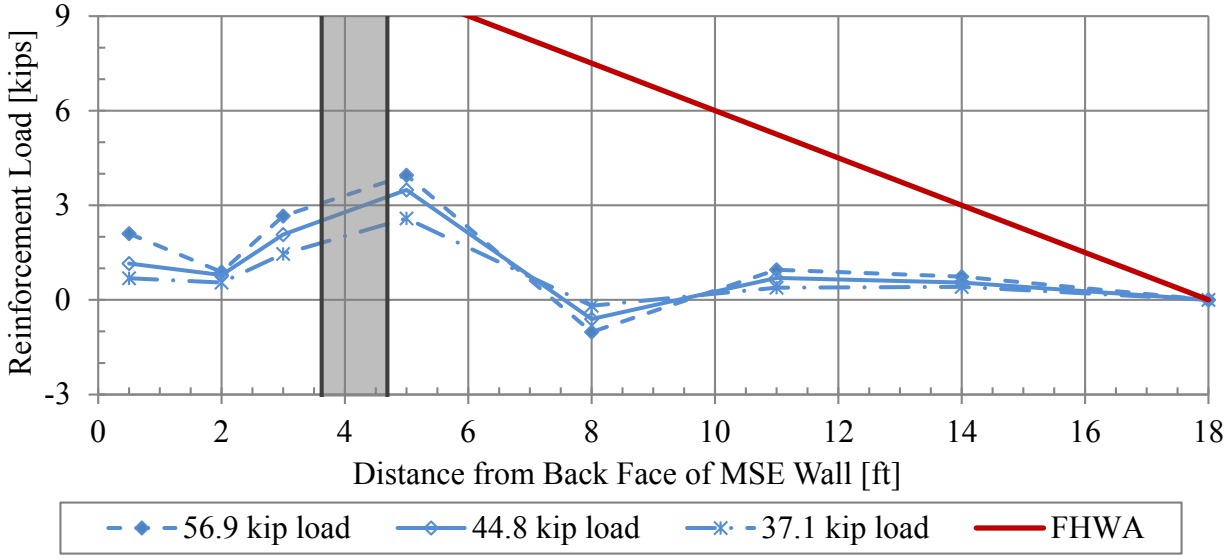

Figure E-30: Induced force in soil reinforcement at varying pile head loads and distances from the back face of the MSE wall for the 3.9D test; 75 in. depth and 50 in. transverse spacing from center of pile.

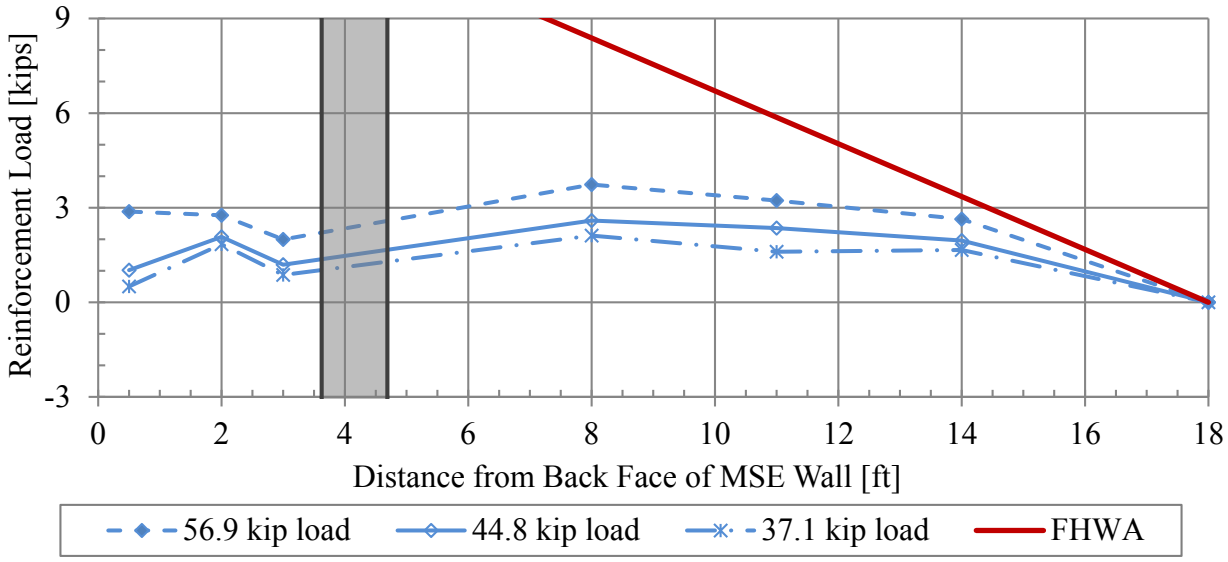

Figure E-31: Induced force in soil reinforcement at varying pile head loads and distances from the back face of the MSE wall for the 3.9D test; 105 in. depth and 24.5 in. transverse spacing from center of pile.

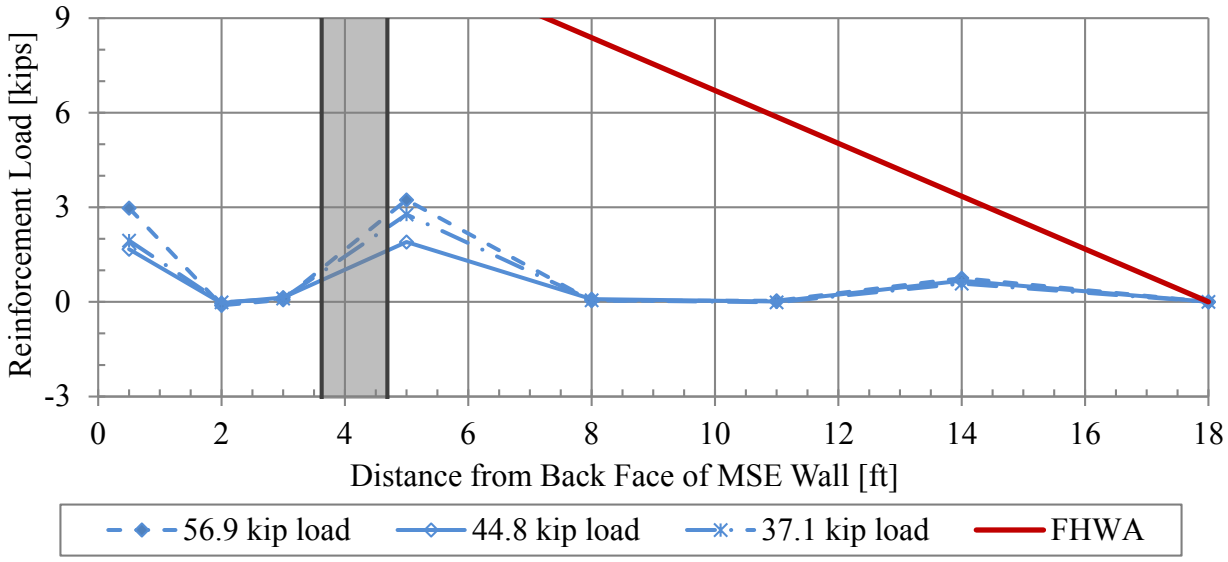

Figure E-32: Induced force in soil reinforcement at varying pile head loads and distances from the back face of the MSE wall for the 3.9D test; 105 in. depth and 51.5 in. transverse spacing from center of pile.

APPENDIX F. PILE DRIVING BLOWCOUNTS

Table F-1: Pile driving blowcounts at various depths for each of the test piles

Depth (ft)	N (blowcount)			
	1.7D	2.8D	2.9D	3.9D
1				
2				
3			2	
4		1		
5	1			
6			1	2
7				
8		2	1	
9	2		1	2
10	1	2	1	1
11	1	1	2	3
12	1	2	5	3
13	3	6	5	5
14	5	5	5	5
15	6	4	5	4
16	4	4	4	2
17	4	1	1	2
18	2	2	3	3
Total	30	30	36	32